Research Department

Technical Report No. 67

Assimilation of altimeter data in a global third generation wave model

P. Lionello[1], H. Günther[2], and P. Janssen[3]

[1] *Presently at ISDGM-CNR, Venice, Italy*
[2] *On leave from GKSS, Geesthacht, Germany*
[3] *KNMI, de Bilt, The Netherlands and ECMWF*

February 1992

Abstract

We investigated the effect of the assimilation of altimeter satellite data in the third generation ocean wave model WAM. We used a sequential method, where analysed significant wave height fields are created by Optimum Interpolation, and the analysed values are used to construct the analysed wave spectrum. The method provides also an estimate of the surface stress showing the possibility of using the analysis of the wave spectrum to derive an analysed surface stress field. In a first set of numerical experiments, the data, that have been provided by the SEASAT altimeter, have been assimilated in the WAM model for 1½ days. The comparison between model results and satellite data during the continuation of the run shows a positive and persistent impact of the assimilation. In a second set of numerical experiments GEOSAT altimeter data have been assimilated for ten days and the resulting analysis has been compared with buoy data. Although the assimilation improves the model results, it is not capable of compensating the differences between model and buoys. Some failures are clearly derived from the absence in the satellite data of the high wave events that were reported by the buoys. Other failures may be the consequence of an excessive swell attenuation in the WAM model, which compromises the effect of a previous correction. In fact, the comparison of WAM model results with altimeter data suggests that there is a tendency of the model to overevaluate initially the windsea, and successively to overestimate the decay of the wave energy, when the waves leave the area of the storm.

CONTENTS

1. INTRODUCTION

The launch of oceanographic satellites has provided wind wave modellers with a new and extensive set of measurements, which represents a remarkable change with respect to the previous situation when only a few measurements were available in scattered locations corresponding to platforms, buoys and oceanographic ships. The assimilation of such few data was not the object of much attention in wave modelling, because it was not necessary to produce an extremely reliable description of the initial wave field. Contrarily to weather forecasting, wave forecasting is in many aspects a boundary value problem and not an initial value problem. The wave field tends to lose the memory of the initial state; its description benefits more from the assimilation that has been performed in the atmospheric model which produced the driving wind fields. The purpose of data assimilation in a wave model is to correct the model, including errors introduced by the driving wind fields and to produce a better performance, but it is not a necessary part of a wave prediction system. While the impact of the few data available in the past was not expected to be very relevant on a global scale, the wide coverage produced by satellite measurements is expected to have a substantial effect.

The improvement of the wave forecast is not the only reason to analyse the wave measurements; another motivation is that, due to the dependence of the wave model results on the surface stress field, a coupled wind and wave assimilation can improve the performance of the atmospheric model, supplying further information on the stress field. Ocean waves can be categorized as windsea (waves that are evolving under the action of the wind), or swell (waves that are freely propagating, the wind being too weak to affect them). This study shows how the surface stress can be derived from the analysis of the wave model results, producing a consistent analysis of the wave spectrum and the surface stress where there is windsea. On the other hand, the consistent modification of surface stress and wave spectrum is a necessary requirement for a wave assimilation scheme. The updating of the wind sea has little effect unless the surface stress is also updated, because the correction would otherwise be erased by the incorrect wind forcing.

The practical target of this study is to develop a system which could use satellite data in an operational framework, i.e. a tool which could be used, for a regular, daily assimilation of satellite data with limited computer resource costs, ready for the ERS-1 mission.

Two devices are mounted on ERS-1 which provide information on the wind waves: the altimeter and the synthetic aperture radar (SAR). The altimeter provides measurements of the significant wave height (SWH) along the satellite track with good accuracy (0.5 m or 10% of significant wave height, whichever is larger). The measurement is based on the modification in the rise time produced by the wavy surface in the backscattered signal. The result is interpreted as SWH. Potentially much more information is contained in the SAR images, from which the wave spectrum can be deduced. Unfortunately the transfer from SAR

image to wave spectrum is not a one to one mapping; waves may be not detected due to excessive noise or to high nonlinearity. The picture of the sea surface is distorted, and the distortion depends on the component of the velocity of the waves normal to the satellite flight direction. It is then not isotropic. Due to these problems a first guess spectrum must be provided by a wave model to interpret adequately the SAR image. A procedure to produce in most of the cases an analysed spectrum is actually available (*Bruning et al.*, 1990), and it has been applied to SEASAT data. Unfortunately, a very limited amount of spectra have been till now produced, and they are not enough to study the impact of SAR on the wave prediction. No SAR was mounted on GEOSAT. Therefore, as no routine inversion of the SAR image was available by the beginning of this study, we sought a method that could analyse the wave field without the need of wave spectra measurements. Therefore, although this method could be readily extended to use peak frequency and peak direction which could be provided by SAR, only altimeter data have been used.

Presently, for wave assimilation, as for assimilation in circulation models, there are two main classes of assimilation methods: sequential methods and variational methods. Sequential methods perform a series of N independent corrections, each at a different time $t_i (i = 1, ..., N)$, each time using the observations available in a time window centred at the time t_i. At each assimilation time t_i, the wave field is modified to agree as much as possible with observations, taking into account the reliability of both model results and measurements. In this respect they may be called single time level schemes. The sequence of fields is not consistent with the model dynamics, a discontinuity in the development being introduced at every assimilation time t_i.

Variational methods aim to find the model solution which minimizes the differences with observations over the whole analysis period by introducing corrections in the sequence of wind fields driving the wave model. In this respect they are also called multiple time level schemes. As the wave model equations are used as constraint, the process produces a sequence of wave fields which are at every time step consistent with the wave model dynamics. Note that the sequence of analysed wind fields will not be in general consistent with the dynamics of the atmospheric model, unless the atmospheric model itself is also involved in the analysis. Presently practical difficulties and enormous costs prevent this solution. The quantity to minimize is the cost function

$$\mathbf{Y} = \mathbf{Y}_{wa} + \mathbf{Y}_{wi} \tag{1}$$

$$\mathbf{Y}_{wa} = \sum_{i=1}^{N_{obs}} (a_P^i - a_O^i) A_{ij} (a_P^j - a_O^j) \tag{2}$$

$$\mathbf{Y}_{wi} = \mathbf{Y}_{wi}(\bar{b}) \tag{3}$$

The a_P^i denotes the model counterparts of the measurements, i.e spectral densities or derived quantities, a_O^i are the observations, A_{ij} a generally diagonal matrix. Therefore the first term represents the difference between model results and measurements. The vector $\overline{b}$ is a suitable set of parameters which describes the modification in the wind field; the magnitude of the second term with respect to the first one can be adjusted to allow a larger or smaller variation in the wind fields. The cost function must be minimized with the constraint of the model equations. The solution of the variational problem using the adjoint method has been proposed by *de Valk and Calkoen* (1989) for a regional implementation of the WAM model. *Hasselmann et al.* (1988) solved it with a different approach using Green's function, which describes the response of the wave field to small perturbations in the stress field.

The advantage of sequential methods is the relative simplicity and the relatively little computer resources required. The minimization of the cost function typically requires a series of runs of the wave model. Consequently the needed computer resources are larger than the ones needed to execute the model itself, while the resources that are requested by a sequential method are, in comparison, negligible. On the other hand the variational approach avoids the problem of specifying correlation scales in model and observations, such scales being automatically produced by the model dynamics; Moreover, as it has been already anticipated, we sought a method that could work using only altimeter data, without the necessity of additional spectral information. The approach by *Hasselmann et al.* (1973) requires explicitly the availability of the measured spectra. In principle this is not true for the adjoint method, although *de Valk and Calkoen* (1989) assumed the availability of SWH, mean period and mean direction in their numerical experiments. Presently there is no evidence that a variational method performs better than a sequential one, but as the research is rapidly progressing in this field, results are expected to be published within the next few years.

Therefore we decided to continue with a sequential approach - using the previous experience of two of the authors (*Janssen et al.*, 1989) - that uses satellite altimeter data to analyse the wave spectra, following a research line common the studies by *Esteva* (1988) and *Thomas* (1988). The input information is therefore the SWH along the satellite track. The advantage of altimeter data is their abundance and reliability; the disadvantage is that the SWH is not a dynamical quantity in the wave models, but only an output information derived from the spectrum. This raises the problem of the reconstruction of the wave spectrum from the altimeter data. Consequently the procedure is split into two steps: first the SWH data are used to construct an analysed field of SWH by O.I. (as described in the second section). The second step consists of the reconstruction of the spectrum from the analysed SWH, i.e. applying a procedure to transform the first guess spectrum into the analysed one, using the information of its total energy only. Since in the WAM model the spectrum has a discrete representation with 300 degrees of freedom (12 direction and

25 frequency bins), its updating, using only the total energy, must involve some assumptions, which are discussed in the third section.

This study presents two realistic data assimilation experiments, which are carried out using the altimeter data supplied by SEASAT and GEOSAT. A short data assimilation experiment is carried out using SEASAT data, with the purpose of investigating in some detail the effect in the subsequent behaviour of the model. Satellite data are assimilated for 1½ days. In parallel, a run without assimilation is carried out. The results of the two runs have been compared with the satellite data available in the forecast period following the end of the assimilation. The comparison describes the relevance and the duration of the effect of the assimilation. A longer experiment (data have been assimilated for ten days at the end of November 1988) has been carried out using GEOSAT data. During it buoy data could be used as an independent dataset, to estimate eventual benefits by comparing them to the analysed wave spectra that were produced by the assimilation.

The wave model used in this study is the WAM model (*WAMDI group*, 1988) in a global implementation with a 3° grid step. This is a third generation wave model which computes the wave spectrum $F(f,\theta,t,\bar{x})$, where the arguments are frequency f, direction θ, time t and position $\bar{x}$. Both the parametrization of the spectral shape and of the source function $S(f,\theta,\bar{x},F)$ are avoided by the explicit solution of the energy transport equation

$$\frac{\partial F}{\partial t} + \nabla.(C_g F) = S \qquad (4)$$

in the prognostic part of the spectrum. Here C_g is the wave group velocity and S is the source function representing the physical mechanisms that are involved in the evolution of the wave field (*WAMDI*, 1988). As it will become clear in the remaining part of the paper, the assimilation approach can be used for other models, although possibly some features (see section 3.2) might be particularly suitable for the WAM model.

2. CONSTRUCTION OF AN ANALYSED WAVE HEIGHT FIELD

No consolidated technique has been used in the past to spread the altimeter data on the model grid. *Janssen et al.* (1989) used the data only at the grid point where the measurement took place. *Esteva* (1988) actually attempted to spread the information preserving the local slope in the forecasted SWH field, but he abandoned this technique because results were unsatisfactory, preferring, as *Janssen et al.*, to use the measured SWH only at the point of the measurement. *Francis and Stratton* (1990) used an exponential spreading function, estimating a correlation length of 1200 km from a collection of wave measurements in the North Sea. In this study, we use Optimum Interpolation (O.I.), that is a standard procedure, which has been extensively used in meteorology for data assimilation (*Hollingsworth*, 1986). Here it is used to construct analysed Significant Wave Height (SWH) fields. At each point x_i the analysed SWH, denoted as H_A^i, is expressed as a linear combination of $H_P^j (j=1, ..., N_{obs})$, the first guess results produced by the model, and of H_O^j, the observations

$$H_A^i = H_P^i + \sigma_P^i \sum_{j=1}^{N_{obs}} W_{ij} \frac{H_O^j - H_P^j}{\sigma_P^j} \tag{5}$$

Here N_{obs} is the number of available observations, σ_P^j is the root mean square error in the model prediction:

$$\sigma_P^j = \langle (H_P^j - H_T^j)^2 \rangle^{1/2} \tag{6}$$

where H_T^j represents the true value of the SWH. The weights W_{ij} are chosen to minimize the root mean square error in the analysis, σ_A^i,

$$\sigma_A^j = \langle (H_A^j - H_T^j)^2 \rangle^{1/2} \tag{7}$$

The $\langle\rangle$ indicates an average over a large number of realizations. Assuming that the errors in the model are uncorrelated with the errors in the measurements the solution is

$$W_{ij} = \sum_{k=1}^{N_{obs}} P_{ik} M_{kj}^{-1} \tag{8}$$

where the element of the matrix M is

$$M_{kj} = P_{kj} + O_{kj} \tag{9}$$

and P and O are the error correlation matrix of prediction and observation respectively (both are actually scaled with σ_P^i):

$$P_{kj} = \left\langle \frac{(H_P^k - H_T^k)(H_P^j - H_T^j)}{\sigma_P^k \sigma_P^j} \right\rangle \tag{10}$$

$$O_{kj} = <\frac{(H_O^k - H_T^k)(H_P^j - H_T^j)}{\sigma_P^k \sigma_P^j}> \tag{11}$$

Therefore the prediction error correlation matrix $\boldsymbol{P}$ and the observation error correlation matrix $\boldsymbol{O}$ must be specified. This would require in practice the determination of statistics for both prediction and the observations, which are presently unavailable. Tentatively for the prediction it is assumed

$$P_{kj} = \exp(-\frac{|\overline{x_k} - \overline{x_j}|)}{L_{\max}}) \tag{12}$$

and the observation errors are assumed to be random and uncorrelated:

$$O_{ij} = \delta_{ij}\left(\frac{\sigma_O^i}{\sigma_P^i}\right) = \delta_{ij} R_i \tag{13}$$

An investigation on the effect of variations of $L_{\max}$ and of the ratio between σ_O^i and σ_P^i on the results of the assimilation is one of the purposes of the experiments, that are discussed in the fourth section.

3. THE ANALYSIS OF THE WAVE SPECTRUM

Since only altimeter data are used in this study, the result of the O.I. is a SWH field. This of course specifies the total energy of the wave spectra but not their shape. Therefore in this kind of sequential method some extra assumptions must be introduced to update the wave spectrum. *Esteva* (1988) simply multiplied the spectrum by the factor $(H_A/H_P)^2$ without modifying the wind speed. The problem of reconstructing the wave spectrum was further addressed by *Thomas* (1989), who attempted to reconstruct buoy spectra by combined measurements of significant wave height and wind speed using the JONSWAP spectrum. The approach used here must be different, because a different type of wave model is involved. Both *Thomas and Esteva* used a second generation wave model with a prescribed windsea spectral shape, while in this study we use a third generation wave model, where there is no prescribed spectral shape. Moreover we prefer not to rely on the altimeter wind speed measurements and to use only wave data. There is an infinite number of transformations which can be applied to the WAM model spectrum in order to match its energy with the measurements and none of the produced spectra will introduce shocks in the model although they may be actually very unrealistic, therefore not producing the expected improvement. Specifically the multiplication of the swell spectrum by the factor $(H_A/H_P)^2$ does not produce satisfactory results in the WAM model (*Lionello and Janssen*, 1990).

The basic assumption of the reconstruction that we propose, is that the model prediction is wrong because the stress field by which it has been driven was incorrect. Consequently we aim to obtain the spectrum that the model would have produced if the stress field were correct, consistently modifying also the wind speed. It is generally believed, at least among wave modellers, that most of the errors in the wave prediction are actually derived from errors in the stress field, and our assumption is in agreement with such an opinion.

The information contained in the first guess spectrum $F_P(f,\theta)$ is used to produce an analysed spectrum $F_A(f,\theta)$ as

$$F_A(f,\theta) = AF_P(Bf,\theta) \tag{14}$$

As no information on the direction of waves is provided by the altimeter, we are forced to consider only errors in the modulus of the stress and not in its direction, but if information on the direction were available a third parameter could easily be introduced to rotate the spectrum. This solution is of course appropriate when no major feature of the true spectrum is absent in the first guess spectrum; if a peak were completely missed, this approach would not be able to produce it. Moreover the ratio among parts of the spectrum having a different origin cannot be changed. Therefore this approach cannot correct for large inaccuracies in the prediction, since this would imply a complete restructuring of the spectrum. We expect it is anyway adequate for the operational framework for which it has been conceived, because both the analysed wind fields driving the WAM model during the analysis and the regular repetition of the data assimilation process

are expected to limit the discrepancies between model and observations. It must be stressed that (14) is not meant to describe the evolution of the wave spectrum, a task for which it is clearly inadequate, but to transform a first guess spectrum into an analysed one, which should have been generated in a relatively similar situation.

To determine the two parameters A and B in (14) is the purpose of the reconstruction procedure. The method distinguishes between the windsea spectrum and the spectrum outside the storm region, reflecting the traditional distinction between windsea and swell in wind wave modelling. The term swell in this study will be used in a relatively loose way to denote the situation in which the waves are not evolving under the effect of the wind. It is therefore applied also to the spectrum immediately outside the storm, which, in spite of being broad, cannot be considered windsea because it has a peak frequency that is lower than the Pierson-Moskowitz frequency.

This section presents three simple situations to illustrate the reconstruction procedure. They are the reconstruction of the windsea spectrum during time limited growth (section 3.1), the reconstruction the spectrum during the subsequent decay when the wind drops (section 3.2), and the reconstruction of a spectrum in which windsea and swell are present together due to a sudden rotation of the wind (section 3.3). The idea is to compare three model runs: a first one, which will be referred to as correct prediction, is used to simulate the truth; a second one, which is obtained by introducing a bias in the surface stress, simulates the wrong prediction; and the third one simulates a run in which the assimilation is carried out (and it will be referred to as assimilation run). The assimilation run reproduces exactly the wrong prediction until the assimilation is carried out, extracting the measured value from the correct prediction and constructing the analysed spectrum from the spectrum of the incorrect prediction. The assimilation produces an analysed spectrum and, if the spectrum is windsea, also an analysed friction velocity. The assimilation experiment is successful if the assimilation run, which in its first part is identical to the wrong prediction, reproduces closely the correct prediction after the assimilation time. In these examples, since no O.I. is carried out, the measured SWH coincides with the analysed one.

The model used is a single point version of the WAM model in which advection is neglected, simulating an homogeneous ocean of infinite extent.

3.1 Windsea time limited growth

The reconstruction of the windsea spectrum is obtained using the energy growth curves and the relations between energy and mean frequency which describe its evolution. Note that these two equations are not explicitly present in the WAM model set-up, because the WAM model solves explicitly the energy transport equation,and they have to be derived by analytical fitting to the WAM model numerical results. The

advantage of the windsea, with respect to the swell, is that total energy and mean frequency can be made dimensionless to provide relations in a form that does not depend on the surface stress ρu_*^2 (*Kitaigorodsky*, 1962). Dimensionless energy E_* time t_* and mean frequency f_{m*} are given as

$$E_* = \frac{u_*^4}{g^2}E, \qquad t_* = \frac{g}{u_*}t, \qquad f_{m*} = \frac{u_*}{g}f_m \tag{15}$$

where g is the acceleration of gravity and u_* is the friction velocity. We fitted the WAM model numerical results and we obtained the following time limited growth curve

$$E_*(t_*) = 955\tanh(6.02\cdot10^{-5}t_*^{0.695}) \tag{16}$$

and the following relation between total energy and mean frequency during the windsea development

$$E_*(f_{m*}) = 1.68\cdot10^{-4}f_{m*}^{-3.27} \tag{17}$$

(The mean frequency is here preferred to the peak frequency because its computation is more stable). The two curves are shown in Figs. 1a and b. These two relations are what we need to correct the effect of an error in the stress. In fact as the first guess friction velocity that has been generating the waves is known, an estimate of the duration T of the windsea can be derived using E_P. Assuming that this estimate of the duration is correct, using the energy E_A provided by the analysis in an analysed value of the friction velocity U_{*A} is computed. An analysed value of the mean frequency f_{*mA} is derived using the computed U_{*A} and E_{*A}. Finally the dimensional quantities E_A and f_{mA} are provided by (15), and the two parameters A and B in (14) are given as

$$A = \frac{E_A}{E_P}B, \qquad B = \frac{f_{mP}}{f_{mA}} \tag{18}$$

where E_P and f_{mP} are energy and mean frequency of the first guess spectrum.

Figs. 2 a,b,c show an instance of windsea assimilation: in the incorrect prediction $u_* = 0.83$ and in the correct prediction $u_* = 0.64$ a shows the time behaviour of the SWH, Fig. 2b of the mean frequency, Fig. 2c of u_*. After 12 hours the correct SWH is assimilated, obtaining, by the previously described procedure, an evaluation of the mean frequency and of the friction velocity. After the assimilation the evolution of the analysed spectrum is very close to the correct prediction. This is a consequence of the correct analysed friction velocity obtained by the analysis and of the correct reconstruction of the spectrum. This is shown in Fig. 2a where correct, incorrect and analysed spectra are compared.

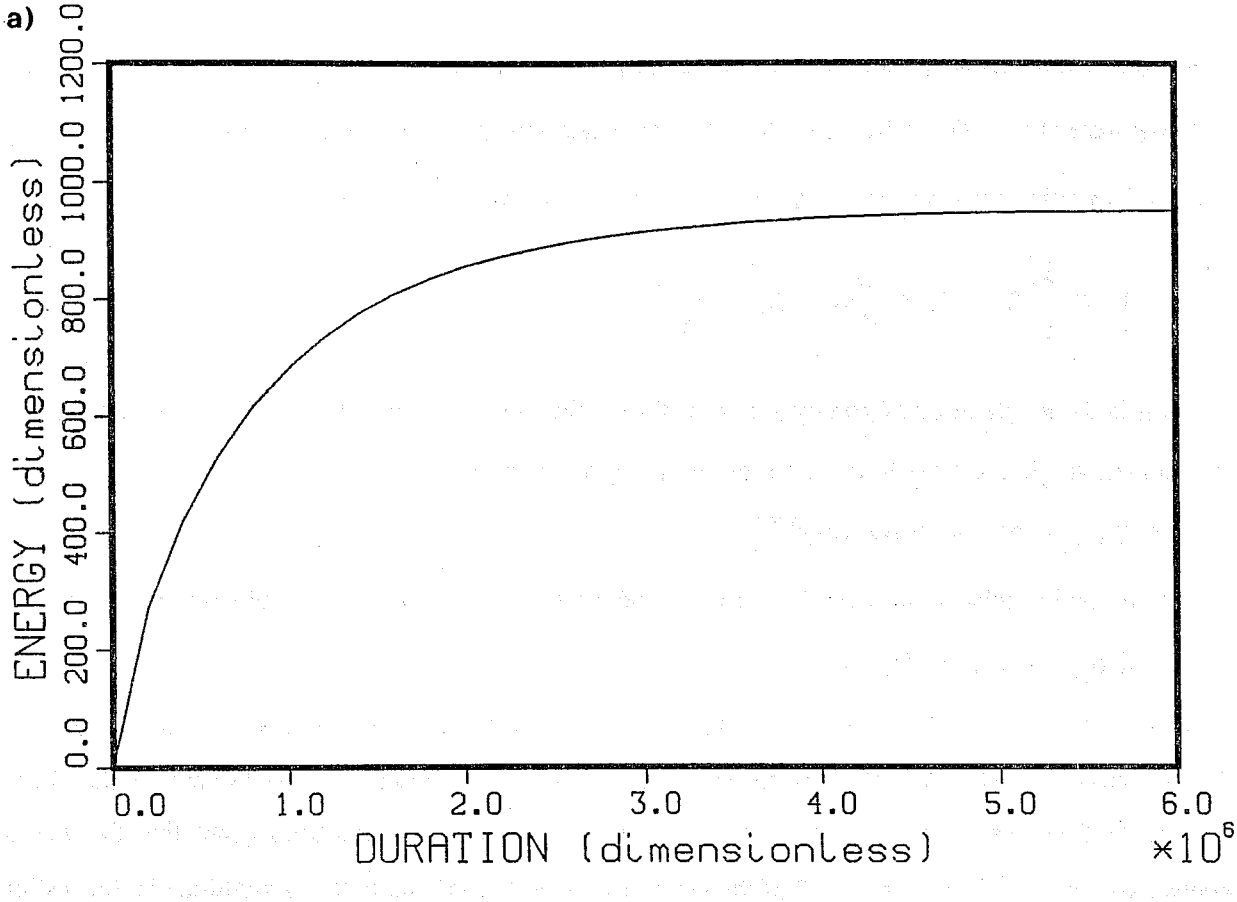

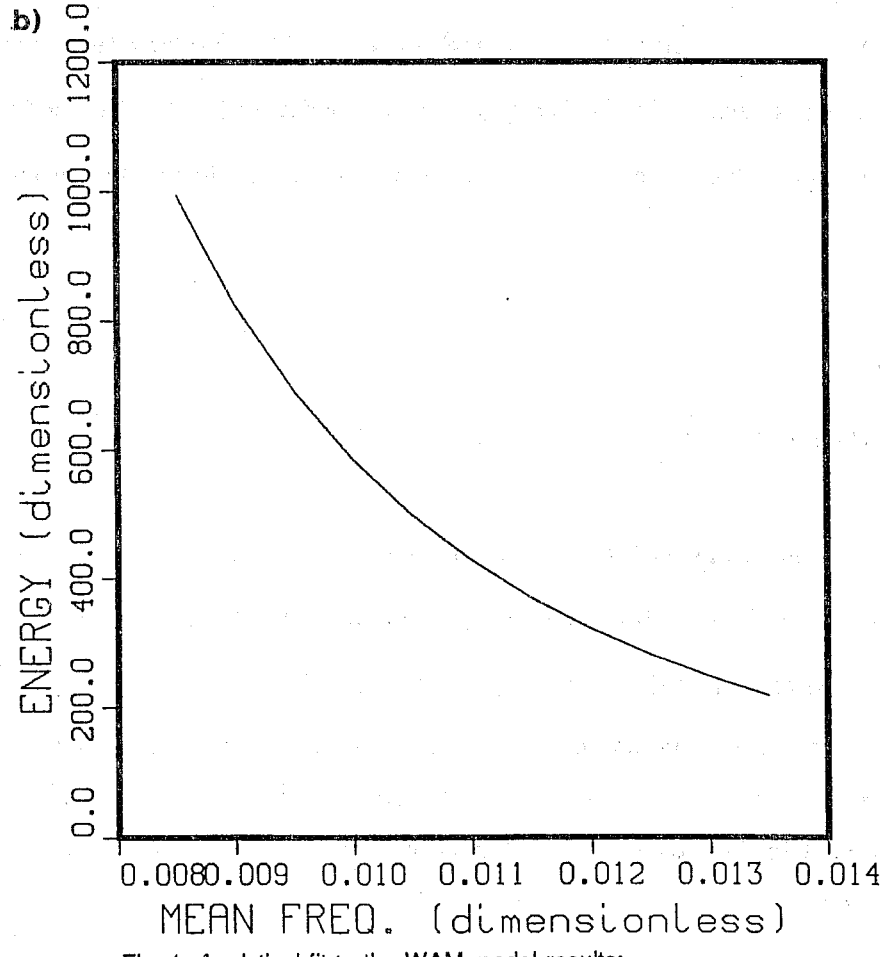

Fig. 1 Analytical fit to the WAM model results:
a) The dimensionless energy as function of the dimensionless time.
b) The dimensionless energy as function of the dimensionless mean frequency.

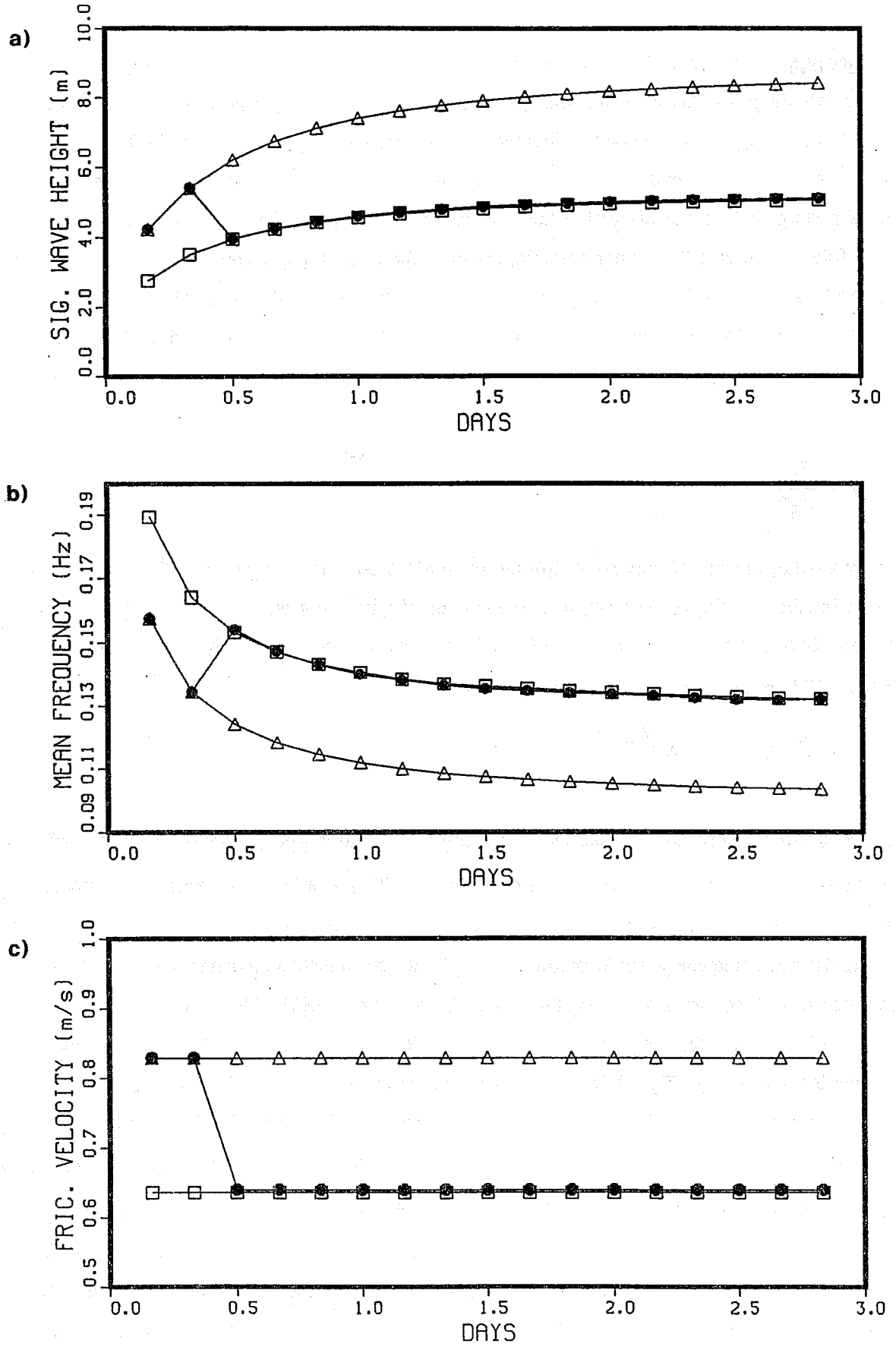

Fig. 2 Time series for case 3.1 (windsea growth). a) significant wave height, b) mean frequency, c) friction velocity. (squares represent the correct prediction, triangles the incorrect prediction, full circles the assimilation run).

3.2 Decay of the spectrum in absence of wind

As second case the possibility to correct the spectrum during its decay is considered. The error is assumed to be due to the wrong friction velocity when the spectrum was generated, but the assimilation takes place when the wind has dropped and the spectrum is decaying. This is meant to simulate what happens on the border of a storm, where the dispersion has not yet spatially separated the different frequencies. The approach followed in case 3.1) is not possible, because there is no way to produce dimensionless decay curves and the spectrum is then modified according to the method proposed by *Lionello and Jannsen* (1990). The authors investigated the decay of WAM model spectra which had been generated by different stresses. They found that, if the spectra have been decaying for the same time, the values of the average steepness s,

$$s = \frac{Ek_m^2}{4\pi^2} \tag{19}$$

were very similar, in spite of very large differences in SWH and mean frequency. Therefore the authors suggested that the updating of the spectrum should not modify its steepness to construct the spectrum which should have been produced if the correct value of the friction velocity would have been used during the generation. This produces for A and B the choices

$$A = \frac{E_A}{E_P}B; \qquad B = \Delta B\left(\frac{E_A}{E_P}\right)^{1/4} \tag{20}$$

where ΔB is a factor very close to one, that can eventually be introduced to account for some variation in the steepness s, that is observed in the model decay curves. This solution corresponds to the intuitive idea that a more energetic spectrum has a lower peak frequency; moreover, increasing the energy without decreasing the peak frequency would produce a swell with an unrealistic steepness and, consequently, a source function with an unrealistic dissipation (see *Lionello et al.*, 1991). Since the swell spectrum is not related to the local stress, the analysis of the friction velocity cannot be carried out in this case, and the first guess value is not changed. Figs. 3.2a, b, c show the numerical experiment. The spectrum was generated by a wind which had been blowing for two days; in the correct prediction the friction velocity had a higher value, $u_* = 0.83$, than in the incorrect prediction where $u_* = 0.64$. After one day of decay the assimilation is carried out according to (20). It results in the correct behaviour of the model for the remaining part of the decay as it is shown in Figs. 3.2a, b, c. The reason for the correct behaviour is clear from the comparison of the spectra: Fig. 3.2 shows the first guess spectrum, denoted by squares, the correct spectrum, denoted by circles, and the result of the reconstruction denoted by triangles. There is very good correspondence between the reconstructed spectrum and the correct one. This implies a correct reconstruction also of the source function and therefore the reproduction of the correct decay, from the assimilation time onwards.

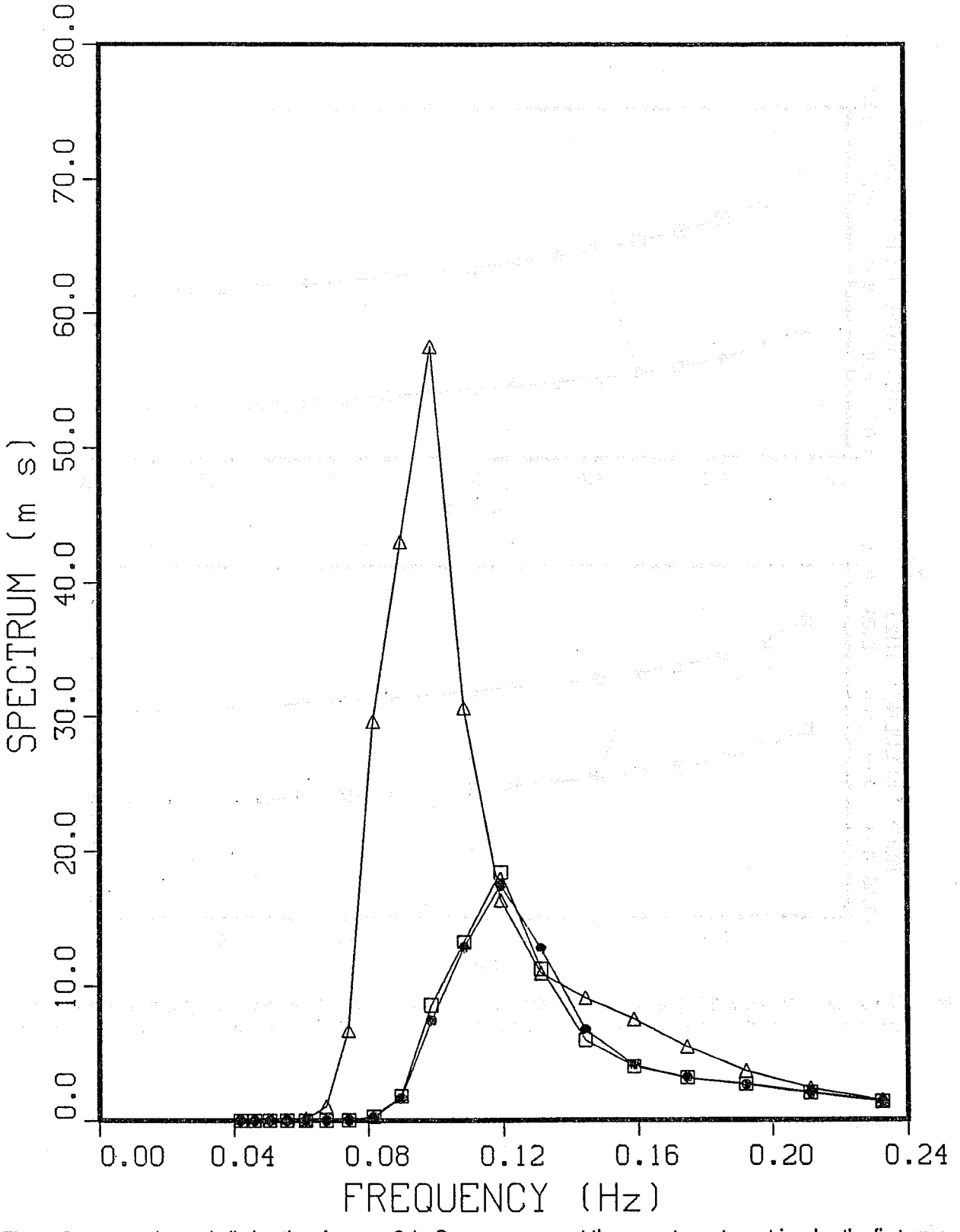

Fig. 3 Spectra at the assimilation time for case 3.1. Squares represent the correct spectrum; triangles the first guess, i.e. the incorrect prediction; full circles the analysed spectrum resulting from the assimilation.

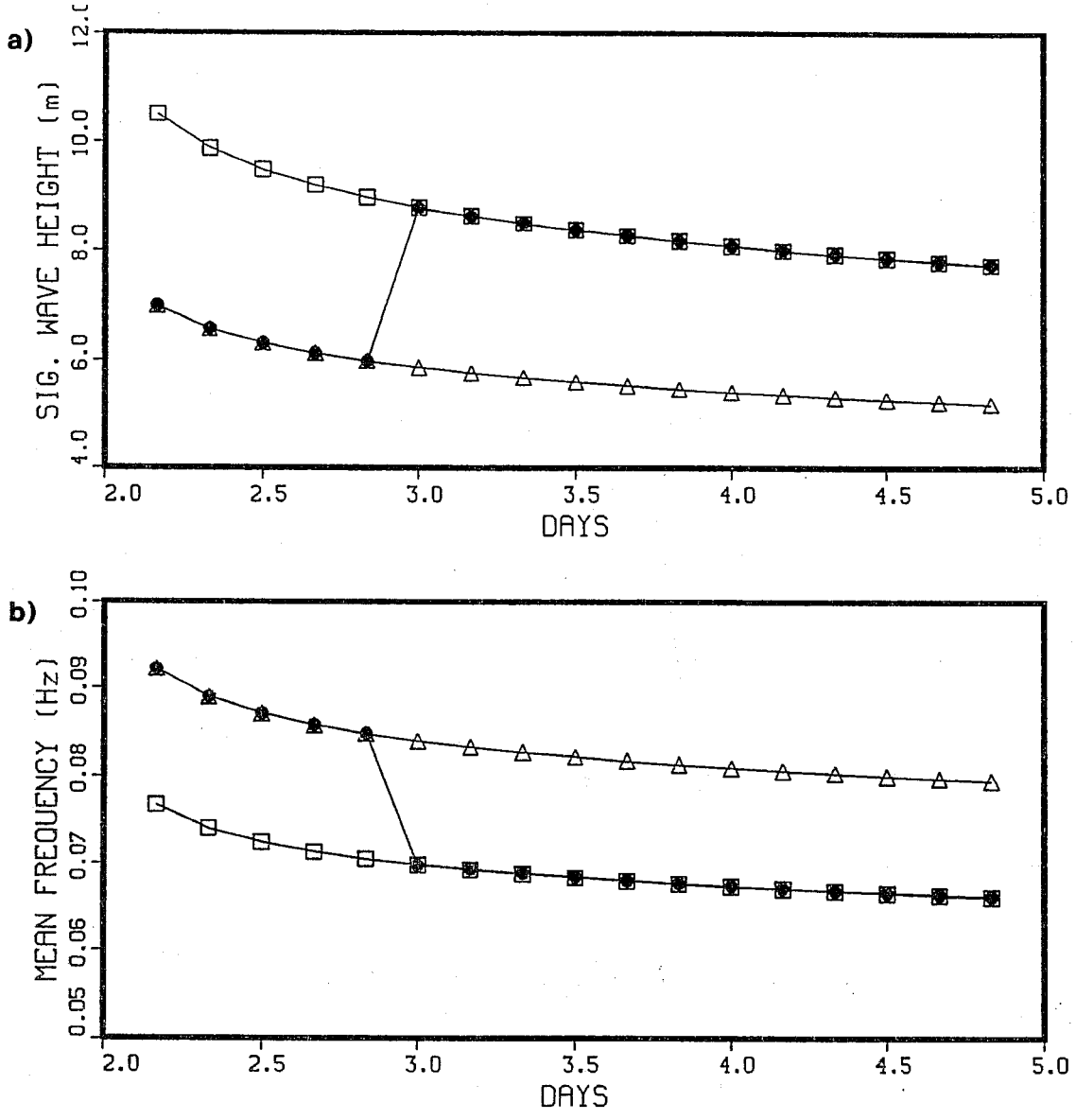

Fig. 4 Time series for case 3.2 (wave decay in absence of wind). a) significant wave height, b) mean frequency. (squares represent the correct prediction, triangles the incorrect prediction, full circles the assimilation run).

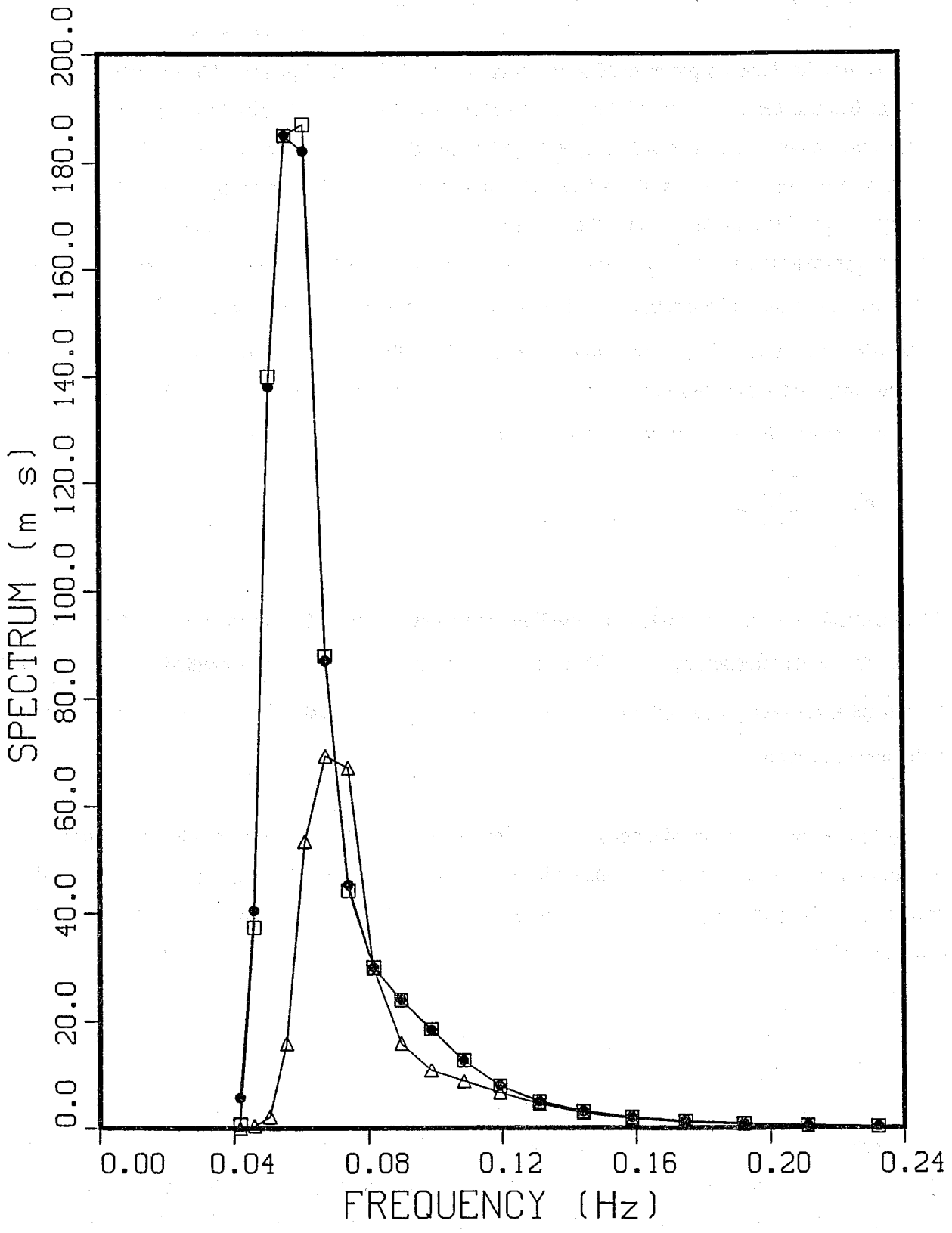

Fig. 5 Spectra at the assimilation time for case 3.2 - wave decay in absence of wind - Squares represent the correct spectrum; triangles the first guess, i.e. the incorrect prediction; full circles the analysed spectrum resulting from the assimilation.

3.3 Spectrum produced by a sudden change in the wind direction

The last case concerns a spectrum evolving under the action of a wind whose direction has changed, producing the simultaneous presence of windsea and swell. The method presented in Appendix A must be changed, because the evaluation of the duration from the total energy is clearly misleading and it will consequently produce an incorrect analysed friction velocity. To produce a reasonable estimate it is necessary to separate windsea, that has been produced by the wind after the change in direction, from the remaining part of the spectrum; only the windsea energy must be used to estimate the duration, which therefore approximates the period of time from the change of the wind direction. The first guess windsea energy E_{Pws} is estimated by locating the windsea peak and computing the energy which has been generated by the wind in an area around it (see *Lionello et al.*, 1991). The assimilation is then carried out as in case A), assuming that the ratio between windsea energy and total energy is the same in the first guess spectrum and in the correct one; the analysed windsea energy E_{Aws} is therefore given as

$$E_{Aws} = \frac{E_A}{E_P} E_{Pws} \tag{21}$$

The numerical experiment is along the same line as the previous ones: The wind blows for three days and then it changes its direction by 90°, without changing intensity. In the correct prediction $u_* = 0.83$ and the first guess has been produced by $u_* = 0.64$. The correct SWH is assimilated half a day after the change in the wind direction.

Figs. 6 a,b,c show how the prediction is corrected by the assimilation. The effect of the assimilation on the two-dimensional spectrum can be evaluated in Figs. 7a, c, d where the first guess spectrum, the analysed spectrum and the correct spectrum are shown respectively. There is a good correspondence between the analysed and the correct spectrum. Fig. 7b shows the part of the first guess spectrum which has been considered windsea.

3.4 Considerations

The reconstruction of the analysed spectrum that is presented here works nicely in these simple cases, but it is expected of course to be less accurate in cases of complicated wind fields; anyway, when the separation of windsea from the remaining part of the spectrum is relatively clear, and the time limited growth curve approximates the model behaviour over a reasonable interval of time, the results of the windsea assimilation using (14), (15), (16), (17) and (18) are reliable. On the other side, in realistic applications, the variability of the natural environment prevents obtaining the persistency of the benefits that is present in these synthetic cases.

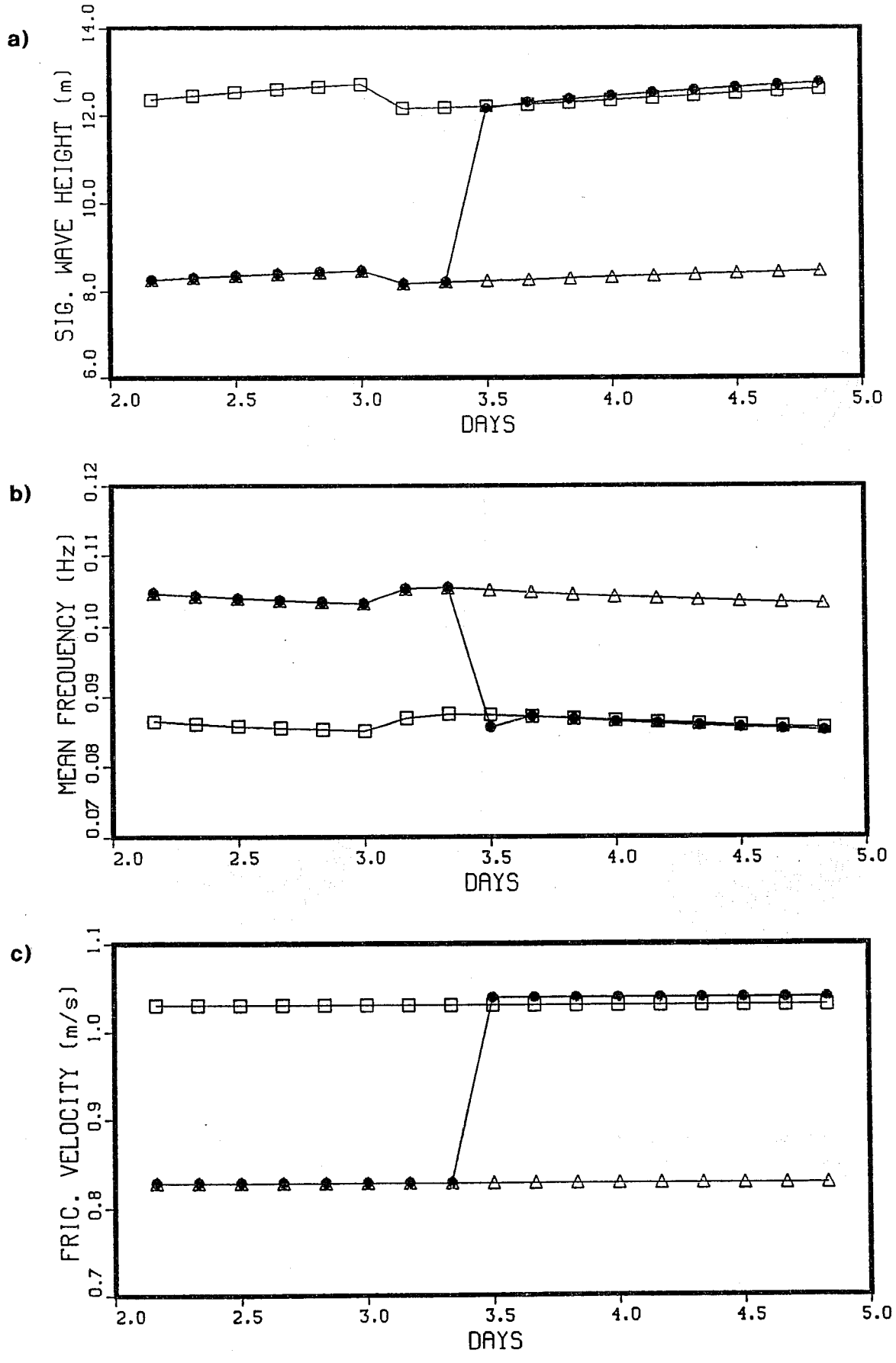

Fig. 6 Time series for case 3.3 --- sudden change in the wind direction --- :a) significant wave height, b) mean frequency, c) friction velocity. (squares represent the correct prediction, triangles the incorrect prediction, full circles the assimilation run).

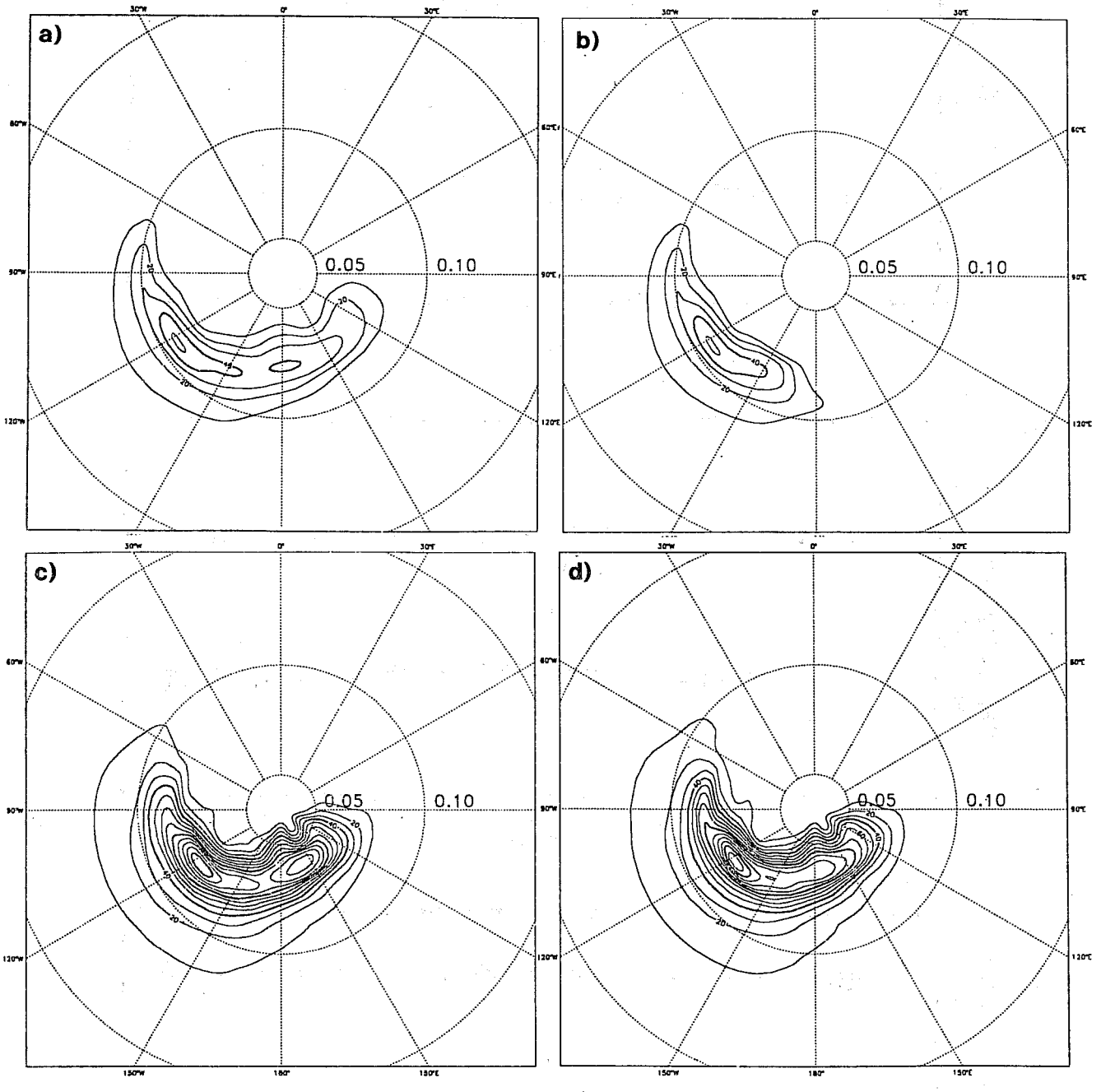

Fig. 7 Two dimensional spectra at the assimilation time for case 3.3 a) first guess spectrum from the incorrect prediction; b) windsea part of the first guess spectrum, c) analysed spectrum, d) correct spectrum.

Numerical experiments on decaying spectra (see *Lionello et al.*, 1991) show that the approach proposed in Appendix B is consistent with the model dynamics over a region around the storm, whose size is comparable to the size of the storm itself. This is because on such a scale, due to the spatial extent of the storm, the spectrum contains a wide range of interacting frequencies, and it has still a quite active dissipation source function. Its extension to a distant region, where, because of dispersion, the components of the spectrum separate in space, is debatable, but it may be supported by the loose argument that, statistically, a higher SWH corresponds to a lower frequency. Anyway if the assimilation is carried out in an operational framework, the continuous updating of the spectra in and around the generation area, is expected to reduce the importance of the updating of the swell in a distant region, unless systematic errors are present in the WAM model. The approach may produce inaccurate results when the interaction of the swell with newly generated windseas or other systems affects the regular decay of the steepness, as observed in this experiment.

Discussing the result of the experiment 3.2), it is natural to ask if this approach has a general validity or it is applicable only to the WAM model. The answer can come only from the study of the decay of the spectrum immediately outside the generation area, where data are now lacking. It is obvious that if the behaviour of the swell spectra in the WAM model is not realistic, the consequent systematic error will not be compensated by this assimilation scheme.

It must be noted however that the steepness of the spectrum is a quantity which must be dynamically relevant: the magnitude of the nonlinear source term S_{nl} is proportional to the square of the steepness

$$S_{nl} \approx \alpha f s^2 F \tag{22}$$

The dissipation source function s_{ds} must moreover be someway depending on the steepness, according to the fact that steep waves are more likely to break than smooth ones. In the WAM model

$$S_{ds} \approx f \left(\frac{f}{f_m}\right)^2 s^2 F$$

Therefore the quasi conservation of the steepness by the assimilation implies that the source function strength is maintained inside a reasonable range, while an increment of the steepness increases the energy dissipation, producing a substantial reduction of the effect of the assimilation (*Lionello and Janssen*, 1990). Although substantial inadequacies in the WAM model physics could make the results of this approach unrealistic, a simultaneous modification of energy and peak frequency is necessary to account for the different peak frequencies of swells which were generated by different wind speeds.

Finally, it is explicitly assumed that the errors in the wind field are mostly due to over or under evaluation, while direction and time behaviour are substantially correct. This is a limitation of the method. Anyway corrections to the stress direction could be considered only if measurements of the wave directional distribution were available, and they could eventually be derived from an estimate of the spectral peak direction produced by SAR.

4. THE EFFECT OF THE ASSIMILATION ON THE FORECAST

This section investigates the effect of the assimilation of real satellite data in the WAM model results. The data that are used were produced by SEASAT from 15 September 12UT 1978 to 17 September 1978 12UT. The period, the satellite data and the wind fields - accurate global wind fields have been made available by *Anderson et al.* (1987) - are the same as in the study by *Janssen et al.* (1989).

A series of experiments was carried out. They have in common a first part, during which the model is spun up for 10 days from 5 September 1978 12UT to 15 September 1978 12UT (spin-up period); the field of spectra at the end of the spin-up period is used as initial condition for the assimilation experiments. The actual assimilation experiments begin at the end of the spin up period, when the data contained in a time window of 12 hours (15/9 12UT to 16/9 00UT) are assimilated in two different time steps, every 6 hours (analysis period). At each time step a field of analysed SWH is produced by O.I. and it is subsequently used to construct the wave spectra; the analysed friction velocity, that has been obtained, is used to drive the wave model, till a new stress field is provided by the atmospheric model (i.e. for the following three hours in the present set up of the WAM model). In the following 1½ days (forecast period) the model is compared with the remaining satellite data which, not having been used in the assimilation, can be used to estimate the impact and the benefit of the assimilation; the degree of agreement between model and observations during the forecast period provides an estimate of the effectiveness of the assimilation. The comparison with a reference run, in which no assimilation has been carried out, allows to study the decay of the effect of the assimilation. The length of the assimilation period has been limited to half a day, in order to analyse the spectrum only once in most of the grid points, providing at the same time a coverage that is good enough to analyse waves over most of the ocean.

This short experiment, the actual length of the model run is only two days, can be performed quite inexpensively, allowing to produce a series of experiments and to obtain an evaluation of the effect of variations in the correlation length L_{max}, and in the root mean square error of the observations σ_O^j. As the method distinguishes between windsea and swell, the eventually different impact of the two distinct contributions and, correspondingly, of the use of (18) or (20) to the assimilation are examined.

Our discussion begins considering the dependence of the results on L_{max}. To this purpose we computed the statistics of the model results against the altimeter measurements. Specifically we discuss here the effect on ***bias*** and root mean square error ***rms*** given by

$$bias = \frac{1}{N_{obs}} \sum_{j=1}^{N_{obs}} h_P^j - h_O^j; \qquad rms = \left\{ \frac{1}{N_{obs}} \sum_{j=1}^{N_{obs}} \left(h_P^j - h_O^j \right)^2 \right\}^{1/2} \tag{23}$$

Figs. 8a and b show respectively the bias and the standard deviation for the whole forecast period as functions of L_{max}, which is expressed in grid units (the grid step is 3°). All the assimilation experiments significantly improve with respect to the reference run (whose ***bias*** and ***rms*** are represented by the continuous line in both the figures). The benefits grow as L_{max} grows; the differences are relevant for low values of L_{max}, but they saturate to a value showing very little dependence on it as L_{max} increases. In our opinion this is the consequence of the separation between adjacent satellite tracks (which is roughly 7 or 8 grid points). Since in half a day the satellite completes almost seven orbits, almost any grid point is updated when L_{max} is larger than 4. A further increase affects the use of the satellite measurements because it compensates interruptions in the series along the tracks and locally it changes the analysed SWH because more observations give their contribution to the interpolation, but the resulting values are not substantially modified.

To investigate how the benefits of the assimilation persist in time the statistics against measurements have been computed every six hours during the forecast period. Results are shown in Figs. 9a and b for various choices of L_{max}. The reduction of the absolute value of the bias with respect to the reference run persists for a long time, a reduction of 25% still being present 1½ days after the end of the assimilation. The reduction of the standard deviation is less prolonged but it is still about 10% one day after the end of the assimilation.

These numerical results indicate that the correlation length L_{max} is larger than 5. This is actually an average over different situations. In fact, windsea has a spatial correlation similar to the spatial extent of the generating storm, which is generally smaller than the spatial correlation of swell.

The results shown in Fig. 8 already indicate that there is not a sensitive dependence on the value of the ratio $R = \sigma_O/\sigma_P$ and in fact differences cannot be considered statistically significant. Fig. 10 shows the time behaviour of the statistics for $L_{max} = 5$ for $R = 0, 1, 2$. The choice $R = 2$ produces the worst results while $R = 0$ and $R = 1$ produce quite similar results. This indicates that the errors in the altimeter are comparable or smaller than the errors in the WAM model.

We now briefly examine the impact of the assimilation, considering the case with $L_{max} = 5$ and $R = 0$. Fig. 11 shows the differences between assimilation and reference at the end of the assimilation period, on 16/9 at 00UT: isolines are plotted every 0.5 m and dots denote areas where the assimilation has reduced the SWH with respect to the reference. Most of the effect of the assimilation is of course in the Southern

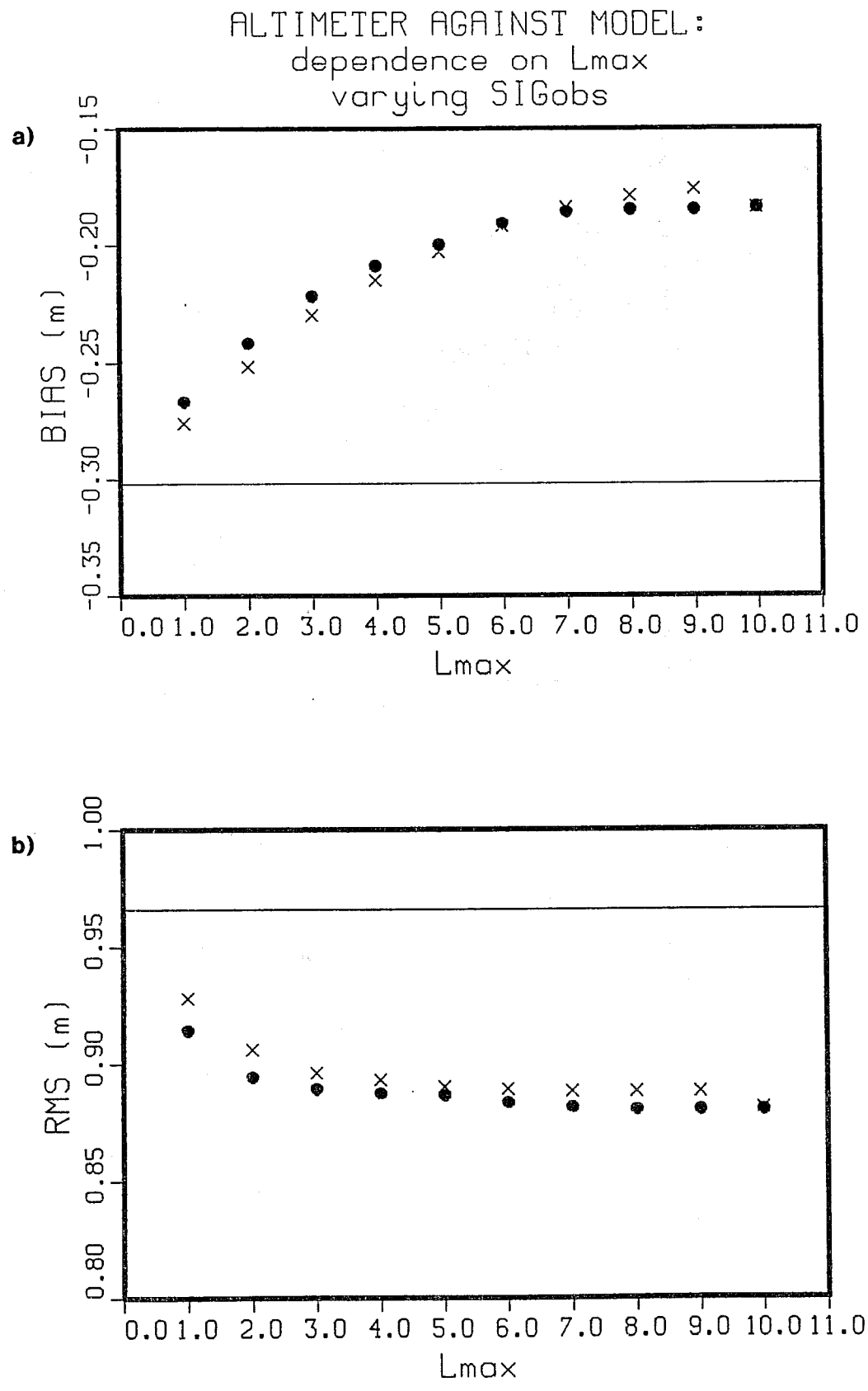

Fig. 8 Statistics of model results against altimeter observations for the whole forecast period: a) bias b) standard deviation. The reference run is represented by the continuous line; dots represent experiments with $R = 0.0$, crosses represent experiments with $R = 1$ $R = \sigma_O / \sigma_P$.

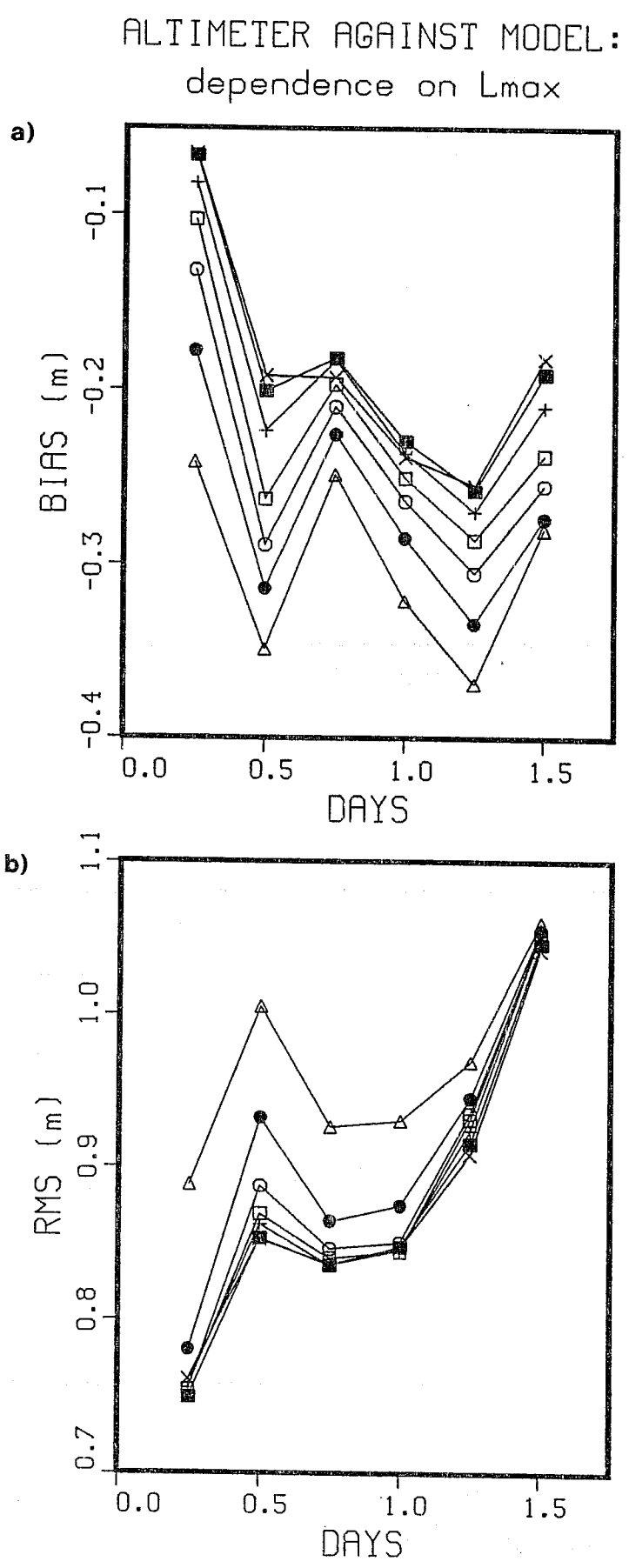

Fig. 9 Statistics of model results against altimeter observations computed every 6 hours during the forecast period: a) bias; b) standard deviation. △ reference, ● $L_{max} = 1$, ○ $L_{max} = 2$, □ $L_{max} = 3$, + $L_{max} = 5$, ■ $L_{max} = 7$, × $L_{max} = 9$.

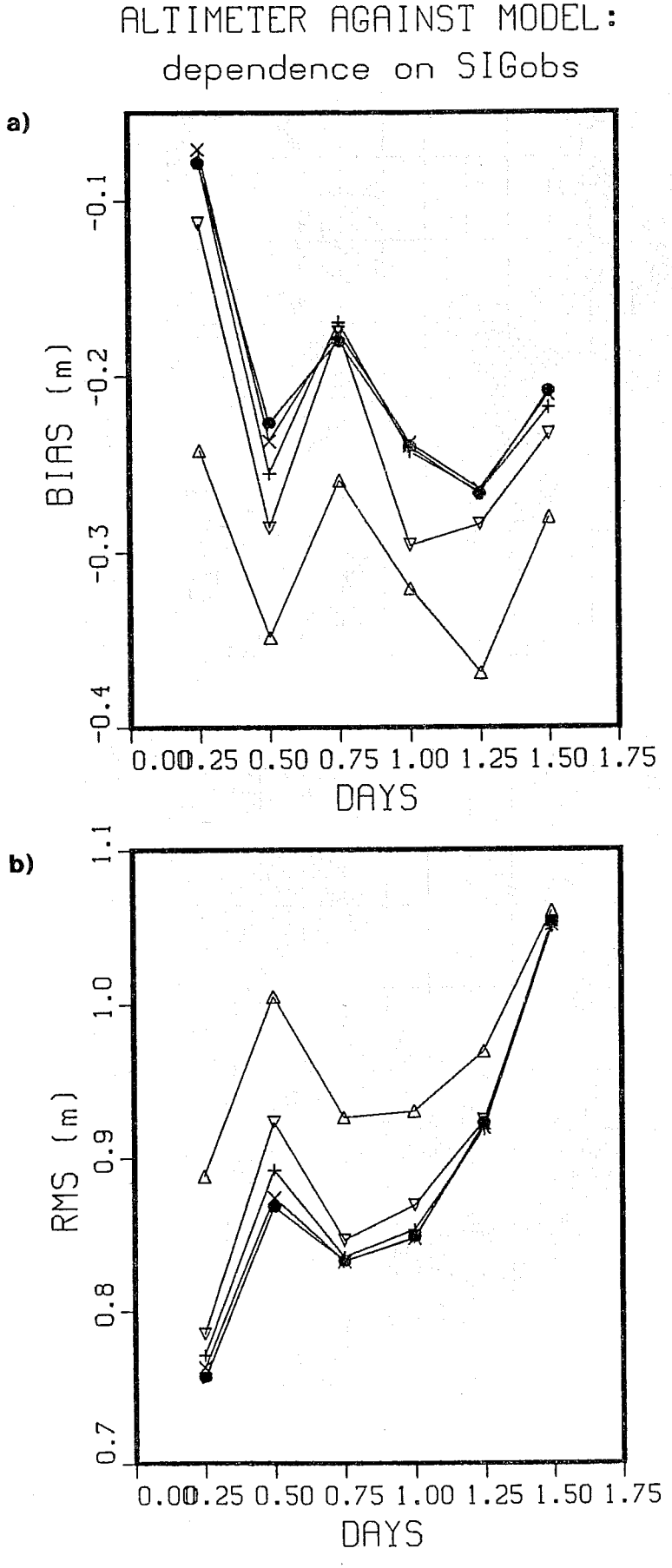

Fig. 10 Statistics of model results against altimeter observations computed every 6 hours during the forecast period: a) bias; b) standard deviation. In all the experiments $L_{max} = 5$. ● $R = 0$, × $R = 1$, ▽ $R = 2$.

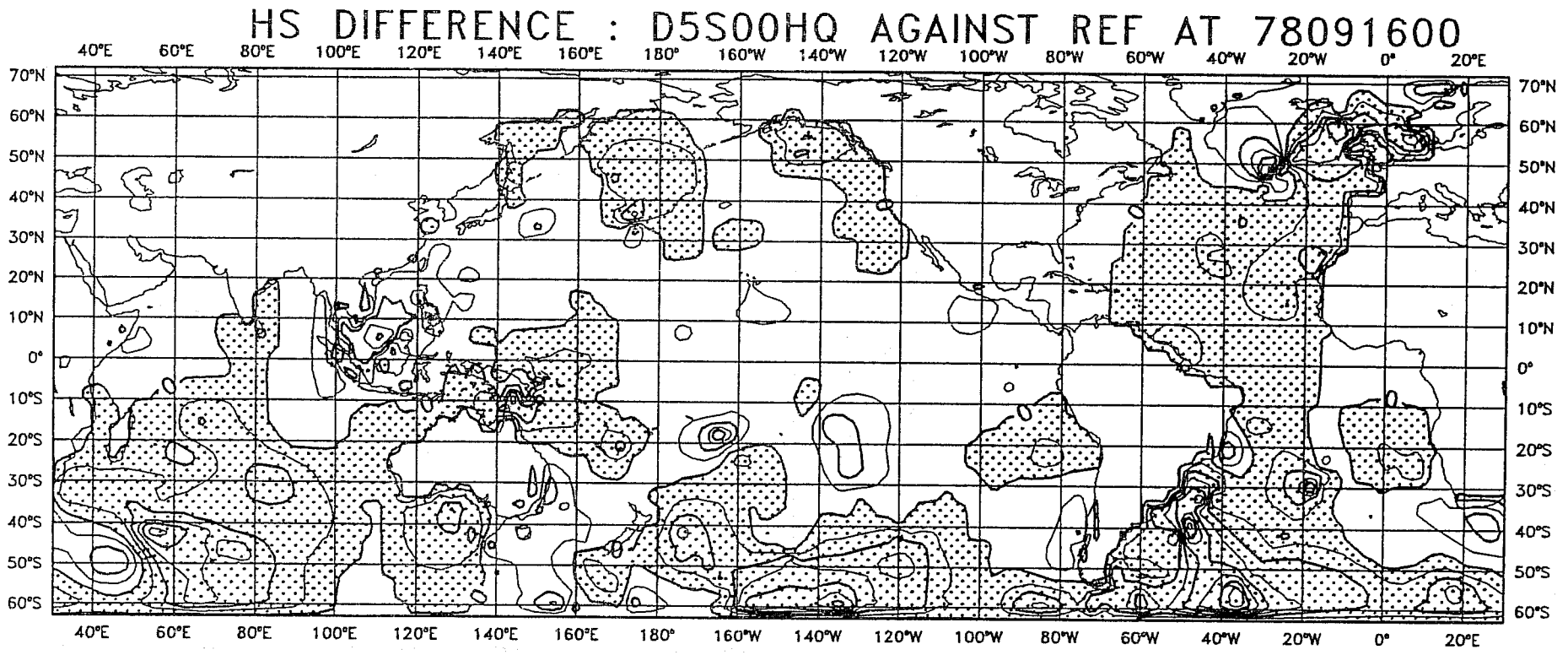

Fig. 11 Differences between assimilation run ($R = 0$, $L_{max} = 5$) and the reference run at the end of the assimilation period. The quantity plotted is $H_A - H_R$; isolines are drawn every 0.5 m; dotted areas indicate negative values.

Hemisphere, on the track of the major storms. The general tendency of the model is to overevaluate with respect to measurements, with the exception of a storm in the Pacific, where the SWH is underevaluated. Since the overevaluation can be clearly distinguished inside the generation areas, it is related to an overevaluation of the wind speed (see Fig. 12). Consequently the swell is generally overevaluated as well. It must be stressed that this is an unlucky situation to obtain large benefits by the assimilation, because, as soon as the assimilation terminates, the action of the wind again produces the growth of the waves, making the decrease of energy not very effective. The opposite case in which the energy of a wave system is increased by the analysis offers more evident benefits, because, at the end of the assimilation, the analysed waves propagate over a field of less energetic waves, losing little energy and determining a persistent feature in the SWH pattern.

Fig. 13 shows what has been left of the differences one day after the end of the assimilation. The pattern is of course much smoother than in Fig. 11, but differences up to 1 m are still present in the Southern Ocean. The individual features tend to move eastward, because of the predominant direction of the waves generated by storms in the Southern Hemisphere. Two updated swell systems, that have been radiated from the mid-latitudes toward the Equator, are present around 170 W, 10 S and 130 W, 18 S. Their origin can be traced back in Fig. 11 at 162 W, 18 S and 129 W, 15 S respectively.

To investigate whether windsea or swell updating is more effective, two experiments were performed analysing only windsea or swell spectra. In the first case, the assimilation was carried out only in the points where, according to the model, most of the spectrum is windsea and using (18); in the second case, only points where most of the spectrum is swell were updated using (20). Of course the windsea is relatively localized on the global scale and this consideration would suggest that the updating of swell could have a much larger impact. Moreover, the swell should have a longer memory. Although supporting these arguments our experiments indicate that the impact of windsea updating is quite comparable to the impact of swell updating. Figs. 14 and 15 show the difference that has been introduced by assimilating swell or windsea respectively with respect to the assimilation run. The swell assimilation determines much wider spread pattern, while the effect of the windsea assimilation is localized in the Southern Ocean, but it is very important in this region. One day after the end of the assimilation, the difference introduced by swell assimilation is slightly larger than the one that was introduced by windsea assimilation (see Figs. 16 and 17) but, because of the large differences, introduced by windsea assimilation in the Southern part of the globe, the impact of the two experiments is quite comparable.

The statistics support the same conclusions. Global statistics (Fig. 18) indicate that updating of windsea and swell have the same importance for the successive forecast. In fact they are important in different regions. Fig. 19 shows the statistics limited to an region around the Equator (i.e. for latitudes between 15° N and 15°)

where the effect of the swell dominates, being responsible for almost the whole improvement obtained by the assimilation. This is of course because the sea state around the Equator is mostly swell radiated by mid-latitude storms. If the statistics are restricted to the Southern part of the globe (i.e. for latitudes south of 15° S) then the effect of windsea analysis is more important because of the many present storms inside which the waves were overvaluated (see Fig. 20). These results indicate that a data assimilation approach should not be limited to the analysis of the windsea, but methods should analyse also swell to be successful on a global scale.

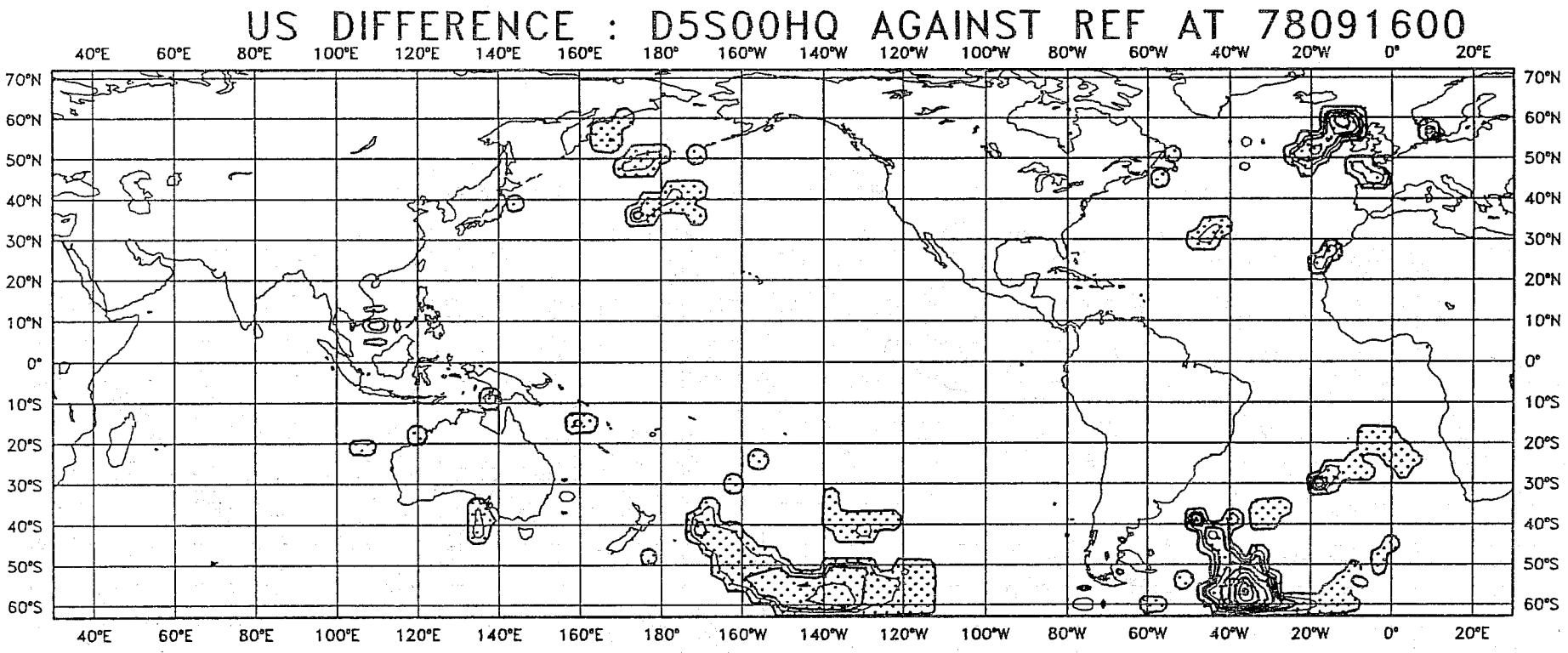

Fig. 12 Differences between assimilation run *(R = 0, L_{max} = 5)* and the reference run at the end of the assimilation period. The quantity plotted is $H_A - H_R$; isolines are drawn every 0.05 m/s: dotted areas indicate negative values.

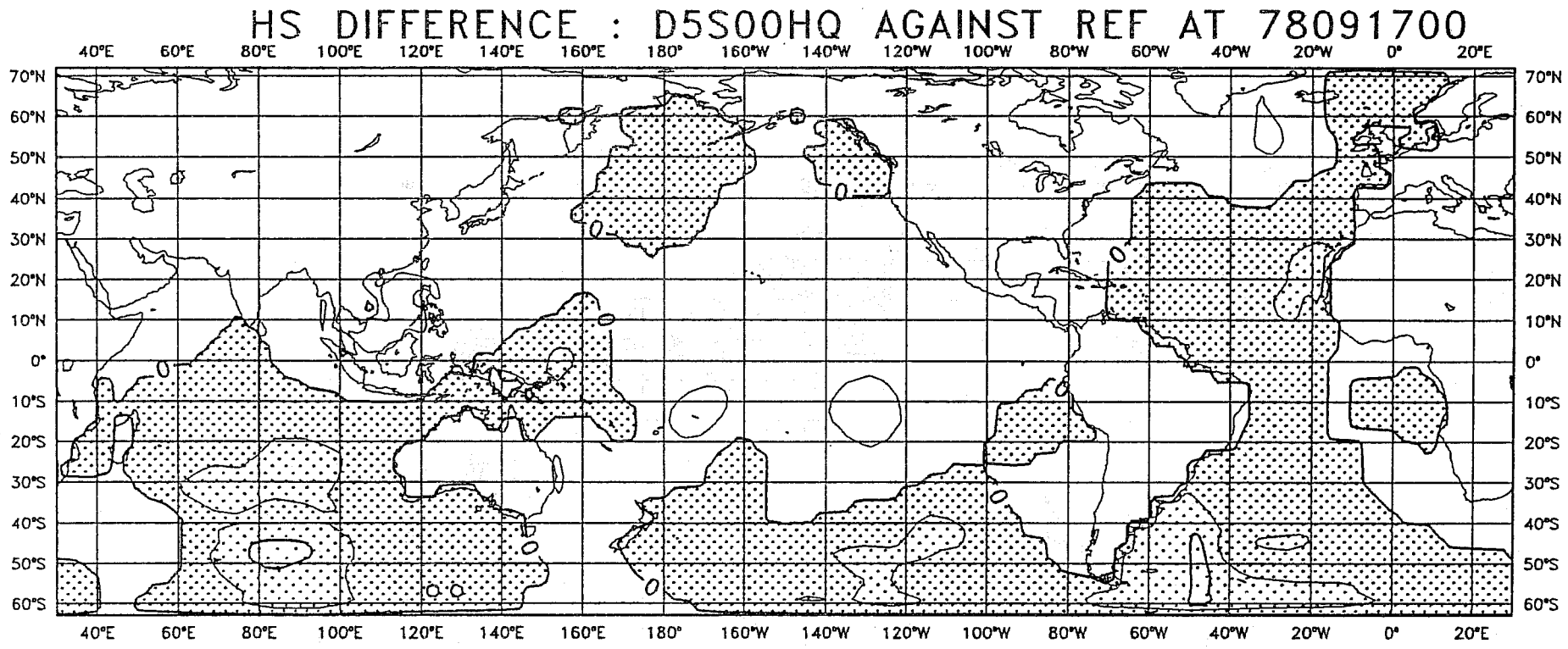

Fig. 13 Differences between assimilation run *(R = 0, L_{max} = 5)* and the reference run one day after the end of the assimilation period. The quantity plotted is H_A - H_R; isolines are drawn every 0.5 m. Dotted areas indicate negative values.

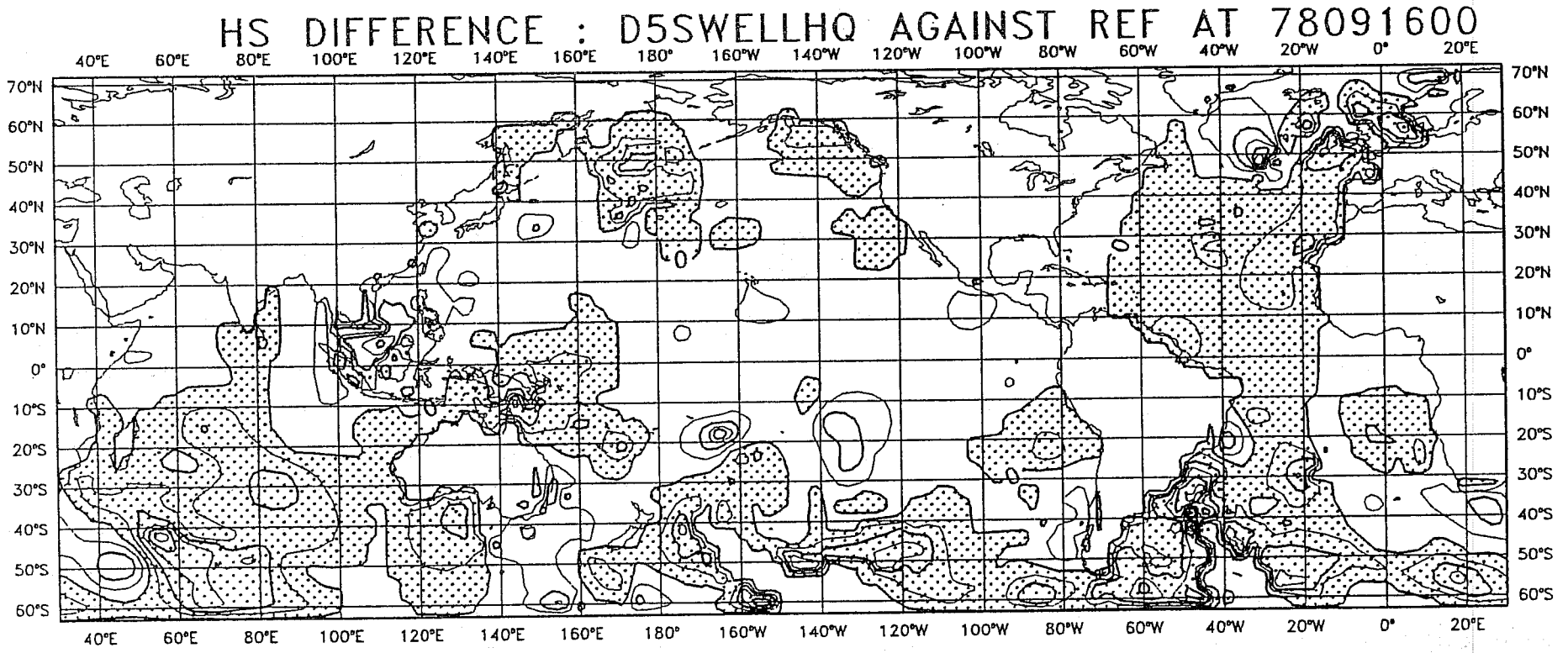

Fig. 14 Differences between swell assimilation run *(R = 0, L_{max} = 5)* and the reference at the end of the assimilation period. The quantity plotted is H_A - H_R; isolines are drawn every 0.5 m. Dotted areas indicate negative values.

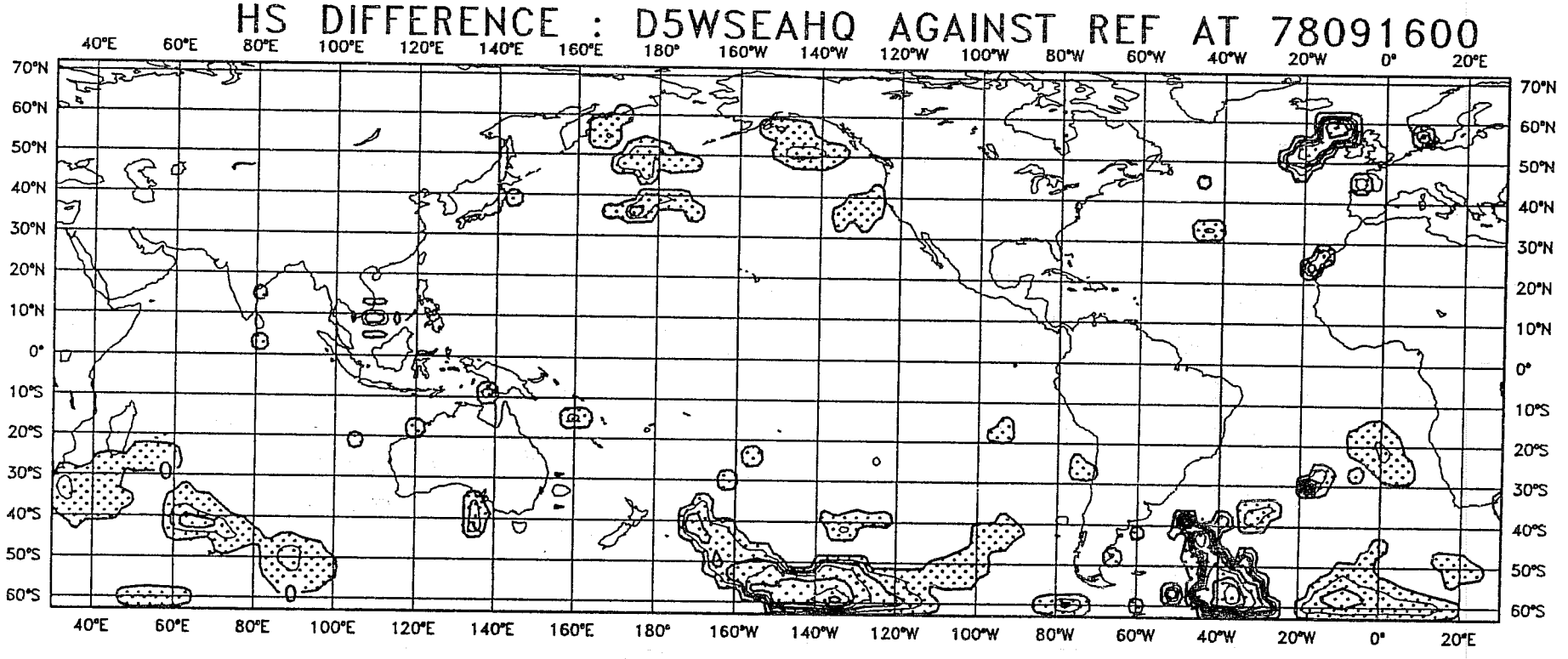

Fig. 15 Differences between windsea assimilation run *(R = 0, L_{max} = 5)* and the reference at the end of the assimilation period. The quantity plotted is H_A - H_R; isolines are drawn every 0.5 m. Dotted areas indicate negative values.

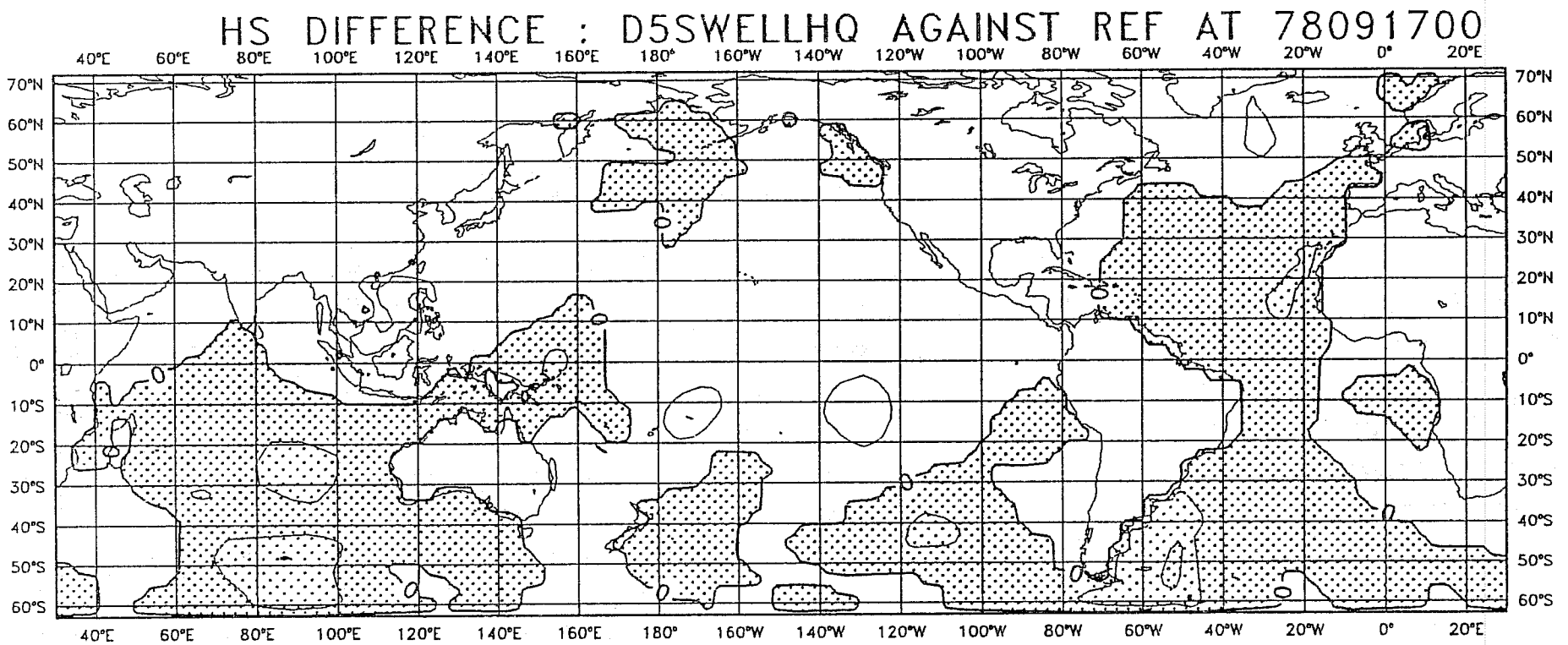

Fig. 16 Differences between swell assimilation run *(R =0, L_{max} = 5)* and the reference one day after the end of the assimilation period. The quantity plotted is H_A - H_R; isolines are drawn every 0.5 m. Dotted areas indicate negative values.

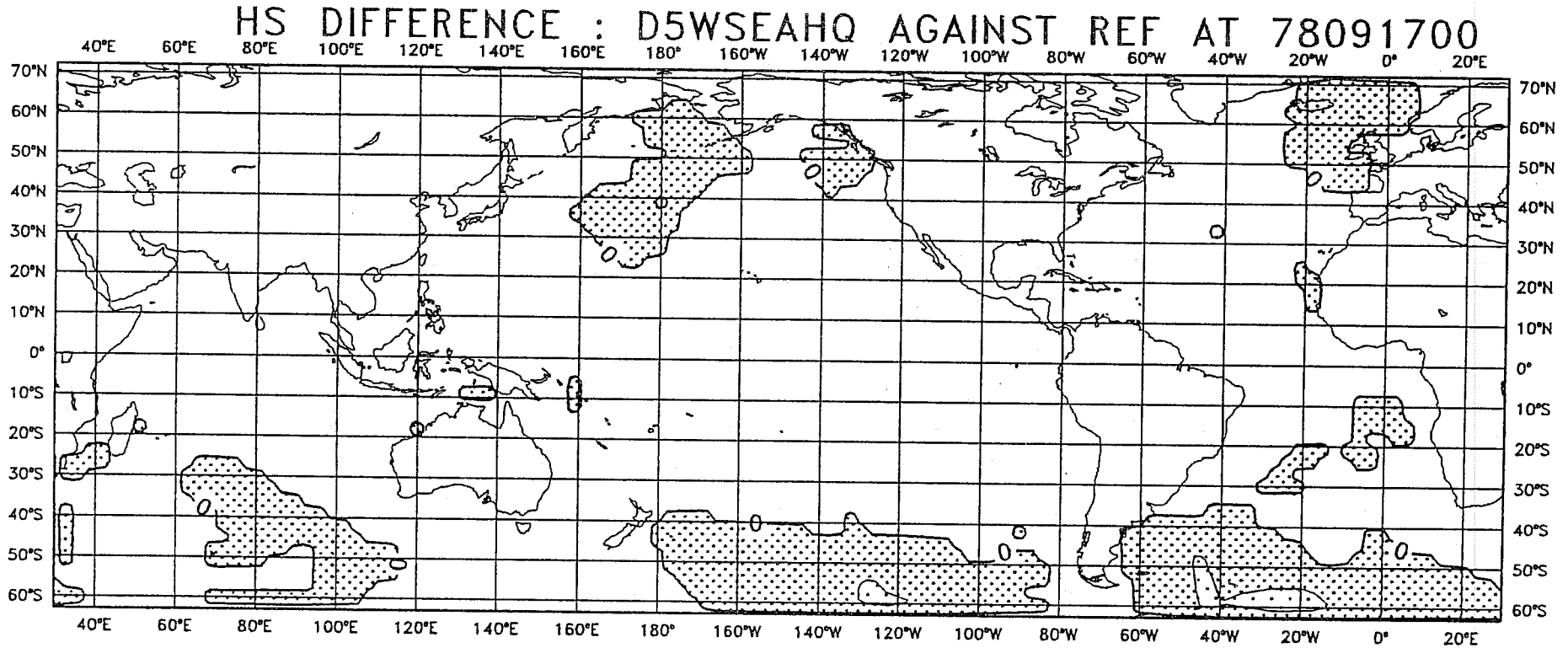

Fig. 17 Differences between windsea assimilation run *(R =0, L_{max} = 5)* and the reference one day after the end of the assimilation period. The quantity plotted is H_A - H_R; isolines are drawn every 0.5 m. Dotted areas indicate negative values.

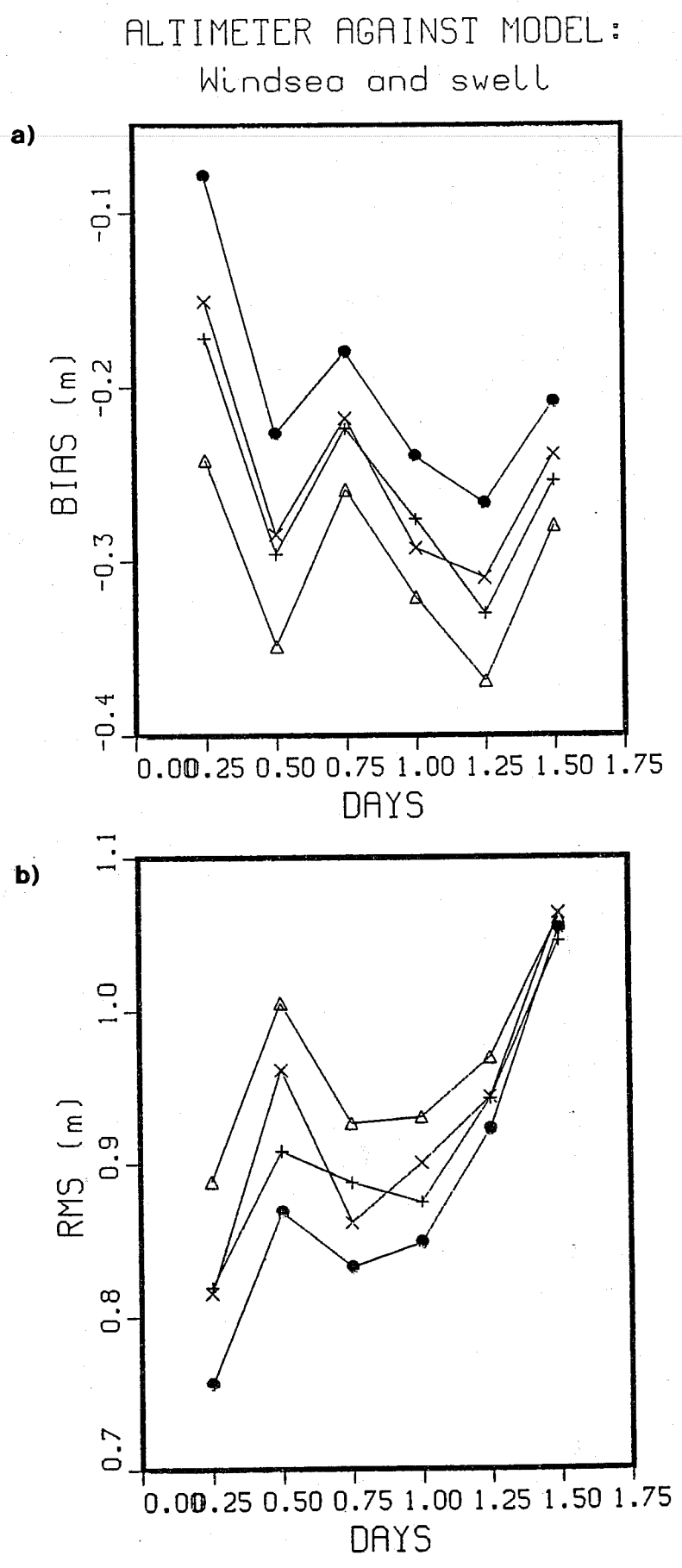

Fig. 18 Global statistics of model results against altimeter observations computed every 6 hours during the forecast period ($L_{max} = 5$; $R = 0$). a) bias, b) standard deviation. Triangle reference run, times only swell assimilation, + only windsea assimilation, bigcirc complete assimilation.

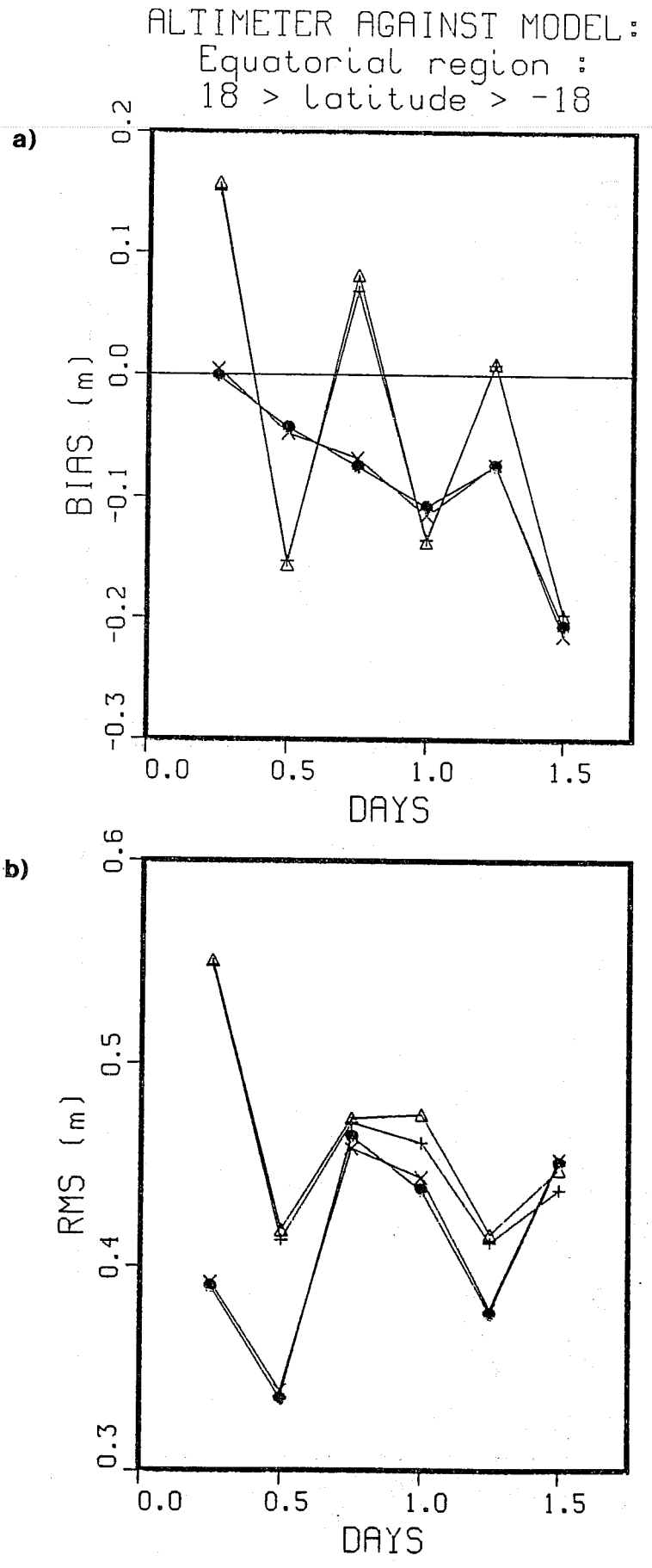

Fig. 19 Statistics of model results against altimeter observations computed every 6 hours during the forecast period for the Equatorial region ($L_{max} = 5$; $R = 0$). a) bias, b) standard deviation. Triangle reference run, times only swell assimilation, + only windsea assimilation, bigcirc complete assimilation.

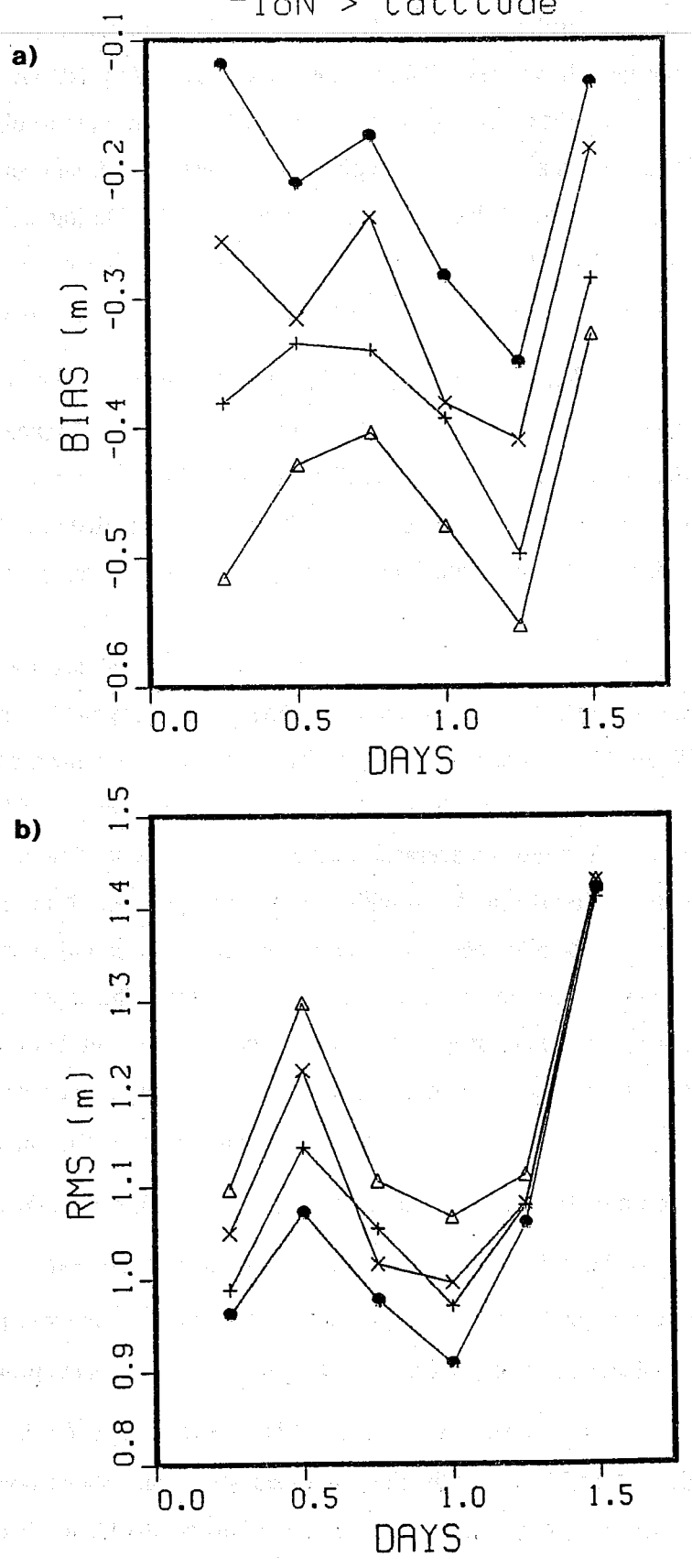

Fig. 20 Statistics of model results against altimeter observations computed every 6 hours during the forecast period for the Southern part of the oceans. a) bias b) standard deviation. Triangle reference run, times only swell assimilation, + only windsea assimilation, bigcirc complete assimilation.

5. VERIFICATION OF THE ANALYSIS AGAINST BUOY OBSERVATIONS

In this section we compare the results of the analysis, performed using altimeter data, with buoy measurements, which are not used in the assimilation. Data are provided by NOAA buoys, that have actually already been used to verify the model results (*Zambresky*, 1988). In order to obtain an extensive set of data for the comparison, the assimilation of wave observations was carried out every six hours in the last ten days of November 1988 (from the 20th at 18UT to the 30th at 24UT). During this period the WAM model was driven by the analysed wind fields produced by the ECMWF atmospheric circulation model. Four experiments were carried out choosing different combinations of the parameters in the O.I.: $L_{max} = 3$ and $R = 0$; $L_{max} = 3$ and $R = 1$; $L_{max} = 5$ and $R = 0$; $L_{max} = 5$ and $R = 1$. The analysed wave data were provided by the altimeter, that was mounted on GEOSAT. In parallel a reference run, without any assimilation, has been carried out for comparison. The discussion involves of course some inspection of specific cases to identify the reasons of the success or of failure of the assimilation. Two relevant and representative situations are discussed, considering buoy measurements at Hawaii and in the Gulf of Alaska.

The area around Hawaii is an interesting location, because the swell that is radiated by the storms in the Northern Hemisphere can be detected. Figs. 21 a-d show the time series of the NOAA buoy 51002 that is located at 17.2 N, 157.8 W, and of the model runs for the four previously mentioned cases. The arrows indicate the time when the spectra are compared in the following Fig. 22. The buoy significant wave height is produced every hour, but measurements are averaged over a six-hour time window for a more adequate comparison with model results, which are produced with a six hour output step. Buoy measurements are denoted with crosses, the results of the reference run with triangles and of the assimilation experiment with full circles. The nearest grid point of the model is taken for the comparison. The impact of the assimilation is clearly positive: a series of relevant wave systems, missing in the reference run, but present in the buoy record, have been detected by the satellite. The improvements corresponding to the satellite passages can be clearly distinguished in the time series in Fig. 21. The differences between the choice $L_{max} = 3$ and $L_{max} = 5$ is caused by use of more distant satellite tracks in the latter case, allowing to update the spectrum a larger number of time at the buoy location. The better results have been obtained with $L_{max} = 5$, indicating a large spatial correlation in the wave field, probably associated with a massive presence of swell. This confirms the trend in the dependence of the results on L_{max} that was found in the previous section (see Fig. 8. The magnitude of the corrections depends on R and it is of course larger for $R = 0$. In this case this is always the best choice. The table reports the time series statistics which shows how the assimilation improves the model results with respect to the reference run, the best results having been obtained using $L_{max} = 5$, $R = 0$. Note that the effect of the assimilation is irrelevant for some periods; this is because

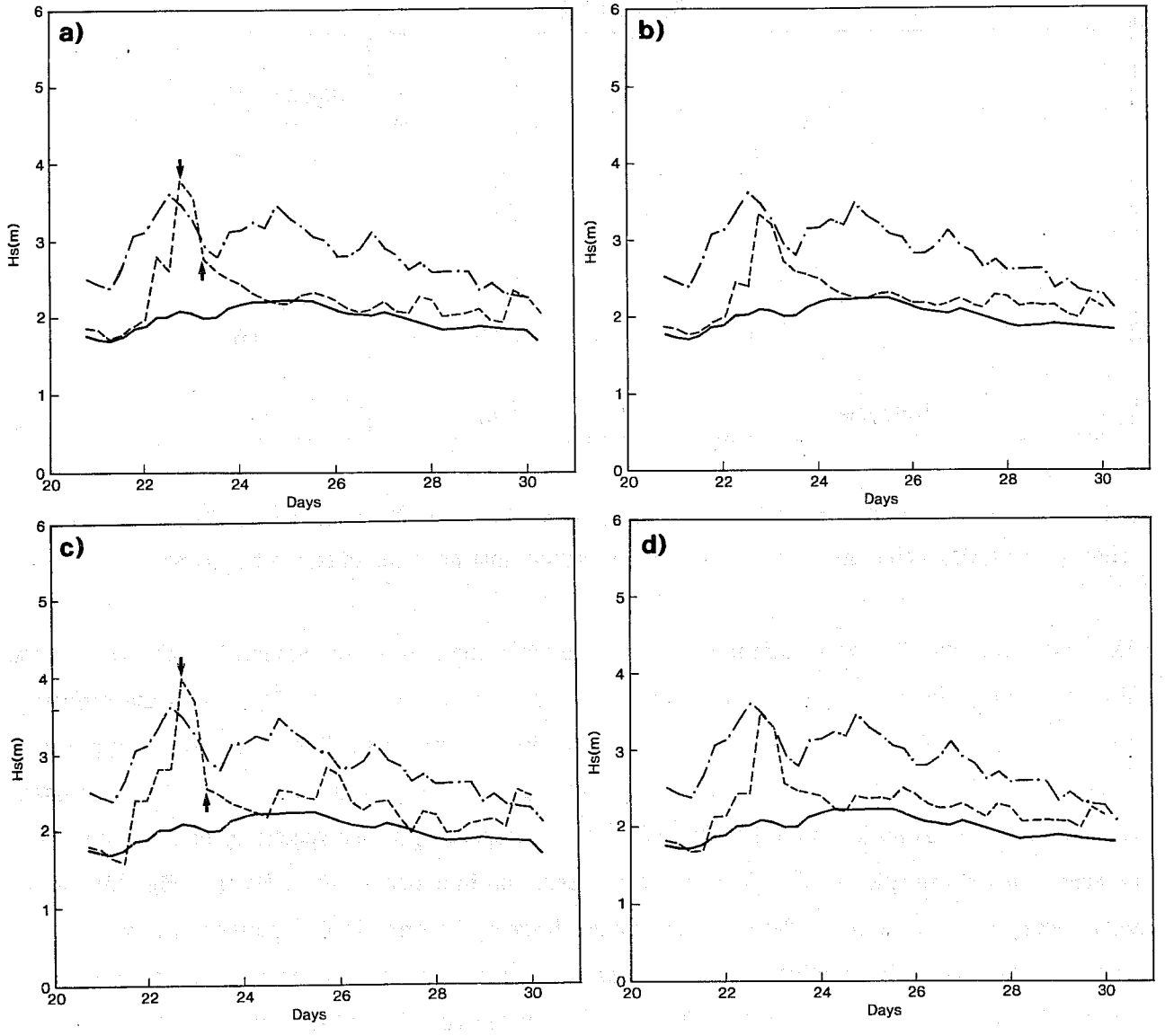

Fig. 21 SWH time series at buoy 51002 —·— buoy measurements; — reference experiment; --- assimilation experiments. In each figure a different data assimilation experiment is shown: a) $L_{max} = 3$; $R = 0$, b) $L_{max} = 3$; $R = 1$, c) $L_{max} = 5$; $R = 0$, d) $L_{max} = 5$; $R = 1$,

of the presence of unreliable spikes in the data close to the buoy location, which prevented the use of data in part of the satellite tracks.

Buoy 51002			
R	L_{max}	Bias	Standard Deviation
0	3	0.60	0.71
1	3	0.63	0.71
0	5	0.52	0.63
1	5	0.59	0.67
Reference		0.87	0.91

Figs. 22 a and b show the 1-dimensional buoy spectra and the model spectra in correspondence to two relevant cases, producing an example of the improvement that has been obtained by the assimilation.

The next two figures 23 and 24 aim to show the situation at the time of the previously compared spectra. The upper large figure shows the wave field in the reference run, and the lower one the difference introduced by the assimilation. In both the figures the line shows the satellite track. The measurements along the satellite track are reported in the upper right figure, where also the time of the satellite passage is displayed. The assimilation on the 22nd at 18UT, corresponding to the spectra in Fig. 22a, corrects a substantial underevaluation of the SWH in the reference run in a area south of Hawaii (Fig. 23). In the second case, on 23rd at 06UT the effect is smaller, because the error in the reference run was smaller (Fig. 24). Although it is tempting to claim a satisfactory success in this case, examining the results of the assimilation at Hawaii, it must be realised that this is a case of a complicated spectrum (many wave systems are present at the same time) for which the reconstruction of the spectrum is not expected to be accurate. In fact windsea and swell are both modified, while they are not necessarily both wrong.

The results in the Gulf of Alaska are less satisfactory. In fact, at buoy 46002, at 42.5° N 130.4° W, the impact is less relevant than at Hawaii, and it does not always improve the results. Although in correspondence to the major event, taking place from 22 to 25 November, the modification has the correct tendency, it is too small to substantially improve the agreement of model and observations. On the other hand, during the second relevant event, which took place from 28 to 29 November, the assimilation acts in the wrong direction, increasing the negative bias instead of reducing it (see Fig. 25). In the statistics, shown

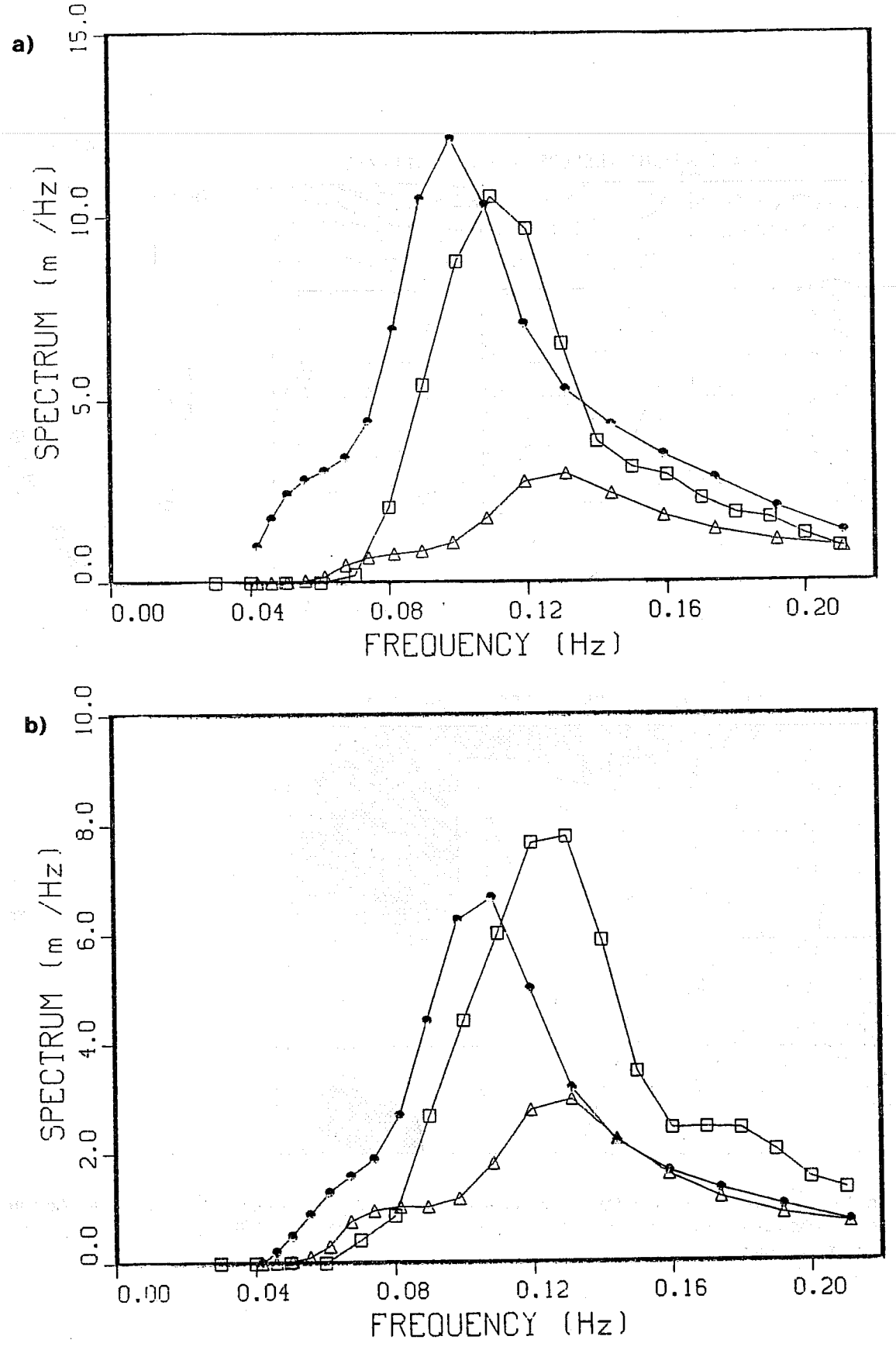

Fig. 22 Spectra at buoy 51002: squares represent the buoy spectrum, triangles the reference and full circles the analysed spectrum $L_{max} = 3$; $R = 0$. a) refers on 22nd at 18UT and b) refers on 23rd at 06UT.

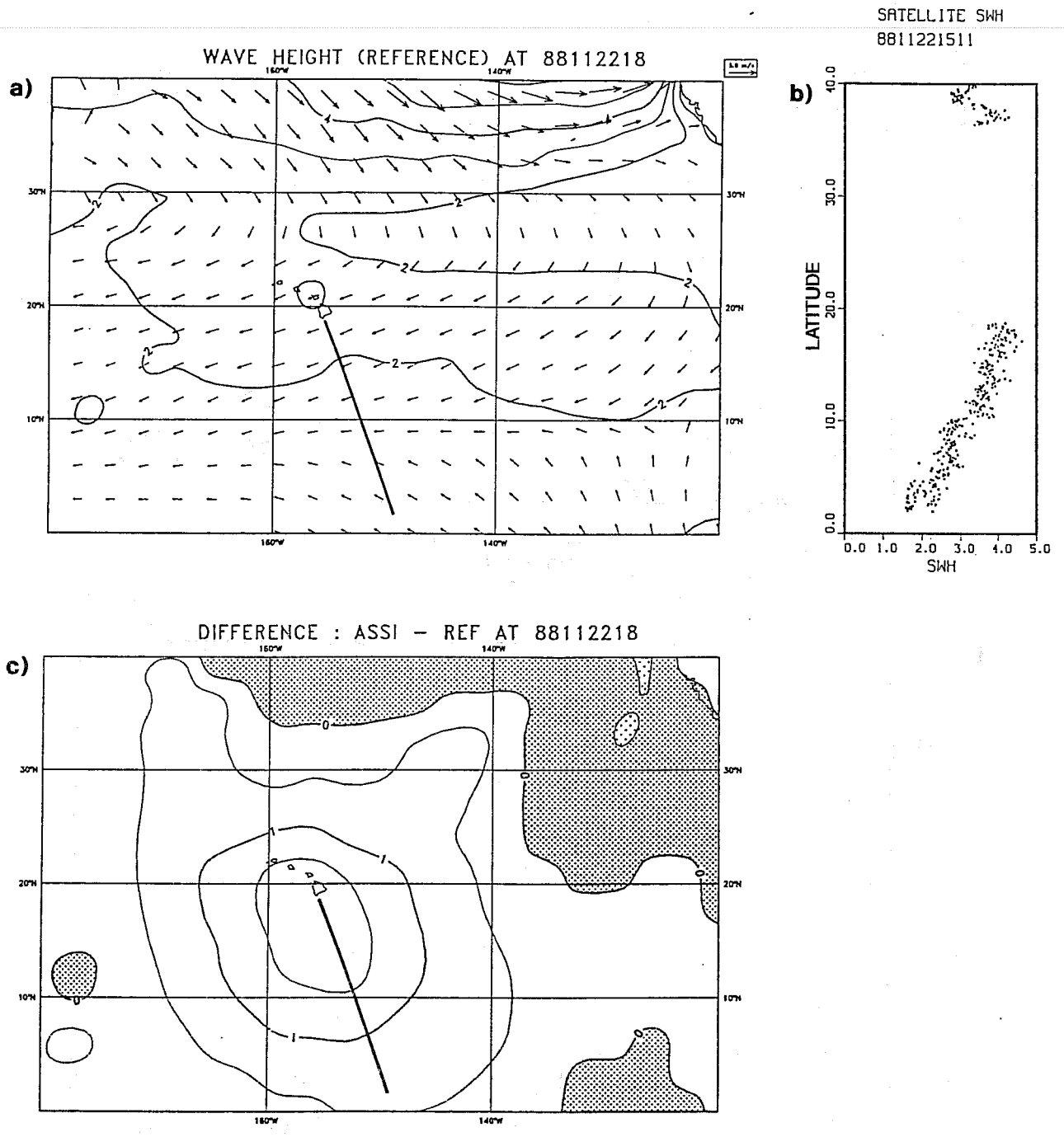

Fig. 23 a) SWH field near Hawaii with the satellite track on 22nd at 18UT. b) altimeter SWH data along the satellite tracks (the approximate time of the passage is displayed in the figure. c) Differences between assimilation run and reference run.

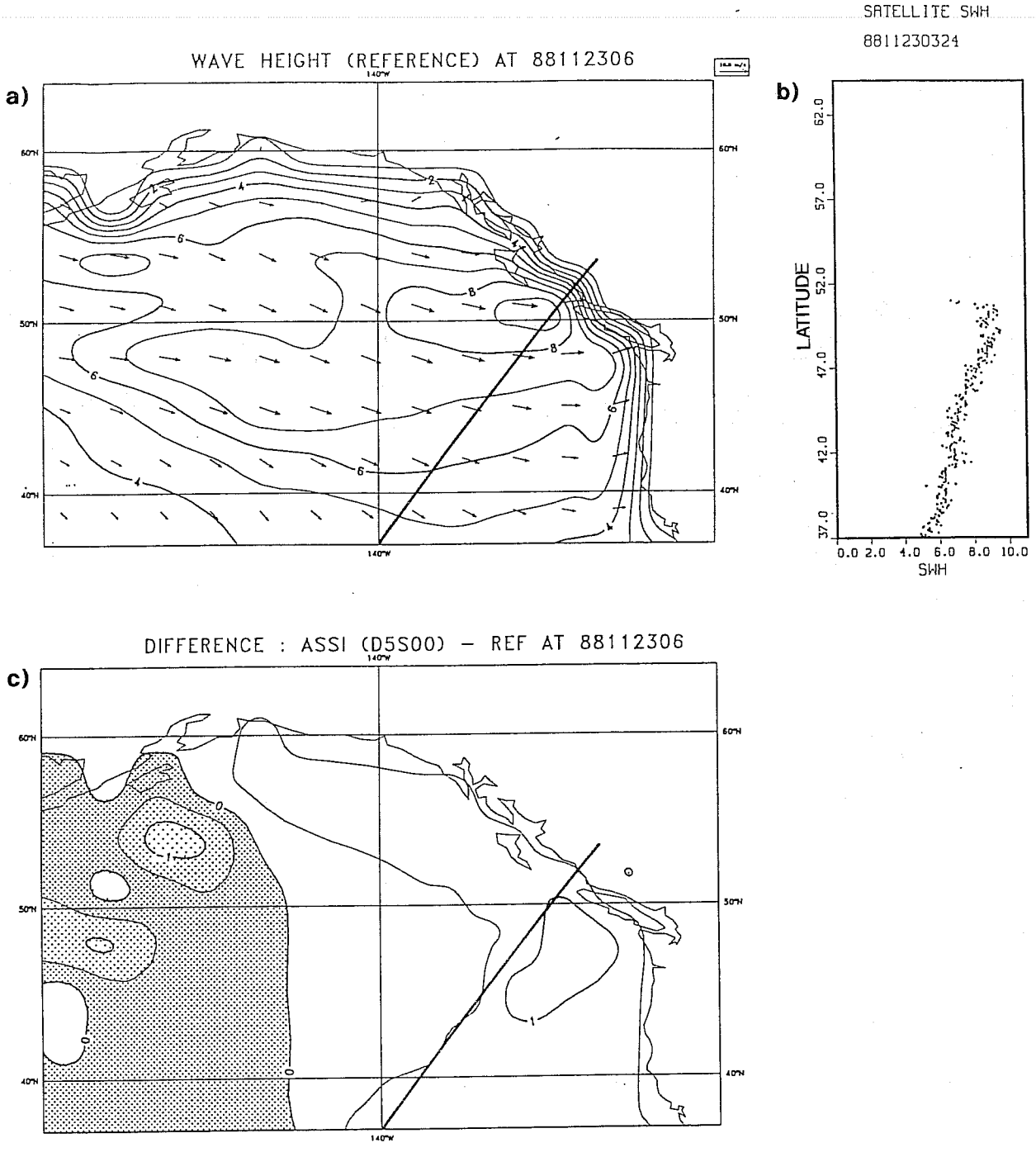

Fig. 24 a) SWH field near Hawaii with the satellite track on 23rd at 06UT. b) altimeter SWH data along the satellite track (the approximate time of the passage is displayed on the figure. c) Differences between assimilation run and reference run.

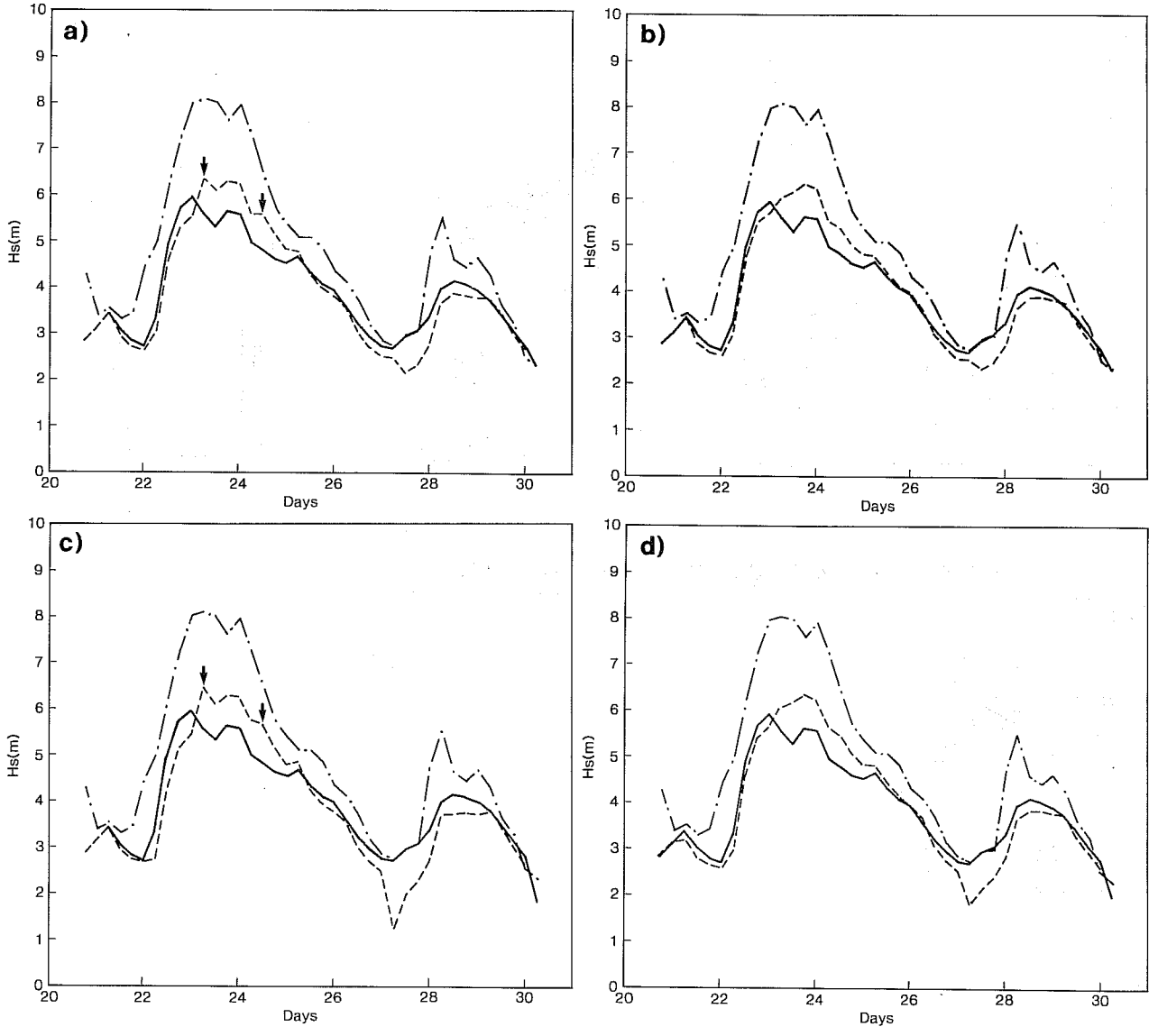

Fig. 25 SWH time series at buoy 46002 —·— buoy measurements; — reference experiment; --- assimilation experiments. In each figure a different data assimilation experiment is shown: a) $L_{max} = 3$; $R = 0$, b) $L_{max} = 3$; $R = 1$, c) $L_{max} = 5$; $R = 0$, d) $L_{max} = 5$; $R = 1$.

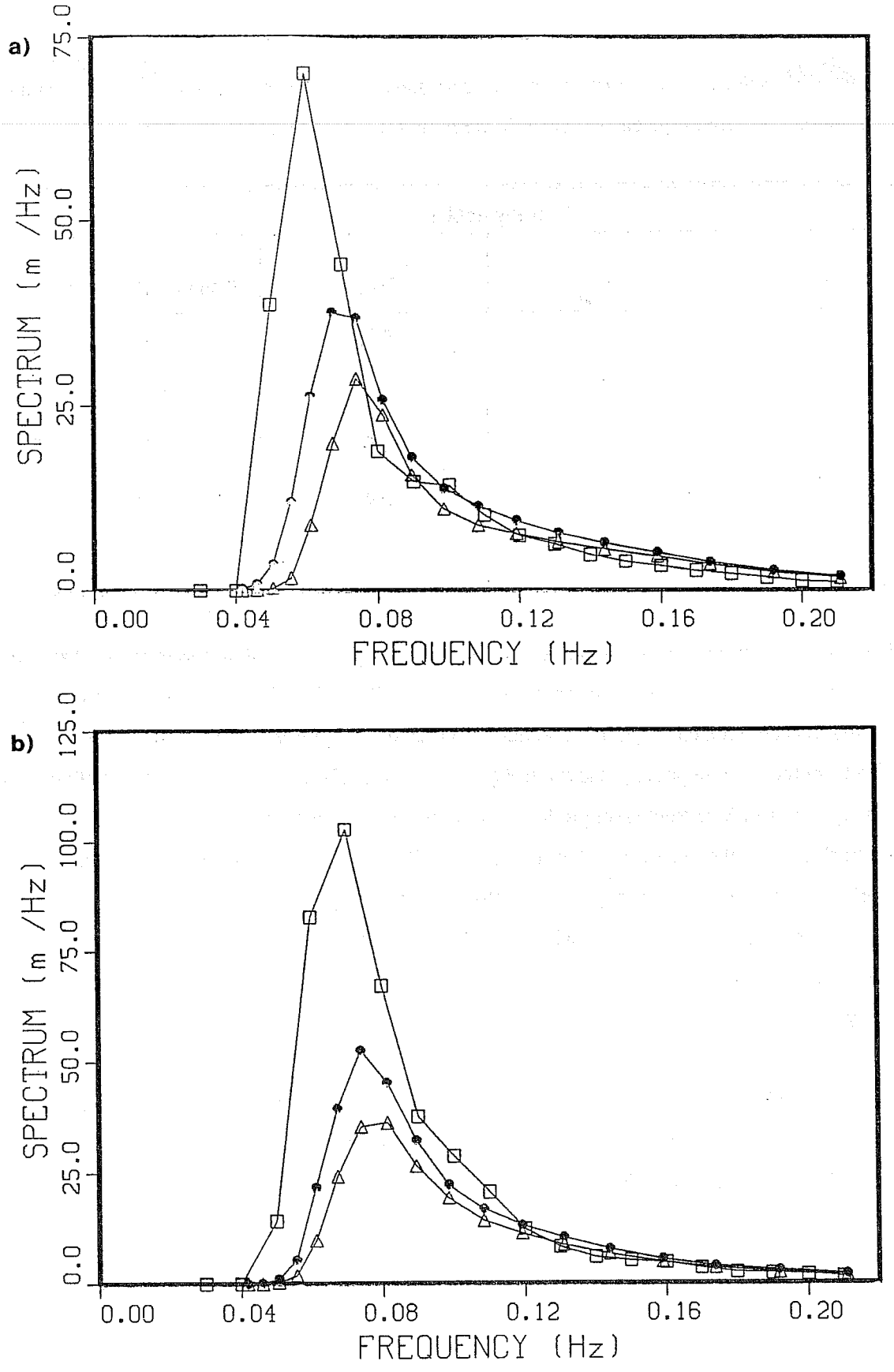

Fig. 26 Spectra at buoy 46002: squares represent the buoy spectrum, triangles the reference and full circles the analysed spectrum ($L_{max} = 5$; $R = 0$). a) refers on 23rd at 06UT and b) refers on 24th at 12UT.

in the following table, the two modifications compensate each other producing very little change in the resulting values. We investigated two specific cases to get a picture of the situation.

Buoy 46002			
R	L_{max}	Bias	Standard Deviation
0	3	0.95	1.17
1	3	0.93	1.14
0	5	1.02	1.23
1	5	0.96	1.16
Reference		0.92	1.22

Consider the situation on 23rd at 06UT, which is shown in Fig. 27. The time series shows that at that time and in the following 24 hours the reference run produced a SWH 2 m. less than the buoy measurement and the assimilation could not compensate it, producing a less than 1 m improvement. The assimilated data were extracted from the satellite passage shown in Fig. 27, which is substantially in agreement with the reference run. Changes in the SWH field were produced more by the symmetric spread of the information across the satellite track than by the measured value themselves. There may be two explanations for the failure of the assimilation: there is an inconsistency between altimeter and buoy measurements (the altimeter being biased low with respect to the buoy), or the real wave field has a strong gradient, which is completely missed by the WAM results, possibly due to local conditions at the buoy location. Both these two factors may eventually contribute.

A successive satellite passage is closer to the buoy than the previous one (see Fig. 28). The reference run in this case produced values 1½ m less than the buoy measurements. Again the assimilation can compensate only partially this discrepancy. This case reinforces the hypothesis that the altimeter is biased low with respect to the buoy. Actually the instrument specification indicates an error of 10% or 0.5 m, whatever the larger, which in this case is in the order of the lacking SWH, but this is not meant to be related to the systematic bias that we may be observing in these cases.

Therefore the data assimilation could not recover the correct value because the extreme waves recorded by the buoys were less energetic in the altimeter measurements. There are indications that this is because of a systematic bias of satellite altimeter and buoy measurements. At Hawaii, where waves were smaller, the problem was not evident; it may be limited only to extreme cases. The other possibility is that local details

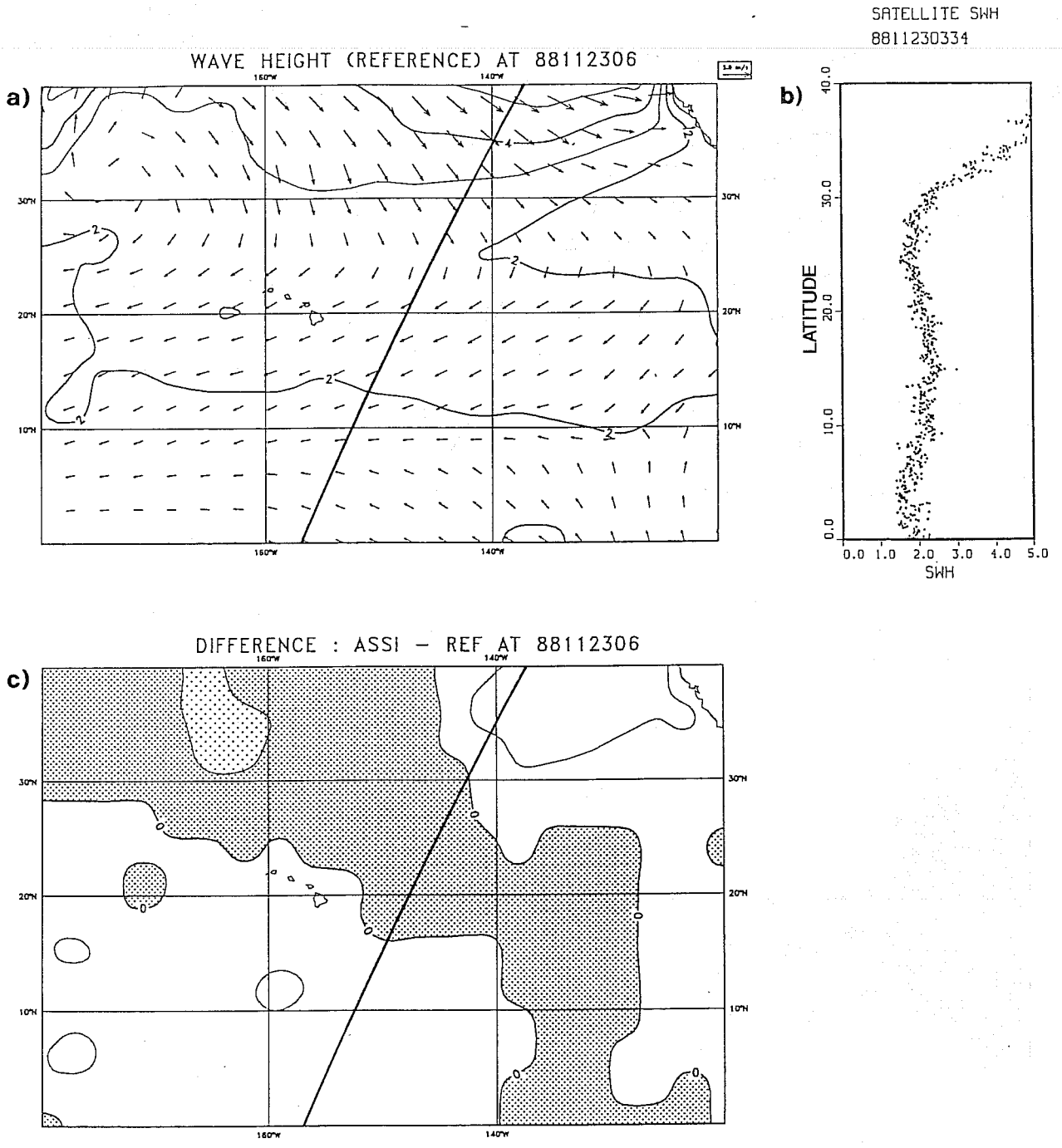

Fig. 27 a) SWH field in the Gulf of Alaska with the satellite track on 23rd at 06UT. b) altimeter SWH data along the satellite track (the approximate time of the passage is displayed in the Figure. c) Differences between assimilation run and reference run.

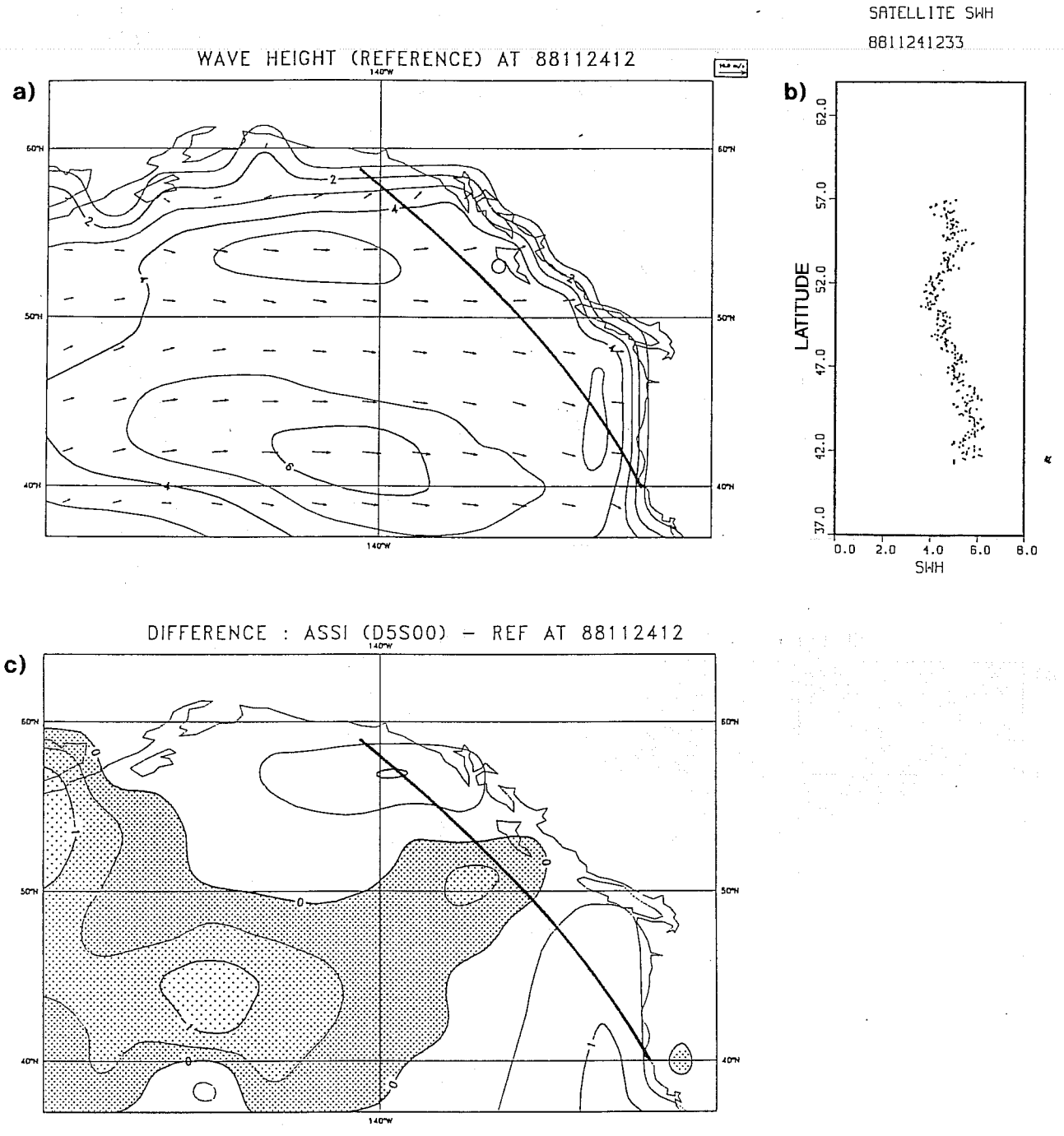

Fig. 28 a) SWH field in the Gulf of Alaska with the satellite track on 24th at 12UT. b) altimeter SWH data along the satellite track (the approximate time of the passage is displayed in the figure. c) Differences between assimilation run and reference run.

have been missed by the satellite passages, and the spread of the information that was obtained by O.I. smoothed them, producing a fake reconstruction of the wave field. Of course the problems may both be present.

Zambresky (1988) already suggested that the WAM model was producing an excessive energy decay on the border of the storms. Examining the results of these experiments we have the same feeling. In fact, at Hawaii a relevant part of the spectrum was presumably swell, and also for the cases in the Gulf of Alaska it is sensible to expect a relevant contribution from waves produced by a distant storm or evolving on the border of the stormy region. In both the cases the WAM model was underpredicting not only with respect to buoys but also to altimeter. This is relatively surprising because it has been shown in the previous section that in the storms SWH was overevaluated and the same conclusion holds in most of the cases also for this experiment. It appears therefore that the energy decay on the border of a storm is excessive in the WAM model, not only compensating the previous overprediction but even determining an underprediction of the wave energy.

6. CONCLUSIONS

With respect to the results of the study by *Janssen et al.* (1989) an improvement has been achieved. In fact benefits are larger and they persist longer. This can be explained by the different approach used to update the swell (see Appendix A and B), by the use of the O.I. to create analysed fields and by the accurate fit to the model growth which improves the evaluation of the surface stress. The benefits are particularly evident from statistics of model results against altimeter data, which show a positive impact of the assimilation.

It appears that analysis of swell and of windsea produce quantitatively comparable benefits. Therefore methods that select only windsea or swell updating are not capable of fully exploiting the satellite data. In fact the improvement due to the updating of swell may have a longer memory than that derived by updating the windsea, but in the presence of large storm systems, which are the most interesting cases, as in the Southern Ocean, the updating of the windsea has a comparable or larger impact.

As anticipated it is obvious that a wave model loses the memory of the correction, because as soon the assimilation stops the forcing tends to erase its effect. In this respect a longer lasting effect can be obtained only if the estimate on the surface stress, derived by analysing the wave field, is used by the analysis in the atmospheric model, having an effect in the wind fields that are successively used.

It must be observed that in many cases the corrections are not dramatic, showing a substantial agreement of WAM model and satellite measurements; consequently no very large modifications of the stress fields are required in most of the cases, but when there is a more substantial disagreement (for instance in the storms in the Southern Ocean during the SEASAT experiment) the analysis of the wave field has a substantial impact on the stress field.

The conclusions from the comparison with the buoy observations are uncertain because of some apparent inconsistency between buoy and altimeter data. In fact, the generally fair agreement of WAM model reference run and altimeter data is surprising because of the many peak events that were recorded by buoys and that were not reproduced by the WAM model. In the cases that we specifically examined, the results suggest that the altimeter did not detect the extreme events recorded by the buoys in the Gulf of Alaska, and their recovery with the assimilation was therefore impossible. Consequently, while at Hawaii both the results presented in sections 4 and 5 show the same dependence on L_{max}, the trend is not confirmed in the Gulf of Alaska.

There are two possible explanations. The first possibility is that for extreme waves the altimeter is systematically biased low with respect to buoys. The second one is that local features, not detected by the

satellite and absent in the WAM model results where present. If this were the case, then the solution would require more data, i.e. eventually more satellites.

The analysis has provided useful indications on the shortcomings of the wave model: in spite of a tendency to overevaluate the windsea, there is a tendency to underevaluate the swell. Some disappointing results may be due to problems in the wave model which cannot propagate adequately an energy initially correctly located in the exact amount. Clearly the assimilation scheme cannot compensate a wrong propagation of the information. Actually the first order propagation scheme that is implemented in the WAM model is likely to produce an excessive diffusion of the wave energy decreasing the effectiveness of the assimilation or misplacing the correction introduced by the assimilation. This could be avoided by using a higher order propagation scheme including an explicit diffusion term (*WAMDI Group*, 1988). An incorrect dissipation source function can be blamed as well. In fact the WAM model dissipation source function has been tuned to reproduce the Pierson Moskowitz spectrum as a final stage of the wave growth. Its extension to the physically completely different situation of the windsea decay is arbitrary, and possibly a different expression should be used in this case. Also this systematic flaw, which cannot be compensated by the assimilation, tends to reduce its effectiveness.

It is clear from this study that the utility of satellite data for wave modelling is not only in the possibility of correcting the model. Because of the wide coverage that they offer, they are a very useful tool to point out the shortcomings of a wave model. This opportunity will be greatly increased by the availability of SAR data and of an efficient algorithm to invert the SAR image. On the other hand, by the cross validation with other data sources, wave models offer the possibility of investigating the weak points of satellite measurements.

ACKNOWLEDGEMENTS

We are indebted to Tony Hollingsworth for discussions during our stay at ECMWF. Liana Zambresky provided us with the data and the software, which she used for a verification study with the WAM model. We thank the GKSS Forschungzentrum for having supplied the GEOSAT data. Finally, the user supporters of ECMWF, Norbert Kreitz and John Greenaway have been a great help.

APPENDICES

APPENDIX A: ASSIMILATION IN CASE OF DECAYING WINDSEA

Wave height measurements provide insufficient information to update the wave spectrum unless extra assumptions on its spectral shape are used. For the wind sea the extra assumptions generally involve the parametrization of the spectrum according to prescribed shapes (*Thomas*, 1988, *Janssen et al.*, 1989) or dimensionless relations of spectral parameters, as in this study (see section 3). Since such a parametrization is not possible for cases with decreasing wind speeds updating the swell spectrum by simple scaling of its energy has become a common choice (*Hasselmann*, 1988; *Janssen et al.*, 1989; *Thomas*, 1988; *Komen*, 1985). We argue that this choice is incorrect, especially when the swell is close to its generation area; the study proposes the relations (18) and (20) and this appendix is devoted to justify them in some detail.

In this study the swell is defined as the part of the spectrum that is not associated with a peak in the wind direction whose frequency is larger than the Pierson-Moskowitz frequency. Consequently, as soon as the wind drops, the spectrum is considered swell, although it is still relatively broad and the source function, not being negligible, still produces a relevant evolution in the sea state. The distinction between windsea and swell is required to determine two different regimes, where different criteria must be used to update the wave spectrum.

The basic flaw of updating the swell energy by simple scaling is that, when the swell is underpredicted, it produces a spectrum where both nonlinear and dissipation source functions are very active, determining a situation which is quite inappropriate for swell. In fact, an increment of the energy without decreasing the peak frequency increases the average steepness of the spectrum; the increment of the average steepness of the spectrum increases the strength of both nonlinear and dissipation source functions, as explained in the third section. The consequence is a quick loss of energy, which strongly reduces the effectiveness of the assimilation. To avoid this inconsistency the steepness is used as a parameter to guide the assimilation when the wind drops. This idea looks particularly suitable to the WAM model.

Fig. 29 shows the evolution of waves for three different values of wind forcing ($u_* = 1.03$, $u_* = 0.83$, $u_* = 0.64$). The steepness of swell spectra, which have been decaying for the same period, is approximately the same, apart from a difference reflecting the original difference in the steepness of the wind-sea spectra from which they were generated (see Fig. 29c). If we assume that the error in the wave field is due to an error in the wind field, Figs. 29a-c imply that discrepancies in the wind produce a strong impact in the SWH and in the peak frequency, but much less impact in the steepness. If a spectrum is updated to compensate an error in the wind field, then the scaling of spectral energy must be combined to a transformation which adjusts the steepness to a sensible value. According to the WAM model dynamics,

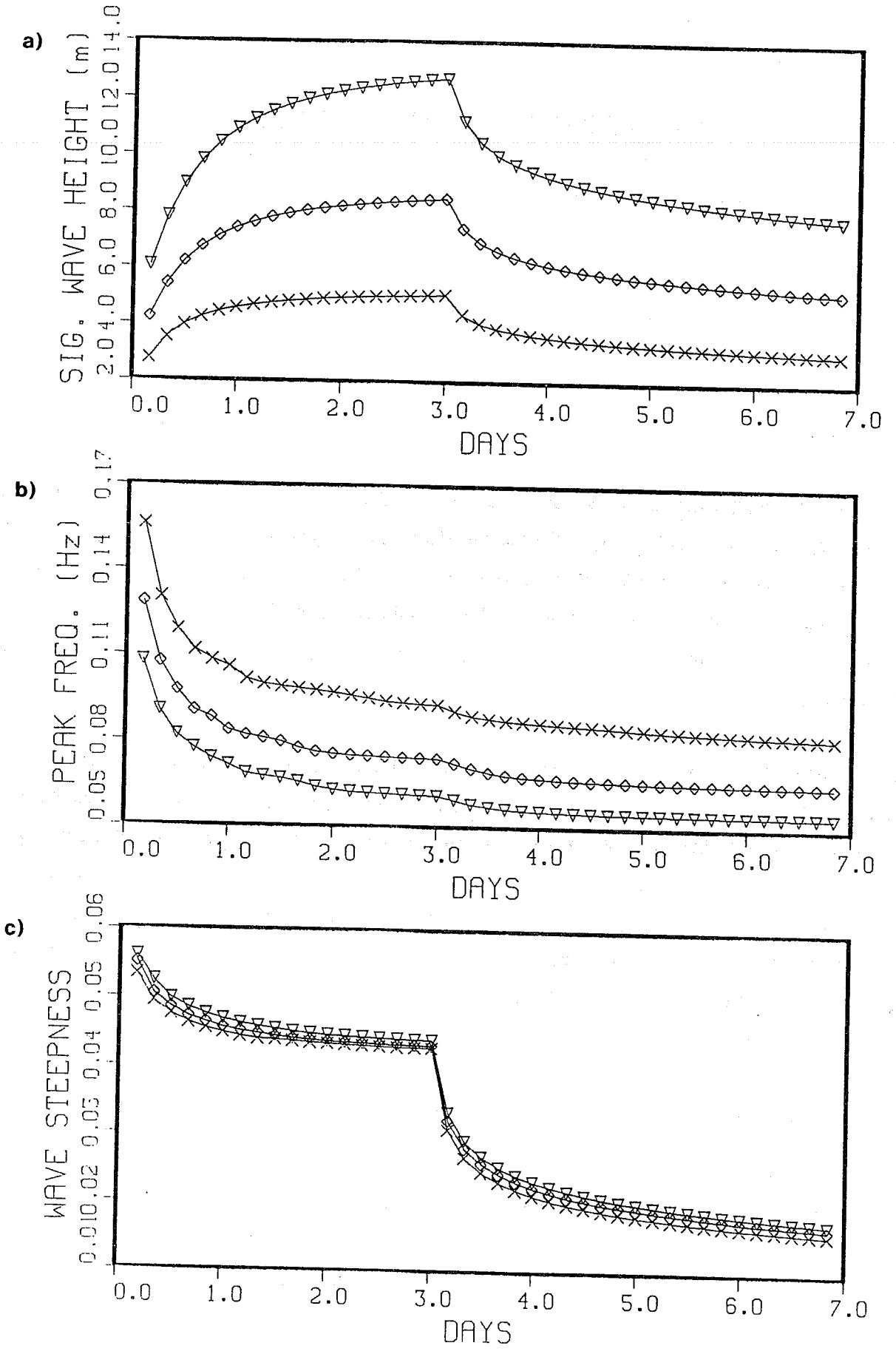

Fig. 29 Time series of wave growth and decay for different values of the friction velocity: a) significant wave height; b) peak frequency; c) average steepness (crosses $u_* = 0.64$, rhombuses $u_* = 0.86$, *reverse triangles* $u_* = 1.03$).

if the energy is increased, or decreased, without changing the peak frequency, the resulting spectrum could not have been produced by a biased wind.

To update the spectrum adjusting its steepness, the analysed spectrum $F_A(f,\theta)$ is derived from the first guess $F_P(f,\theta)$ using (15). If the spectrum is adjusted by simple scaling, then A and B are given as

$$A = \frac{E_A}{E_P}, \qquad B = 1 \tag{24}$$

and, if the steepness was not modified, they are given as

$$A = \frac{E_A}{E_P} B, \qquad B = \left(\frac{E_A}{E_P}\right)^{1/4} \tag{25}$$

Since different values of friction velocity do not actually produce spectra with the same steepness, a small correction to (25) is introduced to take into account such small differences:

$$A = \frac{E_A}{E_P} B, \qquad B = \Delta B \left(\frac{E_A}{E_P}\right) \tag{26}$$

$$\Delta B = 1 - 0.006 \cdot (\sqrt{E_A} - \sqrt{E_P}) \tag{27}$$

This correction is significant only for very large variations of the SWH.

A simple test experiment was set up to evaluate the impact of these considerations on data assimilation. A single point version of the WAM model, simulating an infinite homogeneous ocean, was used to describe the growth of the wave spectrum under the action of the wind (first three days of the experiment) and the subsequent decay when the wind was switched off (second three days). Two parallel runs were performed: an incorrect prediction in which the wind was underestimated ($u_* = 0.86$), represented by triangles in Fig. 30 and a correct prediction where the wind had the correct value ($u_* = 1.03$), represented by squares in Fig. 30. The correct run is used to simulate the truth and supply the wave observations; the incorrect prediction is used to supply the first guess spectrum to be analysed. When the assimilation is carried out, after one day of decay, the first guess spectrum is updated using the value provided by the correct prediction as measurement. The purpose of a correct assimilation process is then to skip from the incorrect prediction to the correct prediction line in Fig. 30. The full dots denote the experiment where (27) is used, while open circles indicate the experiment where (24) is used. The use of (27) gives quite satisfactory results, reproducing the correct significant wave height during the decay of the spectrum following the assimilation; the use of (24) produces the correct value only at the assimilation time itself, the energy being later quickly dissipated as expected from the previously presented arguments. The differences in the results are even

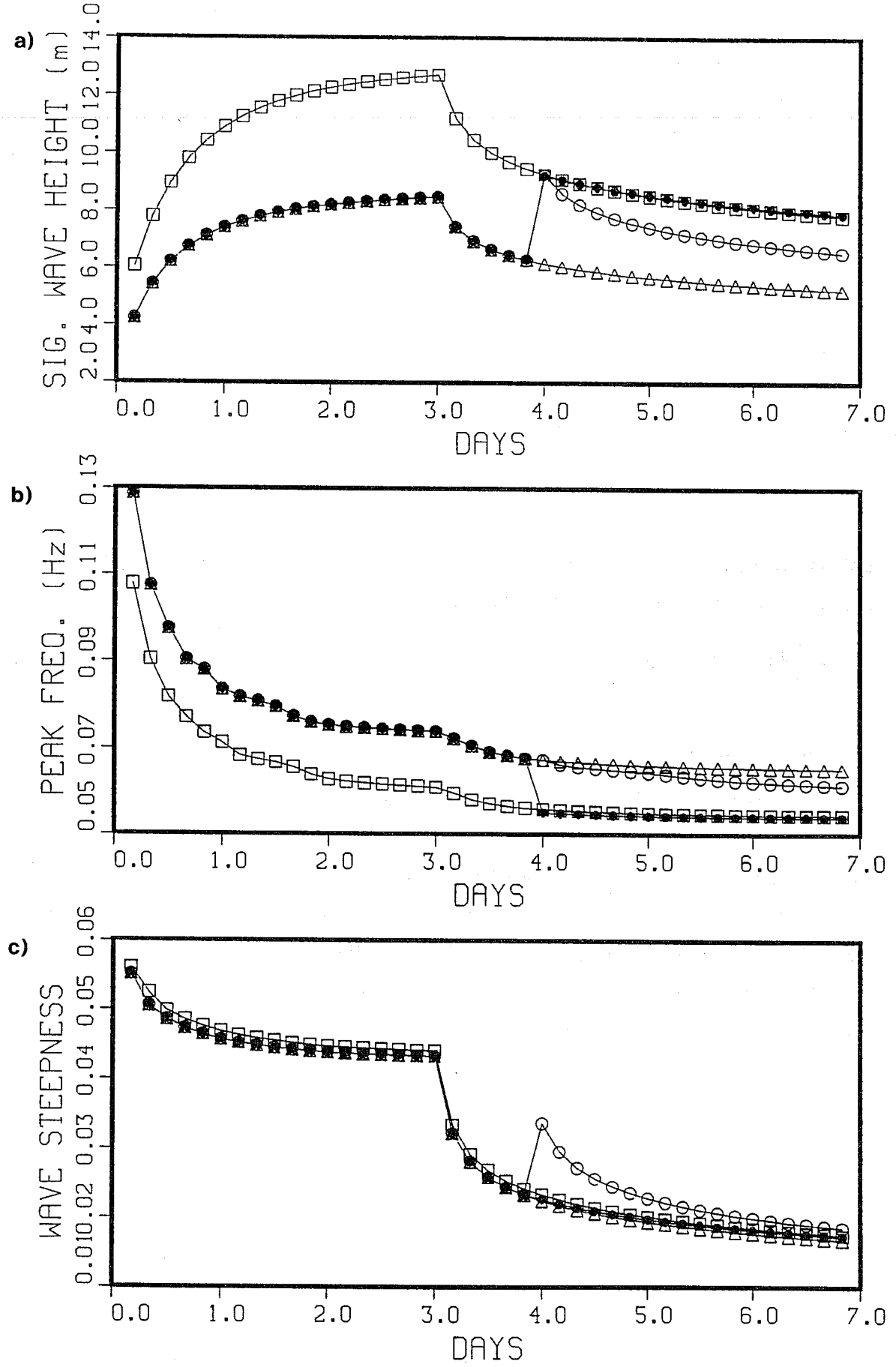

Fig. 30 Assimilation experiment time series a) significant wave height; b) peak frequency; c) average steepness squares represent the correct prediction, triangles the incorrect prediction, open circles the assimilation using (24) and full circles the assimilation using (26).

more striking if the peak frequency or the steepness are considered (Fig. 30), showing that the spectral shape is not updated correctly by the use of (24).

The analysis of the spectra at the assimilation time and of the relative source functions explains the different behaviour of the spectral parameters. Fig. 31a shows the incorrect prediction spectrum - denoted by triangles, the correct spectrum - denoted by squares, the result of the assimilation according to (27) - denoted by full circles and the result of the assimilation according to (24) - denoted by open circles. The similarity of the analysis performed using (27) with the correct result is striking. Fig. 31b shows, using the same symbols, the respective source functions. The use of (24) provides a very active source function, which produces the subsequent decay of the spectrum. This quick decay is not consistent with the evolution of the spectrum which has been generated by the correct friction velocity ($u_* = 1.03$). In fact, the "correct" source function is very weak, since it is an order of magnitude smaller than the source function resulting by the updating using (24). The incorrectness of the source function causes the failure in the updating.

Fig. 32 shows the spectra one day later. As consequence of the unrealistic source function produced by (24) much of the energy has been dissipated and the spectrum is not in good agreement with the correct one. On the contrary the agreement which has been produced at the time of the assimilation using (27) persists in time. The loss of the energy produced by the scaling method, is a typical feature of a third generation wave model, where the source function is also active in a swell spectrum; in second generation wave models where the swell is defined from the outset and its energy is not modified there is no energy loss; nevertheless, the peak frequency and the steepness of the updated spectrum are incorrect. It is necessary to be cautious transferring the result of this experiment to nature, but as far as assimilation in the WAM model is concerned, this numerical experiment indicates that the use of (27) is more consistent with the dynamics of the model itself.

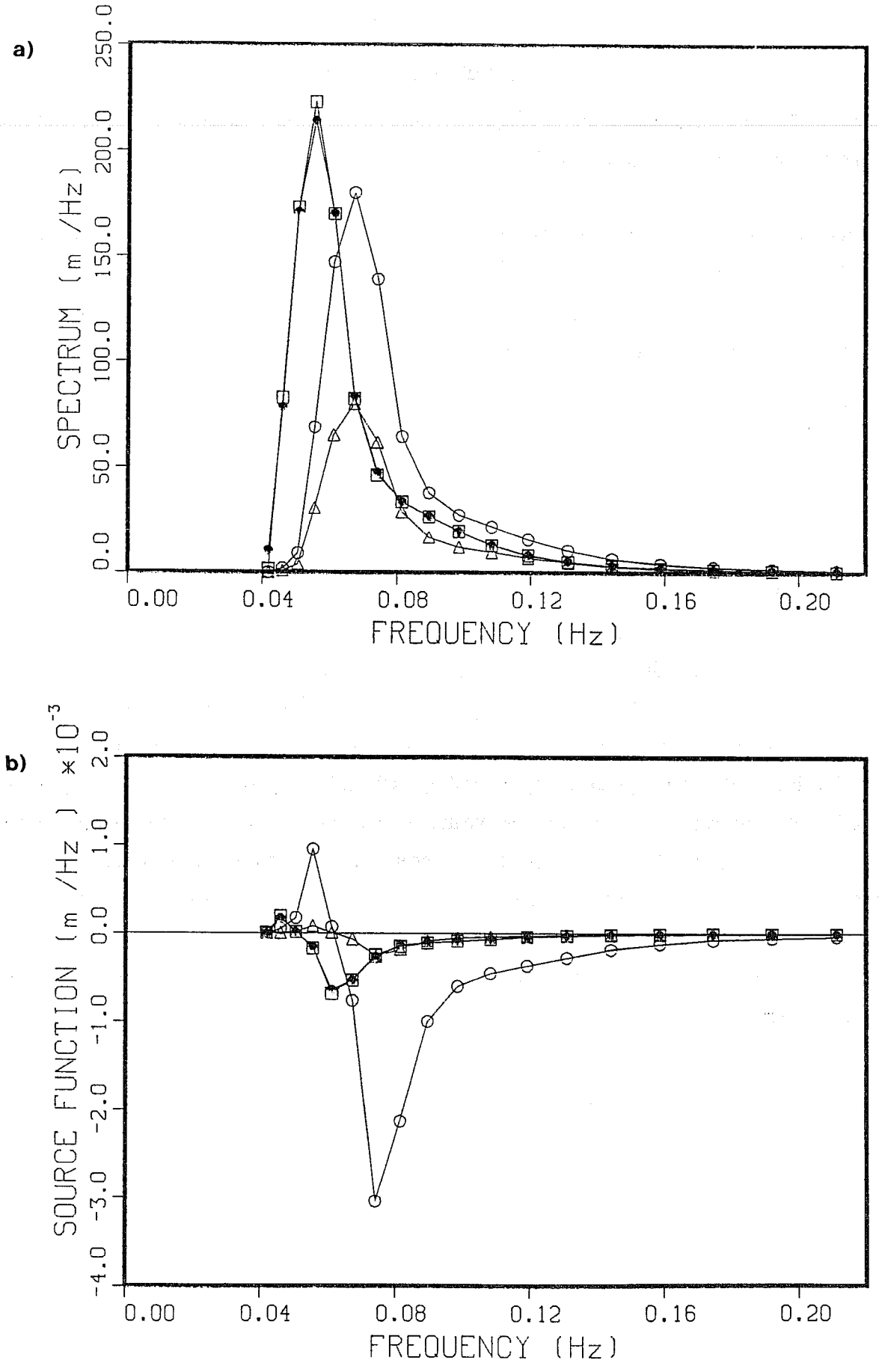

Fig. 31 a) wave spectra intercomparison and b)source functions intercomparison at the assimilation time. Squares represent the correct prediction, open circles the assimilation using (24), full circles the assimilation using (26) and triangles the first guess spectrum.

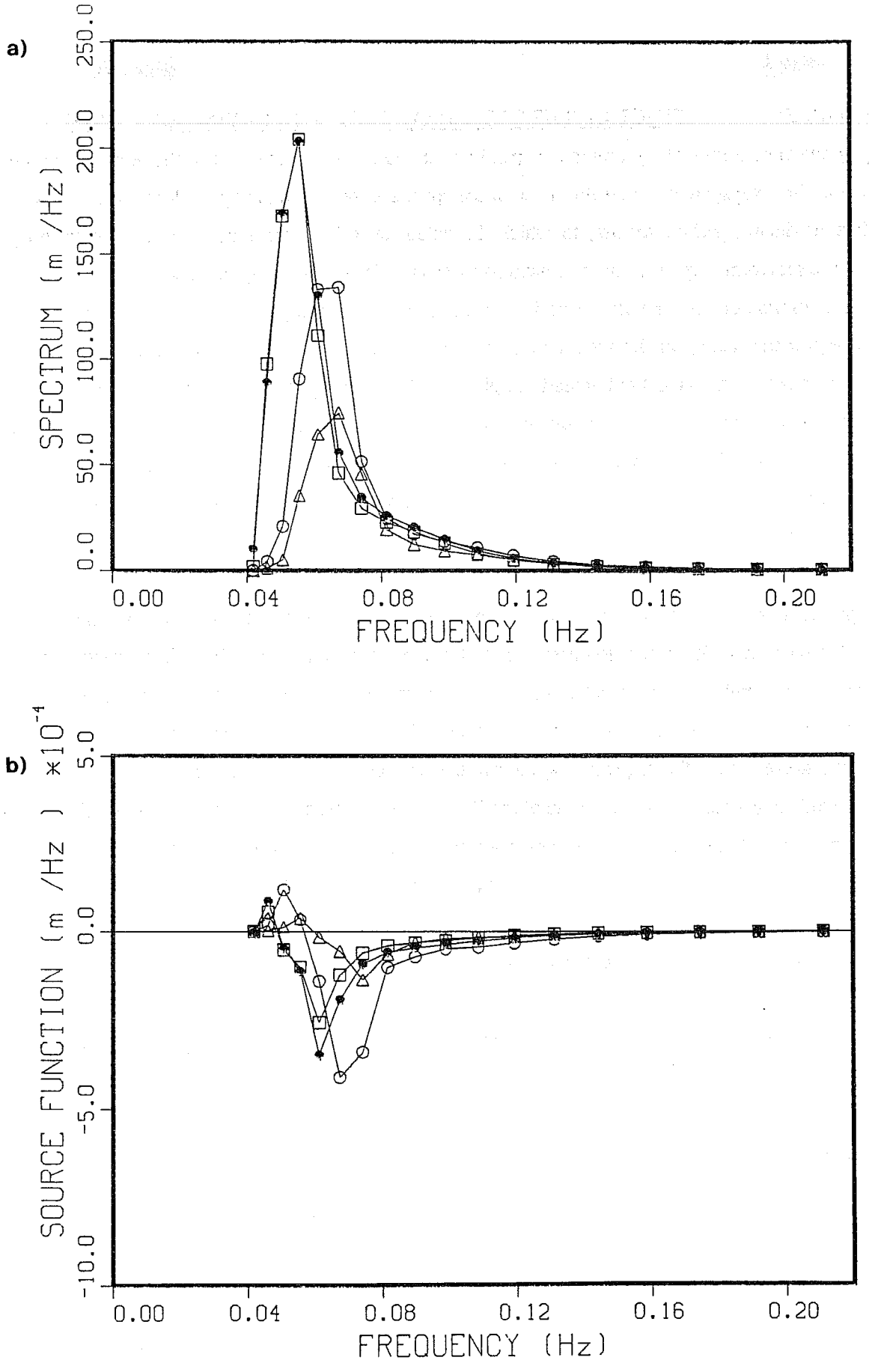

Fig. 32 a) wave spectra intercomparison and b) source functions intercomparison one day after the assimilation time. Squares represent the correct prediction, open circles the assimilation using (24), full circles the assimilation using (26) and triangles the first guess spectrum.

APPENDIX B: EFFECT OF THE PROPAGATION ON A DECAYING SPECTRUM

To apply the conclusions of the previous appendix to a realistic case the effect of the propagation must be examined. The propagation affects the shape of the spectrum, separating in space different frequencies and therefore producing peaked spectra, to which the extension of the previous arguments is arbitrary. In general, if a spectrum very far from the generating area is updated modifying its peak frequency, a time shift in space or in time of the generation area is implied, because the energy propagation velocity is modified. In this respect the scaling of the spectrum, without any change in the peak frequency, is not satisfactory, because an error in the wind field actually implies a different frequency in the area where the swell was generated. Consequently, during the following development of the spectrum, not only the swell energy is incorrect but also its location and its peak frequency. A simple scaling might be appropriate if the errors were due only to an incorrect dissipation in the WAM model, but our assumption is that they are due to inaccuracies in the wind field.

These problems in updating swell are the weak point of sequential methods; the best way to update wave spectra far away from the generation area is actually to consistently correct the whole previous history of the model. This might be the real advantage of variational methods, if they are able to deal properly with swell propagation, with respect to sequential methods. This appendix aims to show that there is a large area around the storm, where the sequential approach, that is presented in this report using (18) and (20), can be used, producing a successful correction of the WAM model. The repetition of the analysis should correct the spectrum over large areas of the ocean, eliminating the errors when the waves are generated or they begin decaying; this should consequently improve the prediction of the following evolution of the wave field, so that the need of a correction far away from the storm area is strongly reduced. Of course, large inaccuracies in the propagation could compromise the result.

To study the response of the WAM model we consider a basin extending 6900 km in the x-direction, infinite in the y-direction; the grid step is 300 km. Both wind and wave fields are homogeneous in the y-direction. The wind blows off-shore, in the x-direction, in a region near the left limit of the basin ($0 < x < 1200\ km$); it is switched off after two days. Therefore for two days swell is irradiated through the basin; after two days, when there is no wind anywhere, the whole basin is covered with swell. In line with the approach that was followed in the previous appendix, two runs are carried out: a wrong prediction, supplying the first guess spectra, and a correct prediction, supplying the measurements for the updating. The experiment is successful if the differences between the two runs are substantially reduced after the assimilation.

Fig. 33 shows the wave height profile across the basin for the correct prediction ($u_* = 1.03\ m/s$). A profile is plotted every 12 hours (the time from the beginning of the experiment is indicated near each curve). The

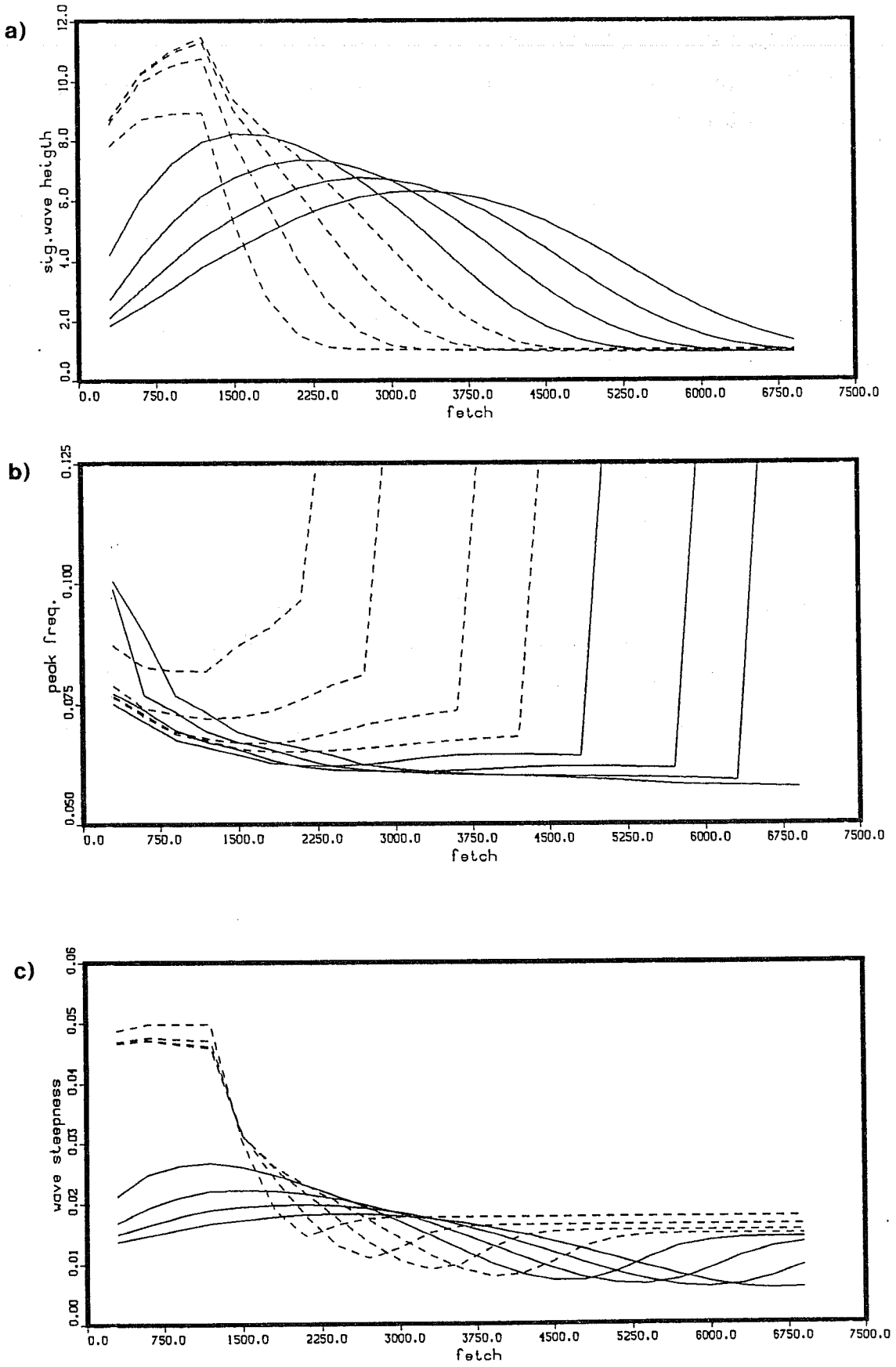

Fig. 33 Time evolution of the profiles across the basin for the correct prediction: a) significant wave height b) peak frequency c) average steepness. Dashed curves refer to the first part of the experiment when the wind was blowing over the first 1200 km of the basin.

first four curves, without dots, show the progressive growth of the windsea and the advance of the swell across the basin. The second four curves, with dots, show the decay and the propagation of the swell, after the wind has been switched off.

The spectrum is updated in four consecutive grid points to simulate the information derived from the passage of a satellite, which is assumed to orbit in the y-direction. The updating time is 12 hours after the wind has been switched off and it affects the part of the basin where the significant wave height is larger. Fig. 34a shows the modification in the wave height profile across the basin at the assimilation time, and Fig. 34b-d the following evolution, with a 12 hour interval. The correct and incorrect predictions are plotted for comparison. The results of the updating using (26), denoted by full circles, are better then the results obtained using (24), denoted by triangles. The comparison of the spectra provides the same conclusion. Fig. 35 shows the spectra at the time of the assimilation, at the eighth point of the one-dimensional grid, corresponding to a distance of 2400 km from the left limit of the basin. Using (26) a strict resemblance of updated and correct spectrum is obtained, while this is not the case using (24). The wrong spectral shape and the corresponding incorrect source function strongly reduce the effect of the assimilation: Fig. 36 shows the spectrum one day later at the twelfth point, which is approximately the point reached at this time by the energy of the peak of the spectrum that has been shown in the previous Fig. 35. The agreement of the spectrum produced using (26) with the correct one is still satisfactory, while the improvement obtained using (24) is arguable.

The same conclusions hold for the comparison of the peak frequency (Fig. 37). The underevaluation produced using (26) in the furthest part of the basin corresponds actually to an improvement in the spectral shape, as shown by Fig. 38, where the spectrum at the eighteenth point (at a distance of 5400 km from the left limit of the basin) is plotted, two days after the assimilation. The reproduction of the low frequency part of the correct spectrum is improved by the assimilation, but energy is missing in the central and high frequency part. This produces an underevaluation of the peak frequency, but it is an improvement with regards to the spectral shape. This situation is actually obvious because the energy that is missing was not inside the region affected by the assimilation at the updating time, but it was located at a greater distance from the left limit of the basin. Note that both the incorrect prediction and the result of the assimilation using (24) produce hardly any energy in this point at this time. With respect to such a poor result the improvement obtained is remarkable. This numerical experiment shows that using (27) the assimilation can be successfully carried out, with evident benefits for the model prediction. This method can therefore be applied to update the WAM model in a region around the storm, or during the decay after a drop in the wind speed.

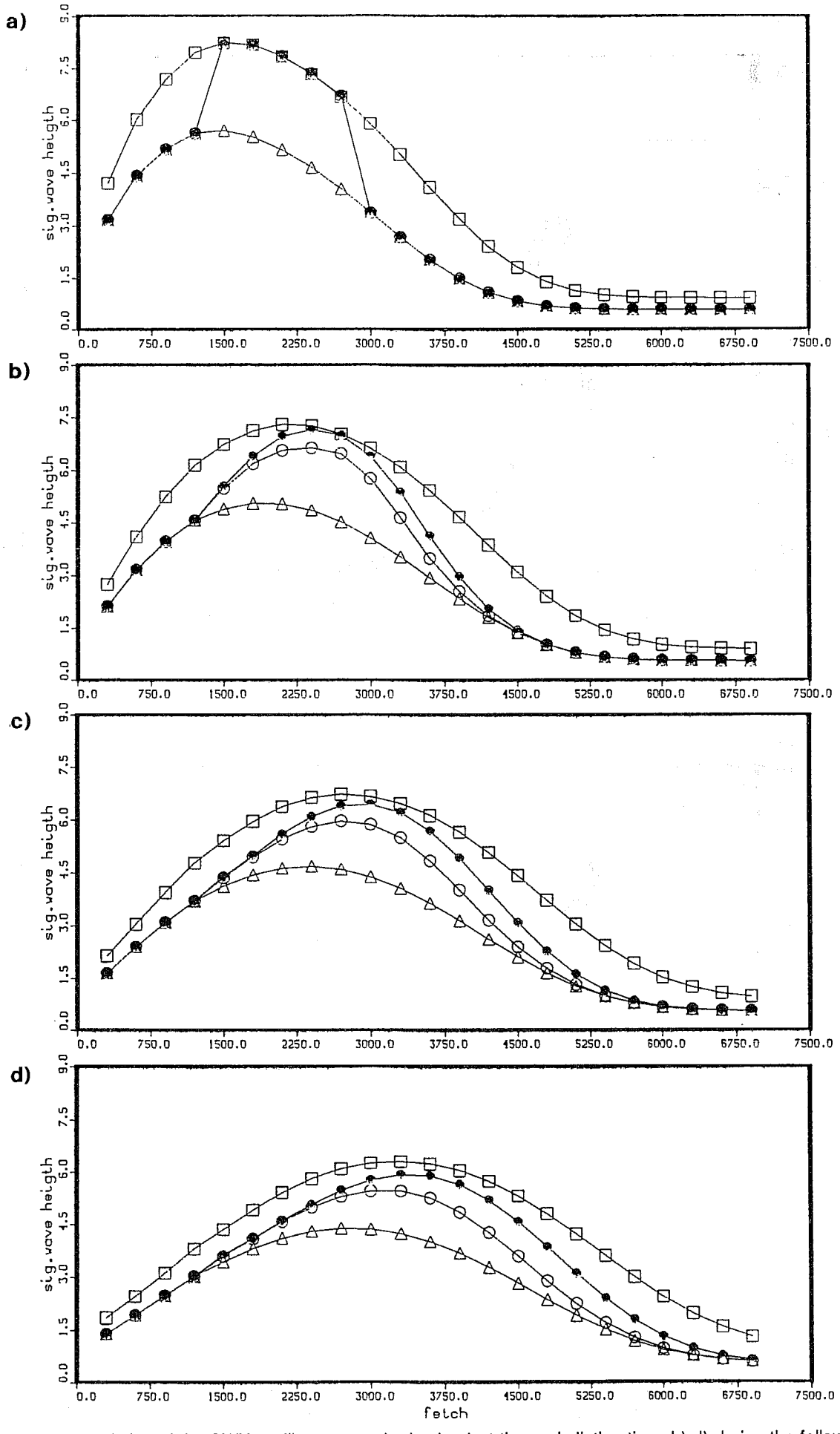

Fig. 34 Time evolution of the SWH profiles across the basin a) at the assimilation time, b)-d) during the following evolution every 12-hour. Squares represent the correct prediction, open circles the assimilation using (24), full circles the assimilation using (26) and triangles the incorrect prediction

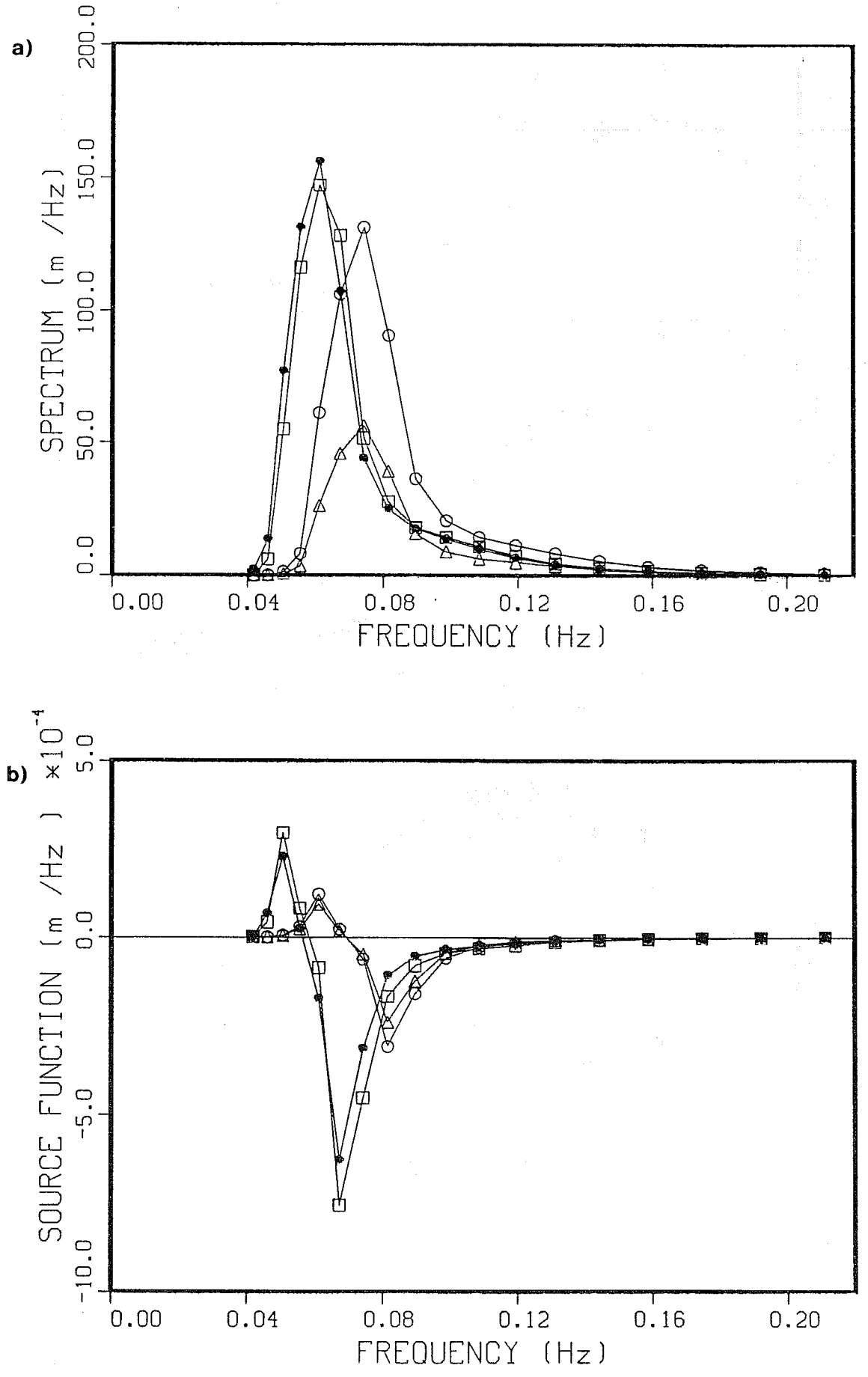

Fig. 35 a) wave spectra intercomparison and b) source functions intercomparison at the assimilation time. The spectra at a distance of 2400 km from the left border of the basin are plotted. Squares represent the correct prediction, open circles the assimilation using (24), full circles the assimilation using (26) and triangles the first guess spectrum.

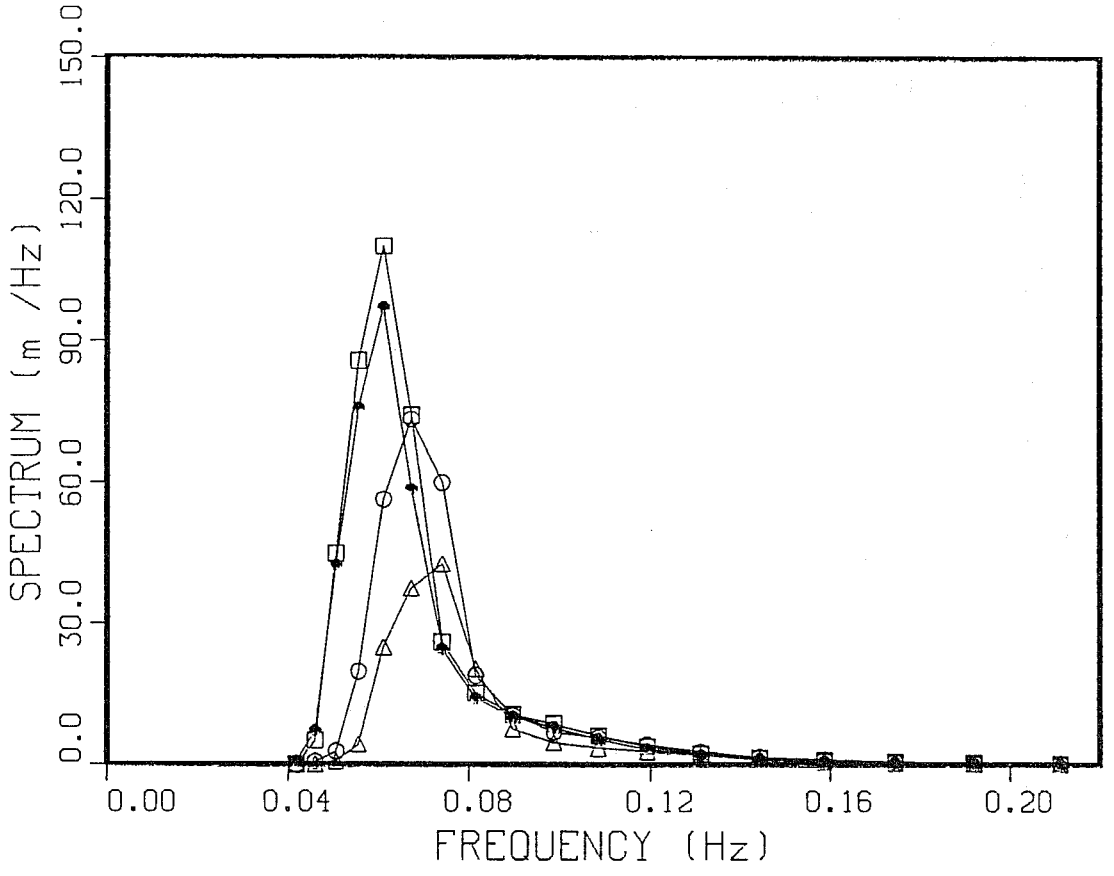

Fig. 36 wave spectra intercomparison one day after the assimilation. The spectra at a distance of 3600 km from the left border of the basin are plotted. Squares represent the correct prediction, open circles the assimilation using (24), full circles the assimilation using (26) and triangles the first guess spectrum.

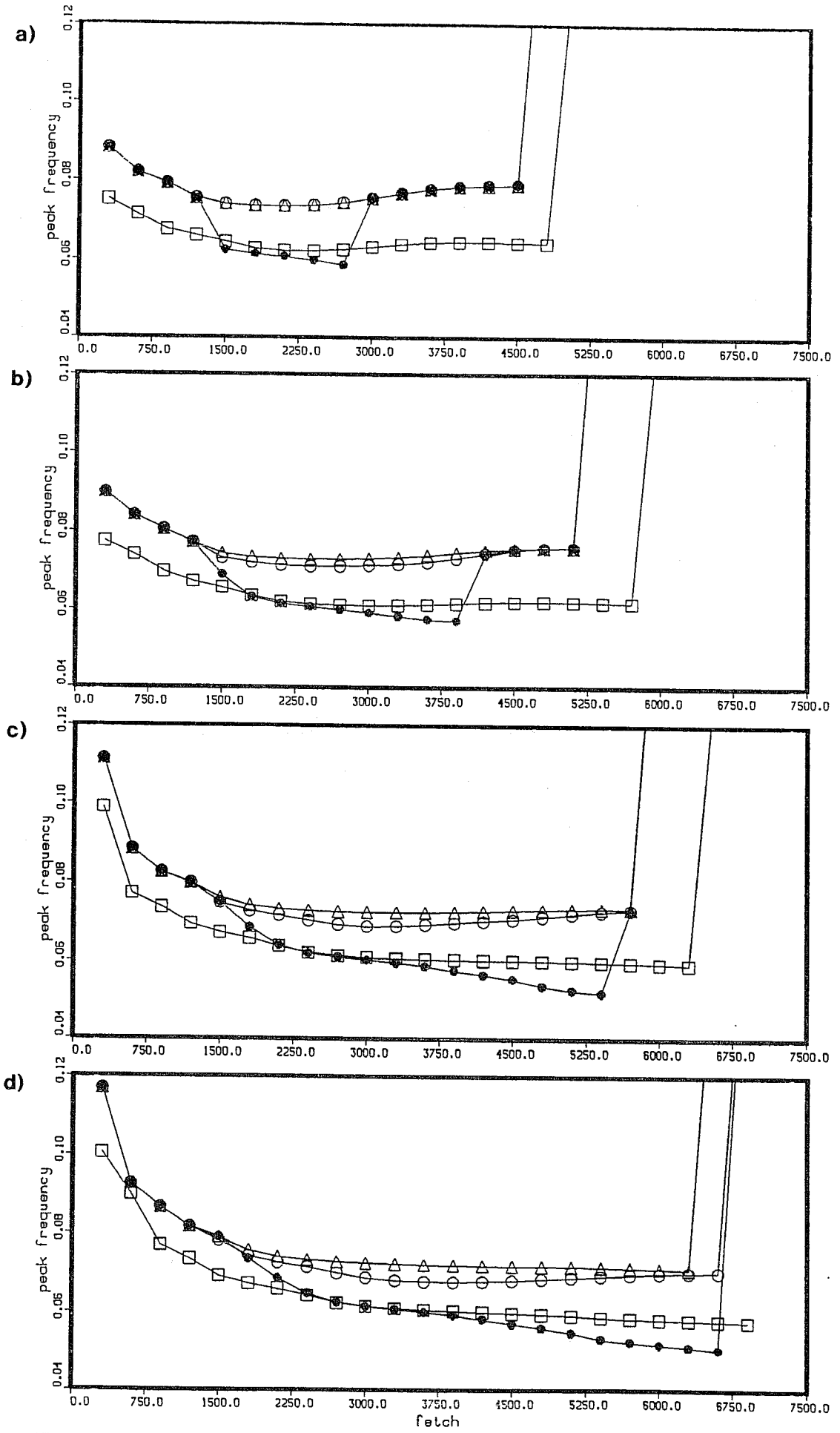

Fig. 37 Time evolution of the mean frequency profiles across the basin a) at the assimilation time, b)-d) during the following evolution every 12 hours. Squares represent the correct prediction, open circles the assimilation using (24), full circles the assimilation using (26) and triangles the incorrect prediction.

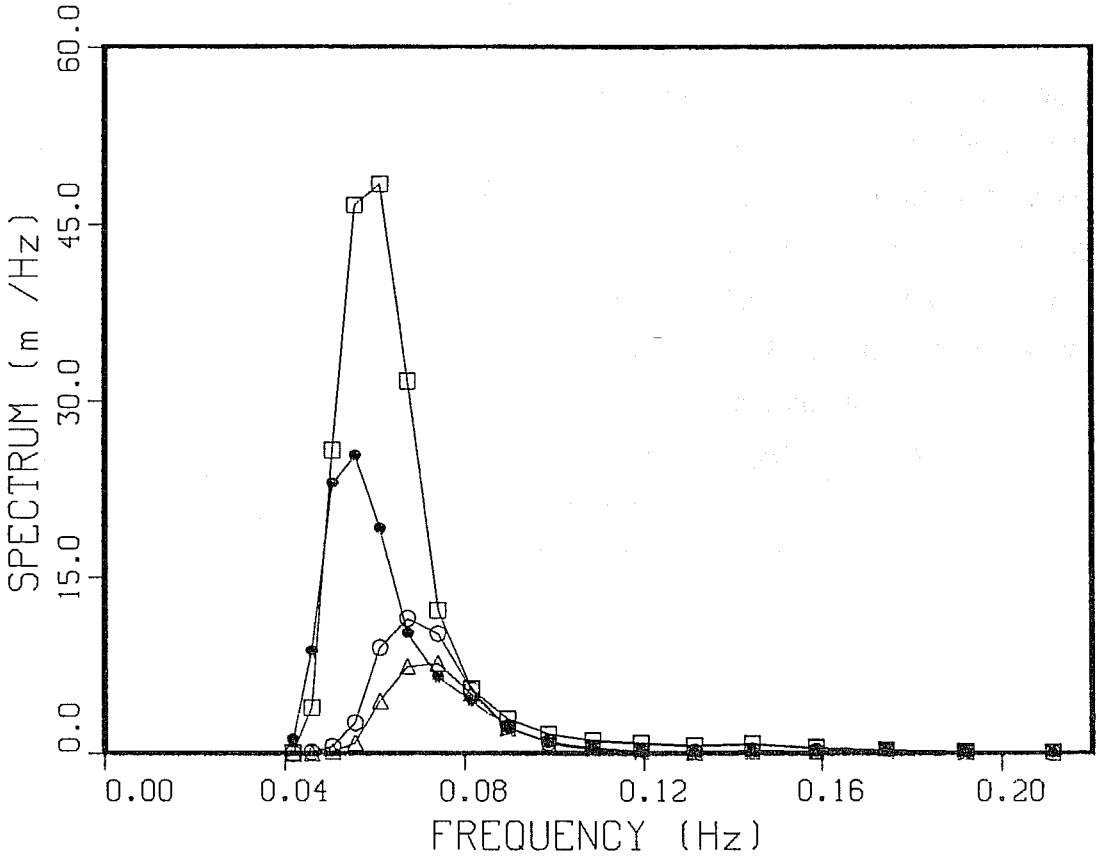

Fig. 38 wave spectra intercomparison one day after the assimilation. The spectra at a distance of 5400 km from the left border of the basin are plotted. Squares represent the correct prediction, open circles the assimilation using (24), full circles the assimilation using (26) and triangles the first guess spectrum.

APPENDIX C: DESCRIPTION OF THE DATA ASSIMILATION PACKAGE

This package has been developed to assimilate altimeter data in the version of the WAM model, that is currently run on a daily basis at ECMWF. It is meant as an extra module to be added to the subroutine version of the WAM model. A library where this assimilation package has been organically added to the WAM model is already available. The package has already been used in two numerical studies, using data provided by SEASAT and GEOSAT (see sections 4 and 5 of this report). There are minor differences in the code used in the two cases, which do not concern the core of the package but only the interface to the satellite data and wind fields used. The GEOSAT run used the ECMWF analysed wind fields, which are accessed with the subroutine GLOWIND. For the SEASAT run this subroutine must be substituted by SATWIND, which accesses the wind fields that have been produced by *Anderson et al.* (1987) for the SEASAT period. In the subroutine GRDATA the statements that access and read the satellite data are different for the SEASAT and GEOSAT run, due to the different formats and management of the data; since the SEASAT run is relatively short the data are all contained in a single file, while GEOSAT data are organized in 31 files (one file per day) which are dynamically fetched during the run. Finally the package is presently adjusted for a periodic grid; its implementation on a regional scale requires minor modifications in the subroutines GRDATA, OIFIELD and ANALYSE.

APPENDIX C

C.1 Subroutine WAMASSI

WAMASSI supervises the whole assimilation. It is called directly by WAVEMDL and therefore the assimilation is added to the subroutine version of the WAM model as an independent module. In the present set up the WAM model consists of three modules (PREWIND, WAMODEL, WAMASSI), which are called successively. Consequently, the assimilation is performed at the end of every wind input time step. Each model run is split into an analysis period, during which the model is driven by the ECMWF analysed wind field and the assimilation of altimeter data is carried out, and into a forecast period, during which the model is driven by the ECMWF forecast wind fields and no assimilation is carried out.

WAMASSI analyses the first guess spectra which are produced by WAMODEL and replaces them with analysed spectra. First guess spectra are read from unit IU10 and analysed spectra are written to unit IU07, exactly as during a propagation time step.

WAMASSI produces the analysed friction velocity in every point where the windsea is found; friction velocity and windsea wave height are consistent with the WAM model growth curve. Friction velocity speed and direction are extracted from the arrays WS1(IJ,IB) and WS2(IJ,IB) respectively and they are replaced in the same arrays at the end of the analysis. Therefore the analysed friction velocity will be used to drive the wave field during the first half of the next wind input time step.

The analysed fields are saved by WAMASSI in the same format as the corresponding first guess output; the unit containing the spectral integrated parameters, the swell integrated parameters and the spectra at the selected output points are called respectively ANAXXXXXXXXXXXX, SWAXXXXXXXXXXXX, OUAXXXXXXXXXXXX, where the date is written in the file name with the usual convention of the WAM model output files. During the analysis period the content of the files MAPXXXXXXXXXXX, SWLXXXXXXXXXXX, OUTXXXXXXXXXXX, which has been saved by WAMODEL before calling WAMASSI, refers to the state of the field before the assimilation. In the present configuration the restart files are saved at the end of the analysis period, overwriting the first guess restart files.

In GRDATA an extra unit is added for the tape containing the measurements (unit IUME='MEAS'L). Extra units are used to store the analysed fields (unit 9 for ANA, unit 49 for OUA, unit 36 for SWA).

APPENDIX C

The following externals are used by WAMASSI:

GRDATA	to read measurements, discard unreliable measurements, transfer measurements to the model grid
OIFIELD	to produce an analysed field by optimum interpolation
MAKEBLO	to transfer data from the global grid to each block
SEMEAN	to compute the mean energy
SPLITBL	to store the second latitude and the latitude before the last of each block in special units
UPDATE	to produce the analysed spectra and the analysed friction velocity field
GSFILE	to save the analysed fields and the restart files on ECFILE
OUTBS	to output spectra at selected points and to transfer a block of integrated spectral parameters to the global grid
OUTINT	to print the global fields of integrated parameters and write them to the output files

Note : SEMEAN, OUTBS, OUTINT, GSFILE, SPLITBL are shared with the remaining part of the programme; they have not been modified. OUTAN is actually OUTGRID but the output unit has been added as an argument. GSFILE has been modified to store the results of the analysis in the file ANAXXXXXXXXXXXX.

The following blocks are used by WAMASSI: FREDIR, GRIDPAR, INTPAR, MAP, MEANPA, OVER, SPEC1, SPEC2, SPEC3, STATUS, TESTO, UNITS, WIND.

C.2 Subroutine GRDATA(WHME,USME)

GRDATA reads the measurements from tape and it transfers them to the model nearest grid point, refusing unreliable data. The data that are contained in a time window whose length is equal to the wind input time step (IDELWO), centred at the assimilation time, are considered.

ARGUMENTS

WHME significant wave height measurements in the global WAM grid.
If there are no data: WHME=-3.
If there are less then 4 data: WHME=-2.
If the scatter is too large: WHME=-1.

USME friction velocity measurements in the global WAM grid.
If there are no data: USME=-3.
If there are less then 4 data: USME=-2.
If the scatter is too large: USME=-1.

METHOD

The subroutine dynamically fetches the file containing the data for the considered time interval. A box of the model mesh size is centred on each grid point. Only model sea points are used. The average value of the measurements inside the box is computed and is stored to update the model. Points where the RMS is larger then 25% of the average value or 0.5 m - whatever the larger - are discarded. Measurements associated with sudden steps or spikes in the altimeter time series are refused, i.e they are not transferred to the grid. The results obtained at the grid point where more than 10% of the data were refused are anyway not used to analyse the spectra. The data are read from unit IUME, and the data input has to be adapted to the data used.

C.3 Subroutine OIFIELDS (XME, XMO, XOI, SIGOBS, SIGMOD, NGX, NGY)

The subroutine produces a map of a given field by optimum interpolation. The resulting values are used to update the model spectra and the friction velocity. The expected value of the error variance in the measurements and in the model must be specified for every field. An estimate of the correlation length must also be provided. The resulting field is produced in the WAM global grid.

ARGUMENTS

XME	measurements XME<0 where there are not reliable data. (input)
XMO	first guess field, produced or used by WAMODEL. (input)
XOI	fields resulting from optimum interpolation XOI=XME<0 where there are no results (output)
SIGOBS	error variance in the observations (input)
SIGMOD	error variance in the model (input)
NGX, NGY	grid dimensions

Note: The correlation length is specified in grid size units by the parameter LMAX in both the subroutines OIFIELDS and ANALYSE.

METHOD

For each grid point the observations contained in a box of size 2*LMAX+1, centred around the point, are selected. The model correlation matrix corresponding to each observation is computed. The standard O.I. technique is used to produce the analysed values. The actual result for a given grid point is produced by the subroutine ANALYSE.

EXTERNALS

SETMAT	to sum two matrices
SYMINV	to invert a matrix
ANALYSE	to compute the analysed field at each grid point

C.4 Subroutine ANALYSE (XM, NOBS, XME, XMO, XOI, IMEAS, JMEAS, I, J)

ANALYSE computes the result of the O.I. producing the field in the point (I,J)

ARGUMENTS

XM	inverse of P+M where P is the model correlation matrix and M is the measurements correlation matrix.
NOBS	number of observations in the box of size 2*LMAX+1 centred at (I,J)
XME	measurements
XMO	corresponding model value
XOI	result of the O.I.
IMEAS	X-indices of the measurements in the global grid
JMEAS	Y-indices of the measurements in the global grid
I	X-index in the global grid
J	Y-index in the global grid

C.5 Subroutine BLOCKER (IB, IJS, IJL, USOIB, WHOIB, WHMOB, USOI, WHOI, WHGTTG, IBG, IUS)

Blocker transfers variables from blocks to the global grid or vice versa

ARGUMENTS

USOI	ustar field from O.I.
WHOI	wave height field from O.I.
WHGTTG	wave height field from blocking
WHOIB	wave height from O.I. (blocked)
USOIB	ustar from O.I. (blocked)
WHMOB	wave height from model (blocked)
IBG	ibg = 1 from global grid to blocks
	ibg = 2 from blocks to global grid
IUS	ius = 1 only ustar is transferred

C.6 Subroutine UPDATE (F, ETOI, USOI, USMO, THMO, IJS, IJL)

UPDATE analyses a block of wave spectra and assimilates significant wave height and friction velocity measurements for a whole block. The method, described elsewhere in the report, produces a consistent analysis of wind and wave spectrum in the case of windsea, using the WAM model growth curve; the quasi-conservation of steepness is used in the case of swell (in such case there is no analysis of the wind)

VARIABLES

F	modified by the subroutine: in input it is the first guess wave spectrum, in output the analysed spectrum
ETOI	total energy after the optimum interpolation as produced by OIFIELD. (input) ETOI<0. where O.I. produced no data to be assimilated
USOI	friction velocity after optimum interpolation, as produced by OIFIELD. (input) USOI<0 where O.I. produced no data to be assimilated
USMO	modified by the subroutine: in input is the first guess friction velocity, in output the analysed friction velocity
THMO	wind direction (input)
IJS	index of the first point where the spectrum is analysed
IJL	index of the last point where the spectrum is analysed
Note:	The first guess energy EMEAN is an input variable in this subroutine, It is stored in the COMMON "MEANPA"

METHOD

By calling FWSEA the presence of windsea is investigated. The windsea energy and frequency are stored in EWFG and FMWFG respectively. If there is no windsea EWFG=-999 and FMWFG=-9999.

The windsea duration (in seconds) is evaluated by FDUR from EWFG and it is stored in T. If the evaluation failed T=-9.

The analysis of the windsea is done by assuming that the ratio between windsea energy and total energy is correct in the first guess spectrum, i.e. it is performed using EWOI

$$EWOI = \frac{ETOI}{EMEAN} EWFG \tag{28}$$

as analysed windsea energy. The analysed values of friction velocity and of the mean windsea frequency are computed by FUSTAR. The results are stored in USA, EWA, FMWA respectively. IF the analysis failed USA=-99., EWA=-999., FMWA=-9999. The analysed friction velocity is substituted in USMO,

which will be used to compute the wave field in the next half wind input time step in the points where the windsea was found and the analysis was successful.

The spectrum is updated according to whether windsea or swell is the dominant contribution: if windsea energy is larger then swell energy then EWFG contains the windsea energy in the first guess spectrum; Otherwise EWFG=-999. EWFG is used as a flag: if it is larger than 0 the parameters A and B in UPSPEC are computed according to (18); if EWFG is negative A and B are computed according to (20) - see description of UPSPEC.

For both windsea and swell the analysed spectrum is built by UPSPEC.

EXTERNALS

FWSEA	to evaluate the windsea energy and the windsea mean frequency in the first guess spectrum
FDUR	to evaluate the windsea duration from the first guess spectrum
FUSTAR	to evaluate the analysed windsea energy and mean frequency using the results of O.I. An analysed friction velocity is also computed
UPSPEC	to produce the analysed spectrum from the first guess spectrum

C.7 Subroutine FWSEA (F, EWFG, THEW, FMWFG, ETOI, USMO, THMO, G, IJS, IJL)

FWSEA finds out if the first guess spectrum contains windsea. If this is the case, it evaluates the windsea energy and the windsea mean frequency.

VARIABLES

F	first guess wave spectrum (input)
EWFG	estimate of the windsea energy (Output) EWFG=-999 if there is no windsea
THEW	direction of the windsea peak (output) THEW=999999999 if there is no windsea
FMWFG	estimate of the windsea mean frequency (output) FMWFG=-9999 if there is no windsea
ETOI	analysed total energy produced by O.I. (input)
USMO	first guess friction velocity, which is currently driving the wave field (input)
THMO	wind direction (input)
G	gravity
IJS	index of the first point where the spectrum is analysed
IJL	index of the last point where the spectrum is analysed

METHOD

The subroutine scans three direction bins around the wind direction, searching for a peak. If a peak is found the spectrum is integrated on three direction bins centred on the bin that contains the peak, to obtain an approximation to the one-dimensional spectrum. The peak frequency is obtained by quadratic interpolation of such one dimensional spectrum. If the peak frequency is larger then the Pierson-Moskowitz frequency then the peak corresponds to windsea.

The direction of the peak is evaluated by quadratic interpolation.

A parametrized spectrum is built to approximate the model windsea spectrum using parametric relations derived from the WAM model. The spectrum shape is substantially a JONSWAP spectrum with a f^{-4} tail and a Toba's constant instead of a Phillips' constant; the level of the tail is therefore depending on the wind speed. The shape of the spectrum around the peak is slightly different from the JONSWAP spectrum.

The spectrum depends on four parameters $\gamma, \sigma, f_p, \alpha_T$. The overshoot parameter γ is derived from the peak frequency as

$$\gamma = 1 + 2.7\left[1 - \left(\frac{f_{PM*}}{f_{p*}}\right)^{1.44}\right] \tag{29}$$

$$f_{PM*} = 0.00608; \quad f_{p*} = f_p \frac{u_*}{g} \tag{30}$$

The width of the overshoot σ is also derived from the peak frequency

$$\sigma = 0.02 + 0.16\left[1 - \left(\frac{f_{PM*}}{f_{p*}}\right)^{2.34}\right] \tag{31}$$

The Toba's α_T constant is given as

$$\alpha_T = 0.145 \tag{32}$$

The previous relations have been derived from a fit with the model windsea spectrum.

The windsea spectrum is built by taking the smaller between the model spectrum and the corresponding windsea parametrized spectrum. In a restricted area around the peak the model spectrum is assumed to be the windsea spectrum.

The energy and the mean frequency of the windsea are computed in the subroutine WSMFEN.

EXTERNALS

WSMFEN	to compute energy and mean frequency of the windsea
F4SPEC	compute the parametric spectrum to approximate the WAM model windsea spectrum

C.8 Subroutine WSMFEN (FSEA, EW, FM, USTT)

WSMFEN computes the energy and the mean frequency of the windsea spectrum which is stored in FSEA.

ARGUMENTS

FSEA	windsea spectrum in a given point (input)
EW	windsea energy (output)
FM	windsea mean frequency (output)
USTT	friction velocity (input)

METHOD

The subroutine produces a first evaluation of energy and mean frequency by simple integration of the spectrum. This implies a underevaluation both of the energy and of the mean frequency, because the energy content of high frequencies is generally under estimated. To compensate this flaw the relation between energy and mean frequency is used providing an overestimated energy from the underestimated mean frequency and a overestimated mean frequency from the underestimated energy. The average of the over and under evaluation is taken as final result.

C.9 Subroutine F4SPEC (ALFA, FM, GAMMA, SA, THETAQ, USTAR, SPINT, SPT)

This subroutine is substantially the same as JSPEC, which was already present in the WAM model program. It has been modified to have a f^{-4} tail and a Toba's constant instead of a f^{-5} tail and a Phillips' constant. This modification improved the fit to the WAM model spectrum.

ARGUMENTS

ALFA	Toba's constant (input)
FM	peak frequency (input)
GAMMA	overshoot parameter (input)
SA	width of the overshoot (input)
THETAQ	peak direction (input)
SPINT	energy of the computed spectrum (output)
USTAR	friction velocity (input)
SPT	parametrized spectrum (output)

METHOD

A spectrum in the form

$$F(\theta,f) = I(\theta)\frac{\alpha_T g u_*}{(2\pi)^3} f^{-4} \exp\left[-\left(\frac{2f}{3f_p}\right)^{\gamma^{\exp(-\frac{1}{2}(\frac{f-f_p}{\sigma f_p})^2)}}\right] \tag{33}$$

is produced. An angular spreading factor

$$I(\theta) = \cos^2(\theta) \tag{34}$$

is used.

EXTERNALS

SPR to compute a $\cos^2$ spreading function

C.10 Subroutine FDUR (EWFG, T, USMO, IJS, IJL)

FDUR provides an estimate of the windsea duration which will be later used to estimate the analysed friction velocity from the analysed windsea energy.

ARGUMENTS

EWFG	first guess windsea energy (input)
T	windsea duration (output)
USMO	first guess friction velocity
IJS	index of the first point where the spectrum is analysed
IJL	index of the last point where the spectrum is analysed

METHOD

The dimensionless growth curve derived from the WAM model time limited growth is used to derive the duration from the windsea energy. Its explicit expression is

$$E_*(t_*) = 955 \cdot \tanh 96.02 \cdot 10^{-5} t_*^{0.69} \qquad (35)$$

C.11 Subroutine FUSTAR (USMO, USA, USOI, EWFG, EWOI, EWA, T, FMWA, G, IJS, IJL)

This subroutine provides an evaluation of the friction velocity consistent with the analysed windsea energy. Originally this value was cross validated with the wind speed value supplied by the altimeter, where a tolerance of 20% was allowed for the expected bad quality of the measured windspeed. Only if the estimation and measurement were consistent, the results of the analysis were used to update the WAM model. In the case of GEOSAT data, this part of the code was commented out, since no windspeed measurements were directly available.

The subroutine evaluates a analysed windsea mean frequency and it stores in EWA the analysed windsea energy, if the analysis is successful.

ARGUMENTS

USMO	first guess friction velocity (input)
USA	analysed friction velocity (output); USA=-99, if analysis is not successful
USOI	friction velocity produced by optimum interpolation (input)
EWFG	first guess windsea energy (input); EWFG=-999, if there is no windsea
EWOI	windsea energy from optimum interpolation (input)
EWA	analysed windsea energy (output); EWA=-999, if there is no windsea or analysis was not successful
T	windsea duration (input); T=-9, if there is no windsea
FMWA	analysed windsea mean frequency (output)
IJS	index of the first point where the spectrum is analysed
IJL	index of the last point where the spectrum is analysed

METHOD

The friction velocity is evaluated from the estimate of the windsea energy EWOI, which was derived by O.I. using (34). Since energy and duration, which is assumed correct in the first guess, are given (34) is in fact an equation for u_*, which can be only solved numerically; a simple iteration procedure is used.

The mean frequency is derived by the analysed windsea energy EWA, which, if there in no cross validation with a wind measurement, is equal to EWOI, using its relation to the windsea energy, as deduced by the model growth curve.

C.12 Subroutine UPSPEC (F, ETFG, ETA, FMWFG, FMWA, IJS, IJL)

The subroutine UPSPEC updates the wave spectrum, using the criterium explained elsewhere in this report. The analysed spectrum F_A is given as a function of the first guess spectrum using (14).

The basic point is the distinction between windsea and swell spectrum. If the spectrum is mainly windsea then (18) is used; if the spectrum is mainly swell then (20) is used.

ARGUMENTS

F	wave spectrum; in input it is the first guess spectrum and in output it is the analysed spectrum
ETFG	first guess total energy (input)
ETA	analysed total energy which resulted from optimum interpolation (input).
FMWFG	first guess windsea mean frequency (input)
FMWA	analysed windsea mean frequency (input)
IJS	index of the first point where the spectrum is analysed
IJL	index of the last point where the spectrum is analysed

METHOD

The new spectrum is built by linear interpolation from the old one, without changing the directional distribution:

$$F_A(IPOINT,K,M) = A \cdot F(B \cdot FRM) \tag{36}$$

where K and M are the frequency and direction bin respectively. $F(B \cdot FRM)$, required value of the first guess spectrum is computed as

$$F(B \cdot FRM) = \frac{F_M(IPOINT,K,M2) - F_M(IPOINT,K,M1)}{FR(M2) - FR(M1)} (B \cdot FR(M) - FR(M1)) \tag{37}$$

$FR(M)$ is the frequency array in the model, which is stored in COMMON/FREDIR/. Note that in the model $FR(M + 1) = 1.1 \cdot FR(M)$.

$M1$ denotes the model largest frequency bin such that $FR(M1) < B \cdot FR(M)$ and $M2 = M1 + 1$. If $M1$ is smaller than 1 or larger than NFRE (number of frequencies), then $F_A = 0$.

References

Allan, T.D. (editor), 1983 : "Satellite microwave remote sensing", Ellis Horwood Limited, pp. 526.

Anderson, D., A. Hollingsworth, S. Uppala and P. Woicheshyn, 1987: "A Study On The Feasibility Of Using Sea And Wind Information From The ERS-1 Satellite I: Wind Scatterometer Data", ECMWF Contract Report ESA, Paris.

Bruning, C., W. Alpers, K. Hasselmann, 1990: "Monte Carlo Simulation Studies Of The Nonlinear Imaging Of A Two Dimensional Surface Wave Field By A Synthetic Aperture Radar", in press in Int.J. Remote Sens.

Esteva, D.C., 1988: "Evaluation of preliminary experiments assimilating Seasat significant wave heights into a spectral wave model". J.Geophys.Res., 93, pp. 14099-14106.

Francis, P.E., and R.A. Stratton, 1990: "Some experiments to investigate the assimilation of SEASAT altimeter wave height data into a global wave model", Q.J.R.Meteorol.Soc., 116, pp. 1225-1251.

Hasselmann, K., 1988: "Development of a satellite SAR image spectra and altimeter wave height data assimilation System for ERS-1", Max Planck Institut fur Meteorologie Report, 19,

Hasselmann, K, T.P. Barnett, E. Bouws, H. Carlson, D.E. Cartwright, K. Enke, J.A. Ewing, H. Gienapp, D.E. Hasselmann, P. Krusemann, A. Meerburg, P. Muller, D.J. Olbers, K. Richter, W. Sell and H. Walten, 1973 : Measurements of wind-wave growth and swell decay during the Joint North Sea Wave Project (JONSWAP). Deut.Hydrogr.Z., Suppl.A, 8, 12, 22pp.

Hollingsworth, A., 1986: 'Objective Analysis For Numerical Weather Prediction' in 'Short and Medium Range Numerical Weather Prediction', special volume of the Meteorological Society of Japan, ed. T. Matsuno.

Janssen, P.A.E.M., P. Lionello, M. Reistad, A. Hollingsworth, 1989 'Hindcasts and data assimilation studies with the WAM model during the SEASAT period', J.Geophys.Res., 94, pp 973-993.

Kidaigorodskii, S.A., 1962: "Application of the theory of similarity to the analysis of wind-generated water waves as a stochastic process", Bull.Acad.Sci. USSR Geophys. Ser. 1, pp 73

Komen, G., 1985: "Introduction to wave models", in European Space Agency Special Publication, ESA SP-221, pp. 21-25.

Lionello, P.and P.A.E.M. Janssen, 1990: "Assimilation of altimeter measurements to update swell spectra in wave models", in Proc. of the International Symposium on Assimilation of Observations in Meteorology and Oceanography, Clermond-Ferrand, France, August 1990.

Lorenc, A.C., 1981: "A Global Three-dimensional Multivariate Statistical Interpolation Scheme", Mon.Wea.Rev., 109, n.4, pp. 701-721.

Talagrand, O., 1988: "Four dimensional variational assimilation", in Proceedings of Data Assimilation and the use of Satellite Data, ECMWF, September 1988, 2, pp. 1-30.

Thomas, J., 1988: 'Retrieval of energy spectra from measured data for assimilation into a wave model', Q.J.R.Meteorol.Soc., 114, pp. 781-800.

de Valk, C.F. and C.J. Calkoen, 1989: "Wave data assimilation in a third generation wave prediction model for the North sea", Delft Hydraulics Report.

WAMDI Group (S. Hasselmann, K. Hasselmann, E. Bauer, P.A.E.M. Janssen, G. Komen, L. Bertotti, P. Lionello, A. Guillaume, V.C. Cardone, J.A. Greenwood, M. Reistad, L. Zambresky, J.A. Ewing), 1988: 'The WAM model - A third generation ocean wave prediction model', J.Phys.Oceanogr., 18, pp. 1776-1810.

Zambresky, L., 1988; "A Verification Study Of The Global WAM Model", ECMWF Research Department Technical Report 63.

LIST OF ECMWF TECHNICAL REPORTS

1	A case study of a ten day forecast. September, 1976	Arpe, K., L. Bengtsson, A. Hollingsworth, and Z. Janjic
2	The effect of arithmetic precision on some meteorological integrations. December, 1976	Baede, A.P.M., D. Dent, and A. Hollingsworth
3	Mixed-radix Fourier transforms without reordering. February, 1977	Temperton, C.
4	A model for medium range weather forecasts - adiabatic formulation. March, 1977	Burridge, D.M., and J. Haseler
5	A study of some parameterisations of sub-grid processes in a baroclinic wave in a two dimensional model. July, 1977	Hollingsworth, A.
6	The ECMWF analysis and data assimilation scheme: analysis of mass and wind field. December, 1977	Lorenc, I. Rutherford and G. Larsen
7	A ten-day high-resolution non-adiabatic spectral integration; a comparative study. October, 1977	Baede, A.P.M., and A.W. Hansen
8	On the asymptotic behaviour of simple stochastic-dynamic systems. November, 1977	Wiin-Nielsen, A.
9	On balance requirements as initial conditions. October, 1978	Wiin-Nielsen, A.
10	ECMWF model parameterisation of sub-grid scale processes. January, 1979	Tiedtke, M., J.-F. Geleyn, A. Hollingsworth, and J.-F. Louis
11	Normal mode initialization for a multi-level grid-point model. April, 1979	Temperton, C., and D.L. Williamson
12	Data assimilation experiments. October, 1978	Seaman, R.
13	Comparison of medium range forecasts made with two parameterisation schemes. - , 1978	Hollingsworth, A., K. Arpe, M. Tiedke, M. Capaldo, H. Savijarvi, O. Akesson, and J.A. Woods
14	On initial conditions for non-hydrostatic models. November, 1978	Wiin-Nielsen, A.C.
15	Adiabatic formulation and organization of ECMWF's spectral model. -, 1979	Baede, A.P.M., M. Jarraud, and U. Cubasch
16	Model studies of a developing boundary layer over the ocean. November, 1979	Økland, H.
17	The response of a global barotropic model to forcing by large scale orography. January, 1980	Quiby, J.
18	Confidence limits for verification and energetic studies. May, 1980	Arpe, K.

19	A low order barotropic model on the sphere with orographic and newtonian forcing. July, 1980	Källén, E.
20	A review of the normal mode initialization method. August, 1980	Du Xing-yuan
21	The adjoint equation technique applied to meteorological problems. September, 1980	Kontarev, G.
22	The use of empirical methods for mesoscale pressure forecasts. November, 1980	Bergthorsson, P.
23	Comparison of medium range weather forecasts made with models using spectral or finite difference techniques in the horizontal. February, 1981	Jarraud, M., C. Girard, and U. Cubasch
24	On the average errors of an ensemble of forecasts. February, 1981	Derome, J.
25	On the atmospheric factors affecting the Levantine Sea. May, 1981	Ozsoy, E.
26	Tropical influences on stationary wave motion in middle and high latitudes. August, 1981	Simmons, A.J.
27	The energy budgets in North America, North Atlantic and Europe based on ECMWF analysis and forecasts. November, 1981	Sävijärvi, H.
28	An energy and angular momentum conserving finite-difference scheme, hybrid coordinates and medium range weather forecasts. November, 1981	Simmons, A.J., and R. Strüfing
29	Orographic influences on Mediterranean lee cyclogenesis and European blocking in a global numerical model. February, 1982	Tibaldi, S. and A. Buzzi
30	Review and re-assessment of ECNET - A private network with open architecture. May, 1982	Haag, A., Königshofer, F. and P. Quoilin
31	An investigation of the impact at middle and high latitudes of tropical forecast errors. August, 1982	Haseler, J.
32	Short and medium range forecast differences between a spectral and grid point model. An extensive quasi-operational comparison. August, 1982	Girard, C. and M. Jarraud
33	Numerical simulations of a case of blocking: The effects of orography and land-sea contrast. September, 1982	Ji, L.R., and S. Tibaldi
34	The impact of cloud track wind data on global analyses and medium range forecasts. December, 1982	Kållberg, P., S. Uppala, N. Gustafsson, and J. Pailleux
35	Energy budget calculations at ECMWF. Part 1: Analyses 1980-81. December, 1982	Oriol, E.

36	Operational verification of ECMWF forecast fields and results for 1980-1981. February, 1983	Nieminen, R.
37	High resolution experiments with the ECMWF model: a case study. September, 1983	Dell'Osso, L.
38	The response of the ECMWF global model to the El-Niño anomaly in extended range prediction experiments. September, 1983	Cubasch, U.
39	On the parameterisation of vertical diffusion in large-scale atmospheric models. December, 1983	Manton, M.J.
40	Spectral characteristics of the ECMWF objective analysis system. December, 1983	Daley, R.
41	Systematic errors in the baroclinic waves of the ECMWF. February, 1984	Klinker, E., and M. Capaldo
42	On long stationary and transient atmospheric waves. August, 1984	Wiin-Nielsen, A.C.
43	A new convective adjustment. October, 1984	Betts, A.K., and M.J. Miller
44	Numerical experiments on the simulation of the 1979 Asian summer monsoon. October, 1984	Mohanty, U.C., R.P. Pearce and M. Tiedtke
45	The effect of mechanical forcing on the formation of a mesoscale vortex. October, 1984	Guo-xiong Wu and Shou-jun Chen
46	Cloud prediction in the ECMWF model. January, 1985	Slingo, J., and B. Ritter
47	Impact of aircraft wind data on ECMWF analyses and forecasts during the FGGE period, 8-19 November. March 1985	Baede, A.P.M., P. Kållberg, and S. Uppala
48	A numerical case study of East Asian coastal cyclogenesis. May 1985	Chen, Shou-jun and L. Dell'Osso
49	A study of the predictability of the ECMWF operational forecast model in the tropics. September 1985	Kanamitsu, M.
50	On the development of orographic. June 1985	Radinovic, D.
51	Climatology and systematic error of rainfall forecasts at ECMWF. October 1985	Molteni, F., and S. Tibaldi
52	Impact of mofified physical processes on the tropical simulation in the ECMWF model. October 1985	Mohanty, U.C., J.M. Slingo and M. Tiedtke
53	The performance and systematic errors of the ECMWF tropical forecasts (1982-1984). November 1985	Heckley, W.A.

54	Finite element schemes for the vertical discretization of the ECMWF forecast model using linear elements. January 1986	Burridge, D.M., J. Steppeler, and R. Strüfing
55	Finite element schemes for the vertical discretization of the ECMWF forecast model using quadratic and cubic elements. February 1986	Steppeler, J.
56	Sensitivity of medium-range weather forecasts to the use of an envelope orography. September 1986	Jarraud, M., A.J. Simmons and M. Kanamitsu
57	Zonal diagnostics of the ECMWF operational analyses and forecasts. October 1986	Branković, Č.
58	An evaluation of the performance of the ECMWF operational forecasting system in analysing and forecasting tropical easterly disturbances. Part 1: Synoptic investigation. September 1986	Reed, R.J., A. Hollingsworth, W.A. Heckley and F. Delsol
59	Diabatic nonlinear normal mode initialisation for a spectral model with a hybrid vertical coordinate. January 1987	Wergen, W.
60	An evaluation of the performance of the ECMWF operational forecasting system in analysing and forecasting tropical easterly wave disturbances. Part 2: Spectral investigation. January 1987	Reed, R.J., E. Klinker and A. Hollingsworth
61	Empirical orthogonal function analysis in the zonal and eddy components of 500 mb height fields in the Northern extratropics. January 1987	Molteni, F.
62	Atmospheric effective angular momentum functions for 1986-1987. February 1989	Sakellarides, G.
63	A verification study of the global WAM model December 1987 - November 1988. May 1989	Zambresky, L.
64	Impact of a change of radiation transfer scheme in the ECMWF model. November 1989	Morcrette, J-J.
65	The ECMWF analysis-forecast system during AMEX. May 1990	Puri, K., P. Lönnberg and M. Miller
66	The calculation of geopotential and the pressure gradient in the ECMWF atmospheric model: Influence on the simulation of the polar atmosphere and on temperature analyses. July 1990	Simmons, A.J. and Chen Jiabin